Diploma thesis

Nonequilibrium Green functions approach to ionization processes

by
David Hochstuhl

Kiel, October 2008

Institut für
Theoretische Physik und Astrophysik
der Christian-Albrechts-Universität zu Kiel

Supervisor/1st examiner: Prof. Dr. Michael Bonitz

2nd examiner: _____

Contents

1. Introduction

New and powerful measurement techniques provide a deep insight into the fundamental properties of our nature. In particular, the research on ionization processes has benefitted from this evolution. The available laser sources, such as X-FEL, FLASH or LCLS, to name a few, have opened the doors to unexplored intensity regimes and peak brilliancies, allowing for a precise and time-resolved investigation of the arising effects on ultra-short time-scales. Their results constitute a major challenge for the theoretical description. The main difficulties thereby emerge from the inclusion of the particle interaction. Whereas several effects observable already in the single-particle picture have been well explained by the one-particle Schrödinger equation, nowadays most important issues elude the single-particle approach. For example, they cover the time-resolved description of Auger processes, the double ionization of atoms or, more involved, the ionization properties of molecules and solids. In this work, for the description of correlation effects, we examine an approach based on quantum kinetic theory. Such one is offered by the formalism of nonequilibrium Green function (NEGF). First invented in 1964 by Kadanoff and Baym and independently in 1965 by Keldysh – basing on pioneering works of Schwinger, Matsubara and others – it has turned out to be a powerful tool for the approximative description of correlated quantum systems. Since that time, the Green function formalism has been applied to almost all topics in quantum mechanical many-body theory, including atoms and molecules, dense plasmas and artificial atoms. Also, many works concerning the ionization properties of real materials have been published. However, these works remain on the equilibrium approach. The application of nonequilibrium Green functions to the descriptions of time-dependent phenomena thus marks an entirely new approach.

The present work is organized in three parts. Part one prepares the required theoretical basis on which the further work is established. In chapter 2, we provide a short overview on the topic of photoionization. After a theoretical introduction based on the single-particle Schrödinger equation, we collect the most important effects arising in the interaction of atoms and laser-fields. The remaining part then will focus on the formalism of nonequilibrium Green functions. In chapter 3, we derive the Keldysh/Kadanoff-Baym equations, the general equations of motion for the Green function, starting from the formalism of second quantization. The following chapter 4 collects the considered self-energy expressions. They include the Hartree-Fock approximation as well as the second Born and GW approximation. Their invention is motivated by diagram technique.
The following part two is devoted to the numerical implementation of several methods from many-body theory. It starts with the treatment of the single-particle Schrödinger equation in chapter 6, whose stationary solutions will provide us a starting basis for the following approaches. Also its time-dependent counterpart is solved to give access to reference results for the noninteracting system. The subsequent chapter 6 constitutes one of the main parts in this thesis. There we investigate the Hartree-Fock approximation for different thermodynamical ensembles and treatments of the spin. Chapter 7 introduces the Configuration Interaction approach, which is also known as Exact Diagonalization. With this tool, we are able to gain a lot of information on the quality of the Green function. The same is considered in chapter 8 for the first time on a numerical footing. In this chapter we face the self-consistent solution of the Dyson equation in imaginary

time space, whereby the particle interaction is approximated within Hartree-Fock, second Born and GW approximation. The following chapter 9 concentrates on the propagation of the thus obtained equilibrium solution in real time. It requires the solution of the Keldysh/Kadanoff-Baym equations, for which an involved algorithm is presented. In every chapter of part two the presented algorithms were tested, yielding some unseen results.
Finally, the last part is devoted to the investigation of ionization processes in terms of the collected schemes. Therefore, in chapter 10, a model is introduced and its equilibrium properties are calculated. From the equilibrium solutions, some properties related to ionization determined. Further an approach to Auger processes is examined. The last chapter concentrates on the propagation of the equilibrium solutions in time under the action of an electromagnetic field. First, we focus on the ideal case to appoint the capabilities of the model. Then, the arising effects are studied, mostly in Hartree-Fock approximation. Also, the double ionization of a one-dimensional Helium model is considered, and its incorporation in the present approach is discussed.

Before beginning with a theoretical introduction, we close with some notational remarks. All parameters and calculational results in this work are given in atomic units. However, they will be suppressed in the following. Further, to introduce a notational scheme, the many body Hamiltonian is written by the capital letter $\hat{H}$, while the single-particle Hamiltonian is denoted by $\hat{h}$. The quantities, which are in equilibrium, i.e. under no influence of an external field, are labeled by the superscript 0, for instance $\hat{H}^0$. Matrices are always indicated by a bold typed letter $\mathbf{H}$.

Part I.

Theory

2. Photoionization

It was in 1905, the "annus mirabilis", when Einstein theoretically founded the description of photoionization. Relying more on Planck's calculations than Planck himself, he proposed a revolutionary explanation of the photoeffect, whose experimental results disagreed with any classical prediction. As it is well-known, Einstein created an as brilliant as simple model, in which light is considered as a carrier of photons, each one able to strike out one electron.
A little more than two decades later the quantum-field theory was invented, which provided an exact description of the interaction between particles and photons. Today, it has turned out to be the most accurate theory in physics at all, though its basic assumptions resemble the ones from Einstein.

In this introduction we will not concern on the quantum-field theory, but restrict ourselves to the description of classical fields. Therefore it is sufficient to consider the Hamiltonian in "minimal coupling". In particular this approximation is valid if the field intensity is strong, i.e. if the number of photons draws near to the thermodynamic limit. However, intrinsic quantum effects, such as spontaneous emission, can then not be observed.

2.1. Atom-field interaction, dipole approximation

The evolution of wavefunctions is governed by the time-dependent Schrödinger equation (TDSE), which in spatial representation surprisingly reads

$$i\,\hbar\,\frac{\partial}{\partial t}\,\psi(\mathbf{r},t) \;=\; \hat{h}(\mathbf{r},t)\,\psi(\mathbf{r},t)\,. \tag{2.1}$$

In the presence of electromagnetic fields the Hamilton operator in minimal coupling is given through

$$\hat{h}(\mathbf{r},t) \;=\; \frac{1}{2m}\big[\hat{\mathbf{p}} \;+\; e\,\mathbf{A}(\mathbf{r},t)\big]^2 \;-\; e\,\Phi(\mathbf{r},t) \;+\; v(\mathbf{r})\,, \tag{2.2}$$

where $v(\mathbf{r})$ is the external time-independent confinement and $\mathbf{A}(\mathbf{r},t)$ and $\Phi(\mathbf{r},t)$ are the vector and scalar potential of the external fields. The fields themselves are related to their potentials by

$$\mathbf{E}(\mathbf{r},t) \;=\; -\,\nabla\,\Phi(\mathbf{r},t) \;-\; \frac{\partial\mathbf{A}(\mathbf{r},t)}{\partial t}\,, \tag{2.3}$$

$$\mathbf{B}(\mathbf{r},t) \;=\; -\,\nabla \;\times\; \mathbf{A}(\mathbf{r},t)\,. \tag{2.4}$$

and are invariant under the gauge transformations

$$\Phi'(\mathbf{r},t) \;=\; \Phi(\mathbf{r},t) \;-\; \frac{\partial\chi(\mathbf{r},t)}{\partial t}\,, \tag{2.5}$$

$$\mathbf{A}'(\mathbf{r},t) \;=\; \mathbf{A}(\mathbf{r},t) \;+\; \nabla\chi(\mathbf{r},t)\,. \tag{2.6}$$

Within a certain gauge, the Hamiltonian (2.2) transforms to

$$\hat{h}(\mathbf{r},t) \;=\; \frac{1}{2m}\big[\,\hat{\mathbf{p}} \;+\; e\,(\mathbf{A} \;+\; \nabla\,\chi)\,\big]^2 \;-\; e\Phi \;+ e\,\frac{\partial\chi}{\partial t} \;+\; v(\mathbf{r})\,. \tag{2.7}$$

We now switch to the Coulomb or radiation gauge , for which $\Phi = 0$ holds and $\mathbf{A}$ satisfies the transversality condition $\nabla \cdot \mathbf{A}(\mathbf{r},t) = 0$ as well as the wave equation

$$\nabla^2\mathbf{A} \;-\; \frac{1}{c^2}\frac{\partial^2\mathbf{A}}{\partial t^2} \;=\; 0\,. \tag{2.8}$$

This choice of gauge is in contrast to the Lorentz gauge not relativistically invariant, but in this work we only focus on non-relativistic regimes. The solution of the wave equation has the form

$$\mathbf{A}(\mathbf{r},t) \;=\; \mathbf{A}_0\,\mathrm{e}^{i(\mathbf{r}\cdot\mathbf{k}\,-\,\omega t)} \;+\; c.c. \tag{2.9}$$

where $\mathbf{k}$ is the wave vector of radiation and $|\mathbf{k}| = 2\pi/\lambda$. For $|\mathbf{r}|$ of typical atomic dimensions (a few Ångströms) and λ of typical optical wavelengths $(400 - 700\,nm)$ is $\mathbf{k}\cdot\mathbf{r} \ll 1$, so that within the considered region the vector potential is spatially uniform, $\mathbf{A}(\mathbf{r},t) \approx \mathbf{A}(t)$. This is the so-called dipole approximation. We now choose a special gauge function, $\chi(\mathbf{r},t) = -\mathbf{A}(t)\cdot\mathbf{r}$ ("length gauge") for that

$$\nabla\chi(\mathbf{r},t) \;=\; -\mathbf{A}(t)\,, \tag{2.10}$$

$$\frac{\partial\chi}{\partial t}(\mathbf{r},t) \;=\; -\mathbf{r}\cdot\frac{\partial\mathbf{A}}{\partial t} \;=\; -\mathbf{r}\cdot\mathbf{E}(t)\,. \tag{2.11}$$

Thus, we obtain the Hamiltonian used throughout this work,

$$\hat{h}(\mathbf{r},t) \;=\; \frac{1}{2m}\,\hat{\mathbf{p}}^2 \;+\; v(\mathbf{r}) \;-\; e\,\mathbf{r}\cdot\mathbf{E}(t)\,, \tag{2.12}$$

which in later chapters is joined by the two-particle interaction part. This result may also be rewritten in terms of the dipole operator $\mathbf{d} = -e\,\mathbf{r}$.

2.1.1. Time-dependent perturbation theory, Fermi's Golden rule

The previous derivation is valid for a quantum or classical electromagnetic field. Now we will focus on the classical case, the only one considered in this work. We assume that the initial state of the atom at time t_0 is $|i\rangle$, where $\hat{h}^0\,|i\rangle = E_i\,|i\rangle$. For times $t > t_0$ we expand the state vector $|\psi(t)\rangle$ in terms of the complete set of eigenfunctions of the uncoupled Hamiltonian $\{|k\rangle\}$:

$$|\psi(t)\rangle \;=\; \sum_k C_k(t)\,\mathrm{e}^{-i\,E_k\,t/\hbar}\;|k\rangle\;. \tag{2.13}$$

Substituting this in the TDSE and multiplying from the left by $\langle l|\;\mathrm{e}^{i\,\omega_l\,t}$ leads to the (exact) set of coupled first order differential equations

$$\dot{C}_l(t) \;=\; -\,\frac{i}{\hbar}\sum_k C_k(t)\;\langle l|\hat{h}^{(I)}(t)|k\rangle\;\mathrm{e}^{i\,\omega_{lk}\,t}\,, \tag{2.14}$$

where $h^{(I)}(t) = -\mathbf{d}\cdot\mathbf{E}(t)$ (the dipole approximation is implied) and $\omega_{lk} = (E_l - E_k)/\hbar$ are the transition frequencies between levels l and k. The expansion coefficients directly determine the

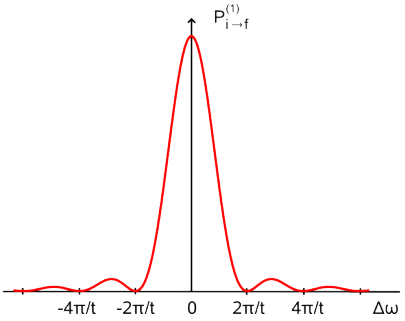

Figure 2.1: *Transition probability $P_{i\to f}$ as a function of $\Delta\omega$ as derived from first-order perturbation theory for a monochromatic electric wave. In the long-time limit this function is well approximated by a delta function.*

transition probability from state $|i\rangle$ to state $|f\rangle$ at time t through $P_{i\to f}(t) = |C_f(t)|^2$.
These equations are analytically solvable only for very simple cases. Thus one has to use the time-dependent perturbation scheme well known from elementary quantum mechanics, valid under the preliminary that $|\langle f|\hat{h}^{(I)}(t)|i\rangle|$ is weak, or equivalently $|C_f(t)| \ll 1$ for $i \neq f$. We expand the probability amplitudes in the power series

$$C_l(t) = C_l^{(0)}(t) + \xi\, C_l^{(1)}(t) + \xi^2 C_l^{(2)}(t) + \cdots . \tag{2.15}$$

Inserting this in (2.14), we obtain the recursive set of equations

$$\dot{C}_l^{(0)}(t) = \delta_{li}\,, \tag{2.16}$$

$$\dot{C}_l^{(n)}(t) = -\frac{i}{\hbar}\sum_k C_k^{(n-1)}(t)\,\hat{h}^{(I)}(t)_{lk}\,\mathrm{e}^{i\,\omega_{lk}\,t}\,, \tag{2.17}$$

whose first-order solution is given by

$$C_f^{(1)}(t) = -\frac{i}{\hbar}\int_{t_0}^{t} dt'\; h^{(I)}(t)_{fi}(t')\,\mathrm{e}^{i\,\omega_{fi}\,t'}\,. \tag{2.18}$$

The transition amplitude $C_f^{(1)}$ accounts for direct transitions from $|i\rangle$ to $|f\rangle$, while the second-order contribution $C_f^{(2)}$ accounts for double transitions $|i\rangle \to \{|l\rangle\} \to |f\rangle$ and so on.

Now we consider the special case of a monochromatic wave, $\mathbf{E}(t) = \mathbf{E}_0\cos(\omega t)$. Expanding the cosine in terms of exponentials, (2.18) integrates to

$$C_f^{(1)}(t) = -\frac{1}{2\hbar}h^{(I)}(t)_{fi}\cdot\left\{\frac{\mathrm{e}^{i\,(\omega+\omega_{fi})\,t}-1}{\omega+\omega_{fi}} - \frac{\mathrm{e}^{i\,(\omega-\omega_{fi})\,t}-1}{\omega-\omega_{fi}}\right\}. \tag{2.19}$$

If the frequency of the radiation ω is near resonance with the atomic transition frequency ω_{fi}, the second term clearly dominates the first. Therefore we can drop the "anti-resonant" first term, making the so-called "rotating wave approximation" [1], with which the transition probability becomes

$$P_{i\to f}^{(1)}(t) = \frac{|h^{(I)}(t)_{fi}|^2}{\hbar^2}\frac{\sin^2(\Delta\omega\,t/2)}{\Delta\omega^2}\,. \tag{2.20}$$

$\Delta\omega$ is the detuning between the radiation field and the atomic transition. In Fig. 2.1 the first-order transition probability is plotted against $\Delta\omega$. In the limit $t\to\infty$, this function converges to

a delta function and we obtain the famous golden rule of Fermi

$$P^{(1)}_{i\to f}(t) \;=\; \frac{|h^{(I)}_{fi}(t)|^2}{\hbar^2}\frac{\pi\, t}{2}\,\delta(\Delta\omega)\,. \tag{2.21}$$

Furthermore, we mention a straightforward generalization to non-monochromatic fields. The transition rate then has to be integrated over the whole frequency spectrum

$$P^{(1)}_{i\to f} \;=\; \frac{t}{\hbar^2}\int d\omega\;\frac{\sin^2(\Delta\omega\, t/2)}{\Delta\omega^2}\,F(\omega)\,, \tag{2.22}$$

where

$$F(\omega) \;\equiv\; |\,\langle f|\mathbf{d}\cdot\mathbf{E}_0(\omega)|i\rangle\,|^2\,, \tag{2.23}$$

is the frequency dependent transition element.

2.2. Phenomenological description

Though the solution of the Schrödinger equation in principle answers all questions on ionization related to one particle, to do physics one needs a more pictorial description of the effects of strong laser fields on atomic systems. As can be seen from (2.12), the atom-laserfield interaction in dipole approximation depends on the electric field $\mathbf{E}(t)$, i.e. on frequency, amplitude and temporal shape of the dipole-approximated wave, as well as on $v(\mathbf{r})$, the atomic confinement. To relate the two quantities, we focus on a free particle in an electromagnetic field [2]. Its classical equation of motion is given by

$$m\,\frac{dv}{dt} \;=\; e\,E_0\,\cos(\omega t)\,, \tag{2.24}$$

respectively

$$v(t) \;=\; \frac{e\,E_0}{m\,\omega}\,\sin(\omega t)\,. \tag{2.25}$$

The averaged kinetic energy of this quiver motion is called the ponderomotive potential

$$U_p = \left\langle \frac{1}{2}mv(t)^2 \right\rangle \;= \frac{e^2\,E_0^2}{4m\,\omega^2}\,, \tag{2.26}$$

that can also be rewritten in terms of the intensity of a dipole field

$$I \;=\; \frac{1}{8\pi}cE^2\,. \tag{2.27}$$

The addressed relation to the atomic confinement was given by Keldysh in a fundamental work from 1965

$$\gamma \;\equiv\; \sqrt{\frac{I_p}{2U_p}} \;=\; \frac{\sqrt{m}}{e}\,\sqrt{2I_p}\,\frac{\omega}{E_0}\,. \tag{2.28}$$

This ratio between the ionization potential I_p and the ponderomotive potential is called “Keldysh-

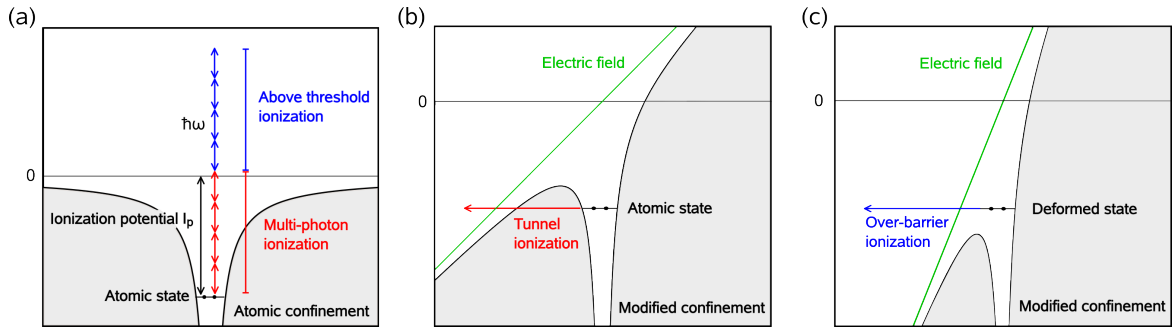

Figure 2.2.: *Different types of photoionization. (a) Multi-photon ionization and above threshold ionization. The Keldysh parameter $\gamma > 1$ is larger than one. (b) Tunnel ionization for $\gamma < 1$. (c) Over barrier ionization for $\gamma \ll 1$.*

parameter". It yields a classification of the strength of a laser-field: If $\gamma < 1$, the ionization potential is small compared to the ponderomotive energy and the dominant energy contribution is given by the electromagnetic field, while for $\gamma > 1$ it is vice versa. Depending on the value of γ, several effects in the ionization process arise, that we will shortly collect in the following.

2.2.1. Multi-photon ionization

According to the treatment in section 2.1.1, in first order perturbation theory transitions occur if the excitation is in resonance to the energy distance of two levels, and the transition probability between those levels is proportional to the field intensity. The validity of the approach requires a small field and thus a large Keldysh parameter $\gamma \gg 1$. If the field gets stronger now, the photon density can be large enough for an electron to pick up more – say N – photons in a certain time Δt. As we know from the Heisenberg uncertainty relation, the variance of the transferred energy is related to the duration of the process by $\Delta E \, \Delta t > \hbar$. By taking several steps of width ΔE, the electron is able to gather the energy $N\hbar\omega$ and can thus be ionized even if the photon energy is smaller than the ionization potential. This process can be illustrated by transitions through intermediate "virtual orbitals", see Fig. 2.2 (a). For a moderate $\gamma \approx 3$ to 6, it can be described by higher terms in the perturbation expansion, what yields a non-linear transition probability proportional to I^N - the probability of N first order steps at the same time.
Of course this effect is not restricted to transitions between bound state and the continuum. The corresponding process, where continuum states with the multiple photon energy get occupied, is called "*above threshold ionization*".
For stronger fields of $\gamma \approx 1$ the atomic levels are modified by the field and the perturbation theory breaks down. The respective ionization probability then normally is given by a smaller power of the intensity, what is caused by the intermediate occupation of real atomic states before the actual ionization. Moreover, a saturation of the ionization is reached when all electrons in the laser focus are already removed.

2.2.2. Strong field effects

In the region $\gamma \approx 1$ we smoothly enter another regime, in that the external field is stronger than the interatomic fields. This leads to a heavy deformation of the atomic confinement by the linear electric potential, as it is sketched in Fig. 2.2 (b), and the diminished barrier allows an electron to tunnel out of the atom. This is the ostensive information in γ: It indicates whether the electron

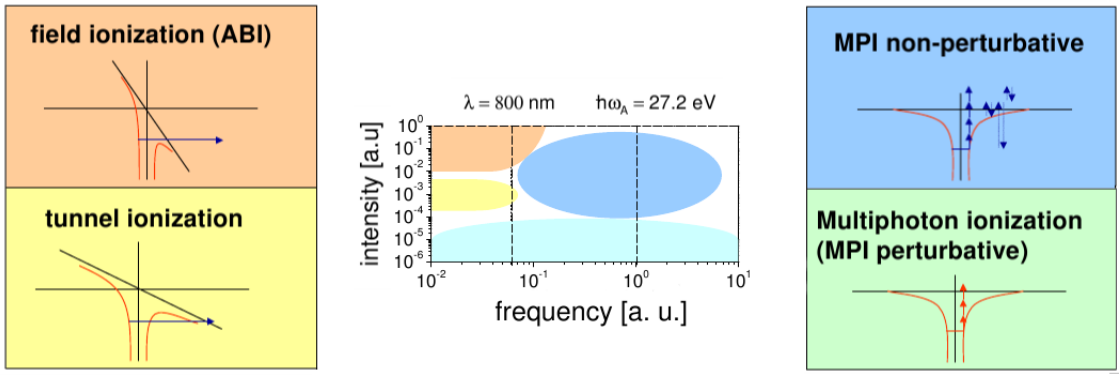

Figure 2.3.: *Ionization regimes of an atom, from [3].*

can pass the barrier before the field changes its sign. Correspondingly, for equal intensities, the fields of smaller frequency are considered as stronger within this theory, as the electron has more time to tunnel through the confinement walls.
If $\gamma \ll 1$, we reach the "*over barrier ionization*" (OBI), in which the atomic structure is so severely modified, that the electron feels no confinement anymore. The process is visualized in Fig. 2.2 (c). Both effects normally lead to a rapid saturation of the ionization probability in the cross-section.

2.2.3. Many-body effects

The previously described effects can all be observed within the single-particle picture, so that for their theoretical investigation the solution of the single-particle Schrödinger is sufficient. The influence of other atomic particles is thereby often approximated by an appropriate constant pseudo-potential ("single-active electron"). The aim of our approach, however, is to include the particle interaction as well as their dynamics in an ab-initio model. The possible applications of such a model are manifold and cover most of the unsolved problems in the theoretical description of ionization processes.
Among them is e.g. the question of re-scattering: An ionized particle can return to the atom if the course and amplitude of the wave is chosen in the right way. There it can be recaptured by the atom under emission of the received energy in radiation, whose energy is a multiple of the field frequency. The emitted electromagnetic waves are called "*higher harmonics*", and their spectrum reaches till the characteristic cutoff, $E < 3.17\,U_p$, which is derived in a classical calculation [2]. This process can still be described in the single-particle picture. The second alternative is that the re-scattered particle ionizes another confined electron. This process is known as "*non-sequential double ionization*" and leads to a so-called knee-structure in the cross section. Clearly, the simulation of this process requires the use of many-body schemes. For two particles it is accessible exactly through the two-particle Schrödinger equation [4], while for a larger particle number accurate schemes are still lacking.[1]
Another common many-body effect is the *Auger process*, which is also known as inner photo-effect. The dynamics of the ionization occurs as illustrated in Fig. 2.4: First a core electron, say from the K-shell, is ionized either through x-ray radiation $(1000 - 2000\,eV)$ or an electron beam $(2 - 50\,keV)$. The generated hole then is filled up by an outer shell electron, for instance

[1] The problem has been investigated in the framework of density-functional theory [5]. However, there is no striking agreement with the experiment. Likewise Hartree-Fock and extended Hartree-Fock calculations are unable to reproduce the knee-structure in the right order of magnitude [6].

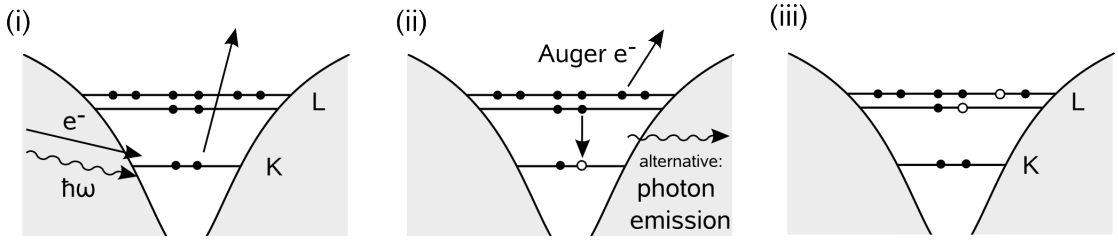

Figure 2.4.: *Schematic progress of the Auger ionization for a Neon atom. (i) Ionization of a core electron. (ii) Transition into the generated hole by an outer shell electron, whereby the energy $|E_K - E_L|$ is is transferred to another outer shell electron, whose ionization energy is roughly E_L. Alternatively a photon can be emitted. (iii) The final state is double ionized. The auger electron can be detected with an energy of roughly $E_{kin} = |E_K - E_L - E_L|$.*

from the L-shell. This transition can take place by emission of a photon. Alternatively, in the Auger process another outer shell electron, for instance again from the L-shell, is ionized by an inner-atomic transfer of the photon. For this reason, the Auger process is also called radiation free transition. The decision between Auger and photon-emission strongly depends on the atomic number Z. For light atoms, the Auger process clearly dominates, while for heavier atoms ($Z \sim 30$) the trend is inversed.
Due to the involved orbitals, the previously considered process is notated by (KLL), respectively by (ABC) in general. The kinetic energy of the Auger electron is roughly given by

$$E_{kin} \;=\; E_A - E_B - E_C \,. \tag{2.29}$$

However, this expression does not account for the relaxation energy. After the Auger process the atom remains in a doubly ionized.

3. Nonequilibrium Green functions

As predicted in the last chapter, we now include the particle interaction in the description. Therefore the Hamiltonian (2.12) must be extended according to

$$\hat{H}(\mathbf{r}_1, \cdots, \mathbf{r}_N, t) \;=\; \sum_{i=1}^{N} \hat{h}(\mathbf{r}_i, t) \;+\; \frac{\lambda}{2} \sum_{i \neq j=1}^{N} \hat{w}(\mathbf{r}_i, \mathbf{r}_j) \tag{3.1}$$

where $\hat{w}(\mathbf{r}_i, \mathbf{r}_j)/2$ is the symmetrized interaction between particle i and j, which, like the one-body part, is assumed to be spin-independent. The prefactor λ is the coupling parameter that determines the interaction strength.[1] Most of the time we will consider the repulsive Coulomb interaction $w(\mathbf{r}_i, \mathbf{r}_j) = |\mathbf{r}_i - \mathbf{r}_j|^{-1}$. Our fundamental Hamiltonian (3.1) only incorporates the electronic degrees of freedom, so the Born-Oppenheimer approximation [7] is implicitly assumed throughout this thesis.
While the solution of the Schrödinger equation with the single-particle Hamiltonian (2.12) requires the treatment of a d-dimensional partial differential equation, where d is the dimension of the physical system, the treatment of the many-body Hamiltonian (3.1) for N particles leads to a system of Nd coupled differential equations, that is numerically feasible only for a small number of particles. Thus approximation schemes become essential, and without lingering on other approaches[2], we directly turn to the formalism of non-equilibrium Green functions (NEGF).
In the following we will give a short introduction into the theory of NEGFs, that is mainly based on the Refs. [8–11].

3.1. Definition and overview

3.1.1. Why Nonequilibrium Green functions?

Before encountering the whole concept of NEGF with all its mathematical and numerical complexity, we try to give a motivation by announcing the main features of this formalism [9]:

- The one-body Green function as a function of two space-time coordinates is compared to the many-body wavefunction a significantly reduced quantity. Despite this reduction, the information on expectation values of all one-body and some two-body operators is fully covered. Among the accessible quantities are e.g. currents and densities, electron addition and removal energies as well as the total energy of the system.

[1] The natural choice is $\lambda = 1$. However, by choosing a special unit system the number of free parameters reduces to one and computational results are valid for a whole class of parameters. For instance, in oscillator units we have $\lambda = E_C/\hbar\Omega$, where E_C is the Coulomb energy and Ω the trap frequency, so that a fixed lambda represents many cases. In the unadjusted atomic unit system, we can think of λ as a chance to vary the Coulomb interaction strength to clarify the influence of interaction effects.

[2] Among them are the density functional theory, multiconfigurational Hartree-Fock and configuration interaction (CI) schemes for nonequilibrium and for equilibirium Monte-Carlo as well as all the other methods known from quantum chemistry.

- The influence of electron-electron correlations can be derived systematically by a perturbation expansion and be included in an effective one-body potential, the self-energy. The necessary approximations to the many-body problem are condensed into this quantity, while the formalism can be established independently of the chosen approximation.
- Approximations on the particle interaction can be derived in a way that macroscopic conservation laws are satisfied.
- The action of external fields on the correlated particles can be treated non-perturbatively, and the reaction of the system can be investigated on arbitrarily short time-scales.

To be honest, we also have to provide some information about the restrictions of the NEGF formalism, as it will be derived within this work, that are mainly related to the numerical application. Due to the great computational demands, up to now only microscopic systems have been treated with the present formalism, what means in plain text an order of magnitude of roughly 10 particles.[3] On account of the same reason, only very few approximations on the self-energy are feasible, and from the first it is not obvious which of them should be used, though there are some hints.
Nevertheless, these numerical reasons can not tear down the attractivity of the elegant NEGF formalism.

3.1.2. Second quantization

Let us shortly recapitulate the basic definitions of the second quantization formalism. For any unanswered questions we refer to the available textbooks on many-body physics, such as [11],[12] or [13].
The foundation of the second quantization is given by the creation and annihilation operators, $\hat{a}_i^\dagger$ and $\hat{a}_i$, that create or destroy a particle in the single-particle state $|i\rangle$, and the observation, that any operator in quantum mechanics can be represented within this picture. For example, we obtain for a one-body operator $\hat{O}$

$$\hat{O} \;=\; \sum_{ij} O_{ij}\; \hat{a}_i^\dagger \hat{a}_j \,, \tag{3.2}$$

where $O_{ij} \;=\; \langle i|\hat{O}|j\rangle$, and the sum runs over all states of the one-particle Hilbert space. From this fact the formalism received its name, as formerly continuous external fields also get resolved into their quanta, while in the "first quantization" only the particle states are treated in a discrete way.
With the corresponding expression for the two-body interaction operator $\hat{w}$, we represent the Hamiltonian (3.1) in second quantization

$$\hat{H} \;=\; \sum_{ij} h_{ij}\; \hat{a}_i^\dagger \hat{a}_j \;+\; \sum_{ijkl} w_{ij,kl}\; \hat{a}_i^\dagger \hat{a}_j^\dagger \hat{a}_k \hat{a}_l \,, \tag{3.3}$$

[3] However, with somewhat different methods, the Green function formalism has also been applied to macroscopic systems like plasmas.

where the matrix elements are given by

$$h_{ij} \;=\; \int d\mathbf{x}\; \varphi_i^*(\mathbf{x})\; \left\{-\frac{1}{2}\nabla^2 + v(\mathbf{r})\right\}\; \varphi_j(\mathbf{r})\,, \tag{3.4}$$

$$w_{ij,kl} \;=\; \iint d\mathbf{x}\; d\mathbf{x}'\; \varphi_i^*(\mathbf{x})\varphi_j^*(\mathbf{x}')\; w(\mathbf{r},\mathbf{r}')\; \varphi_k(\mathbf{x}')\varphi_l(\mathbf{x})\,. \tag{3.5}$$

The variable $\mathbf{x}$ stands for $(\mathbf{r}, m_s)$, and $d\mathbf{x}$ denotes integration over space and summation over the spin quantum numbers. The external potential and the interaction are thereby assumed to be spin-independent.

Any many-body state can be created by applying creation operators on the vacuum state and the resulting wavefunction has to fulfill the right symmetry properties, i.e. under particle exchange it has to be symmetric for bosons and antisymmetric for fermions. One of the main features of the second quantization formalism is that this condition is fully covered only by requiring the following commutation relations:

$$[\;\hat{a}_i^\dagger, \hat{a}_j^\dagger\;]_\mp \;=\; 0\;, \qquad [\;\hat{a}_i, \hat{a}_j\;]_\mp \;=\; 0\;, \qquad [\;\hat{a}_i, \hat{a}_j^\dagger\;]_\mp \;=\; \delta_{ij}\,. \tag{3.6}$$

At the same time the different brackets, namely the commutator for bosons $(-)$ and the anti-commutator for fermions $(+)$, are the only – but fare reaching – difference in the description of both particle species.

The common formulation of the Green function is constructed in terms of the field operators, which are the operators above expressed in the spatial basis. A general change of the single-particle basis can be derived in the following way

$$\hat{a}_\alpha^\dagger\,|0\rangle \;=\; |\alpha\rangle \;=\; \sum_\lambda\; \langle\lambda|\alpha\rangle\,|\lambda\rangle \;=\; \sum_\lambda \langle\lambda|\alpha\rangle\,\hat{a}_\lambda^\dagger\;\;|0\rangle\;. \tag{3.7}$$

This procedure can be repeated for $\hat{a}_\alpha^{(\dagger)}$ acting on any state in Fock space and leads to the operator identities

$$\hat{a}_\alpha^\dagger \;=\; \sum_\lambda\; \langle\lambda|\alpha\rangle\,\hat{a}_\lambda^\dagger\;, \qquad\qquad \hat{a}_\alpha \;=\; \sum_\lambda\; \langle\alpha|\lambda\rangle\,\hat{a}_\lambda\,. \tag{3.8}$$

As it is familiar from elementary quantum mechanics, for a transformation to a continuous basis the sum becomes an integral over all single particle states.

Now we switch to spatial representation and define the field operators, that create or destroy a particle at the space point $\mathbf{r}$ with spin projection m_s, or more abstract in the state $|\mathbf{r}, m_s\rangle \;=\; |\mathbf{x}\rangle$. Instead of $\hat{a}_{\mathbf{r},m_s}^{(\dagger)}$ the somewhat confusing notation $\Psi_{m_s}(\mathbf{r}) \;\equiv\; \Psi(\mathbf{x})$ is used for them:

$$\Psi^\dagger(\mathbf{x}) \;=\; \sum_i \varphi_i^*(\mathbf{r})\chi^*(m_s)\;\hat{a}_i^\dagger\;, \qquad\qquad \Psi(\mathbf{x}) \;=\; \sum_i \varphi_i(\mathbf{r})\chi(m_s)\;\hat{a}_i\,. \tag{3.9}$$

$\chi(m_s)$ is thereby the spin function, i.e. a basis state of the spin Hilbert-space whose dimension is $2s+1$. As we only consider spin-independent interactions – except for the intrinsic Pauli exclusion principle – most of the time we will suppress the spin variable.
Together with the spatial matrix elements of the one- and two-body part of the Hamiltonian [13]

$$\langle\,\mathbf{x}_1\,|\,\hat{h}\,|\,\mathbf{x_2}\,\rangle \;=\; \delta(\mathbf{x}_1-\mathbf{x}_2)\,h(\mathbf{r}_1)\,, \tag{3.10}$$

$$\langle\,\mathbf{x}_1,\mathbf{x}_2\,|\,\hat{w}\,|\,\mathbf{x}_3,\mathbf{x}_4\,\rangle \;=\; \delta(\mathbf{x}_1-\mathbf{x}_4)\,\delta(\mathbf{x}_2-\mathbf{x}_3)\;w(\mathbf{r}_1,\mathbf{r}_2)\,, \tag{3.11}$$

where $\delta(\mathbf{x}_1 - \mathbf{x}_2) \equiv \delta_{m_{s_1},m_{s_2}}\,\delta(\mathbf{r}_1 - \mathbf{r}_2)$, the Hamiltonian (3.3) transforms to

$$\hat{H} \;=\; \int d\mathbf{x}\;\Psi^\dagger(\mathbf{x})\,h(\mathbf{r},t)\,\Psi(\mathbf{x}) \;+\; \frac{1}{2}\iint d\mathbf{x}\,d\mathbf{x}'\;\Psi^\dagger(\mathbf{x})\,\Psi^\dagger(\mathbf{x}')\,w(\mathbf{r},\mathbf{r}')\,\Psi(\mathbf{x}')\,\Psi(\mathbf{x})\,, \tag{3.12}$$

while the commutation relations become

$$[\;\hat{\Psi}^\dagger(\mathbf{x}),\hat{\Psi}^\dagger(\mathbf{x}')\;]_\mp \;=\; 0\;,\quad [\;\hat{\Psi}(\mathbf{x}),\hat{\Psi}(\mathbf{x}')\;]_\mp \;=\; 0\;,\quad [\;\hat{\Psi}^\dagger(\mathbf{x}),\hat{\Psi}(\mathbf{x}')\;]_\mp \;=\; \delta(\mathbf{x}-\mathbf{x}')\,. \tag{3.13}$$

In this work we aim at describing systems, which are in equilibrium for times $t < t_0$, such that $H(t < t_0) = H^0$ equals the equilibrium Hamiltonian, and which are disturbed by an external time-dependent field for $t > t_0$. The expectation value of an arbitrary operator $\hat{O}$ at $t > t_0$ in the Heisenberg representation is then given by a trace over the initial density operator $\hat{\rho}^0$,

$$O(t) \;=\; \langle\,\hat{O}_H(t)\,\rangle \;\equiv\; \mathrm{Tr}\{\hat{\rho}^0\hat{O}_H(t)\}\,, \tag{3.14}$$

where the operator in the Heisenberg picture has a time-dependence according to

$$\hat{O}_H(t) \;=\; \hat{U}(t_0,t)\,\hat{O}(t)\,\hat{U}(t,t_0)\,. \tag{3.15}$$

The evolution operator $\hat{U}(t,t')$ is the solution of the equations

$$i\,\frac{d}{dt}\,\hat{U}(t,t') \;=\; \hat{H}(t)\,\hat{U}(t,t')\,, \tag{3.16}$$

$$i\,\frac{d}{dt'}\,\hat{U}(t,t') \;=\; \hat{U}(t,t')\,\hat{H}(t')\,, \tag{3.17}$$

with the boundary condition $\hat{U}(t,t) = 1$. By integration of (3.16) we get the equation

$$\hat{U}(t,t') \;=\; 1 - i\int_{t'}^{t} d\bar{t}_1\;H(\bar{t}_1)\,\hat{U}(\bar{t}_1,t')\,, \tag{3.18}$$

that can be iterated to yield the Dyson series (that should not be confused with the Dyson equation)

$$U(t,t') \;=\; 1 + \sum_{n=1}^{\infty}(-i)^n\int_{t'}^{t} d\bar{t}_1\int_{t'}^{t_1} d\bar{t}_2\cdots\int_{t'}^{t_{n-1}} d\bar{t}_n\;\hat{H}(\bar{t}_1)\cdots H(\bar{t}_n) \tag{3.19}$$

$$\;=\; 1 + \sum_{n=1}^{\infty}\frac{(-i)^n}{n!}\int_{t'}^{t} d\bar{t}_1\int_{t'}^{t} d\bar{t}_2\cdots\int_{t'}^{t} d\bar{t}_n\;T\big[\hat{H}(\bar{t}_1)\cdots H(\bar{t}_n)\big]\,. \tag{3.20}$$

In the last step we could make all integrals run from t' to t by introducing the time-ordered product, where operators acting at later times are ordered to the left, formally written as

$$T\big[\hat{H}(\bar{t}_1)\cdots H(\bar{t}_n)\big] \;=\; \sum_P \theta(\bar{t}_{P(1)} - \bar{t}_{P(2)})\cdots\theta(\bar{t}_{P(n-1)} - \bar{t}_{P(n)})\,\hat{H}(\bar{t}_{P(1)})\cdots\hat{H}(\bar{t}_{P(n)})\,. \tag{3.21}$$

P runs over all permutations of the numbers $1...n$. The adjoint equation can be treated in the same way, and both results can be formally summarized in the short-hand notation

$$\hat{U}(t,t') \;=\; \begin{cases} T\,\mathrm{e}^{-i\int_{t'}^{t} d\bar{t}H(\bar{t})} & \text{for } t > t' \\ T\,\mathrm{e}^{\,i\int_{t'}^{t} d\bar{t}H(\bar{t})} & \text{for } t < t' \end{cases}\quad. \tag{3.22}$$

3.1.3. The Green function

The following definition of the Green function is a general one, what means that it applies to any type of Green function, whatever averaging procedure or intrinsic coordinates are used. We will try to give a short overview on the common types of Green functions and finally motivate the introduction of a special time contour needed for the nonequilibrium Green function. But at first we give the definition:

$$G(1,2) \;=\; \langle\, T\{\hat{a}_{\alpha_1}(t_1)\,\hat{a}^\dagger_{\alpha_2}(t_2)\}\,\rangle\ . \tag{3.23}$$

Here $1 = (\alpha_1, t_1)$, and α_1 stands for any complete observable.[4] The Green function has a very ostensive interpretation: for $t_2 < t_1$ it provides the probability for a particle at time t_1 to be in the state α_1, if it was added to the many-body system at t_2 in the state α_2. Due to this property, the Green function is often called a propagator, as it propagates an additional particle through the system.
Similarly, if $t_2 > t_1$, a particle in the state α_1 is removed from the system at t_1, and the Green function gives the probability that the original system is restored if a particle is added at t_2 in the state α_2. One can also think of this process as the propagation of a hole through the system.

Let us first consider the equilibrium zero-temperature Green function, where the average in (3.23) is formed over the groundstate $|\Psi_0\rangle$ of the interacting system, $H\,|\Psi_0\rangle \;=\; E\,|\Psi_0\rangle$.

$$G(1,2) \;=\; -i\frac{\langle\Psi_0|\,T\,[\Psi(1)\Psi^\dagger(2)]\,|\Psi_0\rangle}{\langle\Psi_0|\Psi_0\rangle} \tag{3.24}$$

To mention it again, this expression directly yields the probability, that if a particle or hole is added at (x_2, t_2) to the groundstate, the original system is restored after its removal at (x_1, t_1). The problem in this expression is that the exact groundstate of the system is involved, though this is just one of things we want to compute with the Green function. Thus we have to express the groundstate in terms of quantities we know, such as the noninteracting groundstate $|\Phi_0\rangle$. The connection is formed by the Gell-Man/Low theorem[5]

$$|\Psi_0\rangle \;=\; U(t_0,-\infty)\,|\Phi_0\rangle\ , \qquad \langle\Psi_0| \;=\; U(\infty,t_0)\,\langle\Phi_0|\ , \tag{3.25}$$

with that (3.24) transforms into

$$G(1,2) \;=\; -i\frac{\langle\Phi_0|\,U(\infty,-\infty)\,T\,[\Psi(1)\Psi^\dagger(2)]\,|\Phi_0\rangle}{\langle\Phi_0|U(-\infty,\infty)|\Phi_0\rangle}\,. \tag{3.26}$$

This result generates the systematic perturbation expansion scheme for the Green function. To evaluate this expression, (3.20) is inserted for the time-evolution operator. The operator product is then evaluated by means of Wick's theorem [11], which states that a time-ordered product can be expressed as a sum of all pairwise contractions.
The extension of the previous results to finite temperatures is achieved by averaging in a thermodynamic ensemble. As the interaction then also appears in the density operator, the perturbation

[4] For notational clarity however we will consider only the spatial representation given in terms of the field operators. In addition this is also convenient for the inhomogeneous systems we want to describe. For homogeneous systems though, a representation in momentum space is more useful.

[5] In standard textbooks, such as [11] or [10], the following derivation is done in the interaction picture. Especially for the application of Wick's theorem this is much more convenient. We stay in the Heisenberg picture, not only to keep it short, but also because we do not evaluate Wick's theorem explicitly.

expansion becomes quite difficult. A way around this problem was given by Matsubara through the introduction of a complex time branch, which allows for a rewriting of the thermodynamic density operator as an evolution in complex time,

$$\hat{\rho} \;=\; \frac{\mathrm{e}^{-\beta\hat{H}_0}}{\mathrm{Tr}\{\mathrm{e}^{-\beta\hat{H}_0}\}} \;=\; \frac{\hat{U}(t_0-i\beta,t_0)}{\mathrm{Tr}\{\hat{U}(t_0-i\beta,t_0)\}}\,. \tag{3.27}$$

Here the time-independence of the equilibrium state was used, and the chemical potential arising in the grand-canonical average has been absorbed in the single-particle Hamiltonian, $h^0(\mathbf{r}) \to h^0(\mathbf{r}) - \mu$. By means of this replacement, the thermodynamic average (3.14) of an operator $\hat{O}$ in Heisenberg representation becomes

$$O(t) = \frac{\mathrm{Tr}\{U(t_0-i\beta,t_0)\,U(t_0,t)\,\hat{O}(t)\,U(t,t_0)\}}{\mathrm{Tr}\{U(t_0-i\beta,0)\}}\,. \tag{3.28}$$

The extension to nonequilibrium requires a few more thoughts. In the above relations it was implicitly assumed that $U(\infty,t) = U^\dagger(t,-\infty)$ [14], so that the product $U^\dagger(t_0,-\infty)\,U(t_0,-\infty)$ could be casted in the form $U(\infty,-\infty)$, what formally evolves the noninteracting groundstate (respectively the noninteracting density matrix in the finite temperature case) to infinity.[6] The basis for this assumption is the adiabatic theorem, which states that under an adiabatic transformation the groundstate (or equilibrium state) can transform only into itself, possibly multiplied by a phase factor, that is however canceled by the denominator in (3.24). In nonequilibrium, this is not generally valid as there is no guarantee for the system to return to its initial state for asymptotically large times. If we thus replace the time-evolution operator by its adjoint in the above formulas, one observes that the propagation goes from $-\infty$ to t, and then back again to $-\infty$. The time-ordering however is preserved, what gives rise to a special contour, that has been invented by Keldysh in 1964 [15].

3.2. The Keldysh-Contour

The Keldysh-contour $\mathcal{C}$ can be regarded as a mathematical trick to extend the previously obtained formulas and the diagram technique to nonequilibrium theory. It runs from an arbitrary starting time t_0 to the considered time t (both times can be placed at infinity), and anti-chronologically back to t_0. Further by means of the rewriting (3.27), at t_0 the contour is continued in the complex plane to $t_0 - i\beta$.[7] The essential change to equilibrium occurs in the time-ordering – now "later times" means later on the contour – and the corresponding operator is denoted by a subscript $T_\mathcal{C}$. The visualization of the contour is given in Fig. 3.1.

Having prepared these necessary preliminaries, we can define the one-particle Green function on

[6] Note that because of the group property of the evolution operator and the time-independence of the equilibrium state also (3.28) can attain this form.

[7] This is only necessary if one starts with the determination of the equilibrium state; for a description solely on the real track see the approach in [16]. In this context one often neglects the impact of initial correlations on the long-time limit result by assuming "Bogolyubov's weakening of initial correlations". An application is e.g. steady-state transport.

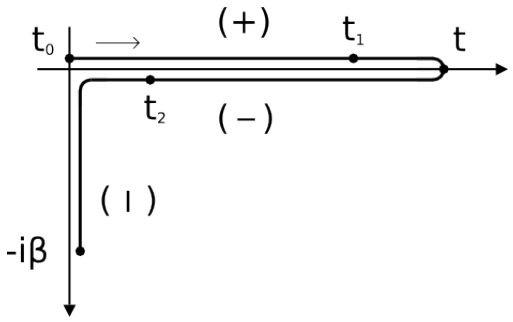

Figure 3.1: *The Keldysh-Contour $\mathcal{C}$, running from t_0 to the considered time t, back again to t_0 and finally to $t_0 - i\beta$. It can be regarded as a mathmatical trick to extend the Green function formalism to non-equilibrium while preserving the time-ordering. Respectively, on the contour the time t_1 is earlier than the time t_2.*

the contour by

$$G(1,2) \;=\; -i\,\langle\, T_{\mathcal{C}}\,[\Psi_H(1)\,\Psi_H^\dagger(2)]\,\rangle \tag{3.29}$$

$$\;=\; -i\,\frac{\mathrm{Tr}\{U(t_0 - i\beta, t_0)\,T_{\mathcal{C}}\,[\Psi_H(1)\,\Psi_H^\dagger(2)]\}}{\mathrm{Tr}\{U(t_0 - i\beta, 0)\}}\,. \tag{3.30}$$

The corresponding generalization of this definition to the s-particle Green function is also achieved [16] in a straightforward manner

$$G_{1..s}(1..s, 1'..s') \;=\; (-i)^s\,\langle\, T_{\mathcal{C}}\,[\Psi_H(1)\cdots\Psi_H(s)\,\Psi_H^\dagger(s')\cdots\Psi_H^\dagger(1')]\,\rangle \tag{3.31}$$

However, in our approach we will only meet the two-particle Green function. For all these many-body Green functions, there exist equations of motion similar to those derived in the next section.

Any two-time function defined on the contour is said to belong to the Keldysh space [17]. In general such functions can be written as

$$k(t,t') \;=\; \delta(t,t')\,k^\delta(t) \;+\; \theta(t,t')\,k^>(t,t') \;+\; \theta(t',t)\,k^<(t,t') \tag{3.32}$$

where the spatial coordinates are omitted for notational clarity. Examples of such quantities are of course the Green function, whose singular part G^δ is zero, and the self-energy, where the singular part is given by the Hartree-Fock self-energy. The greater and lesser term respectively denote the correlation parts.
From this expression we can define several subordinated functions. These functions no longer depend on contour time variables, but on two real values, so that after their introduction we can forget about the contour right again. It is replaced by an algebraic structure, which can be represented in a matrix form.

i. **Correlation functions**, $k^{\gtrless}(t,t')$
Assuming that one time argument lies on the chronological real-time axis $(+)$ and the other on the anti-chronological $(-)$, we define the correlation functions by

$$k^>(t,t') \;=\; k(t_+, t'_-)\,, \tag{3.33}$$

$$k^<(t,t') \;=\; k(t_-, t'_+)\,. \tag{3.34}$$

They mainly carry the dynamical information.

ii. **Mixed functions**, $k^{\rceil\lceil}(t,t')$
The counterpart of the correlation functions, where now one time-argument is situated on the

vertical track (|) and the other may lie on both real branches (±), are the mixed functions

$$k^{\rceil}(t,\tau) \;=\; k^{\rceil}(t,-i\tau) \;\equiv\; k(t_\pm,t^{|})\,, \tag{3.35}$$

$$k^{\lceil}(\tau,t) \;=\; k^{\lceil}(-i\tau,t) \;\equiv k(t^{|},t_\pm)\,. \tag{3.36}$$

They account for the influence and evolution of initial correlations. Following Ref. [18], in the further work we comprehend $k^{\rceil}(t,-i\tau)$ as fully equivalent to $k^{\rceil}(t,\tau)$.

iii. **Matsubara functions**, $k^M(t,t')$
If both times are situated on the imaginary branch, the corresponding quantity is

$$k^M(\tau,\tau') \;=\; k(-i\tau,-i\tau') \tag{3.37}$$

For completeness, we also introduce the causal and anti-causal components for both times lying on the (anti-)chronological branch

$$k^{c/a}(t,t') \;=\; \delta(t-t')\,k^{\delta}(t) \;+\; \theta(\pm[t-t'])\,k^{>}(t,t') \;+\; \theta(\pm[t-t'])\,k^{<}(t,t')\,. \tag{3.38}$$

The upper sign denotes the causal, the lower the anti-causal Keldysh function (and not the particle species !). As only two nonequilibrium Keldysh functions are independent, these functions carry the same information as the correlation functions. The introduced Keldysh functions can be regarded as components of a matrix in Keldysh space. Every function belonging to Keldysh space has therefore the structure of a 3×3 matrix

$$k(t,t') \;=\; \begin{pmatrix} k^{++} & k^{+-} & k^{|+} \\ k^{+-} & k^{--} & k^{|-} \\ k^{|+} & k^{|-} & k^{||} \end{pmatrix} \;=\; \begin{pmatrix} k^{c} & k^{<} & k^{\rceil} \\ k^{>} & k^{a} & k^{\rceil} \\ k^{\lceil} & k^{\lceil} & k^{M} \end{pmatrix} \tag{3.39}$$

As already mentioned above, once this result is achieved and carefully considered in the calculations, one does not need to bother with the Keldysh contour anymore.
Furthermore, as a combination of the different types, the retarded and advanced functions are defined by

$$k^{R/A}(t,t') \;\equiv\; \delta(t,t')\,k^{\delta}(t) \;\pm\; \theta(\pm[t-t'])\;\left[k^{>}(t,t') - k^{<}(t,t')\right]\,. \tag{3.40}$$

The retarded function $k^R(t,t')$ vanishes for $t < t'$, while the advanced function $k^A(t,t')$ vanishes for $t > t'$. We introduce them mostly for notational convenience, though they could also be used to calculate the response at time t for an earlier perturbation of the system at t' [10].

Of particular interest is the decomposition of the function

$$c(t,t') \;=\; \int_{\mathcal{C}} d\bar{t}\,a(t,\bar{t})\,b(\bar{t},t') \tag{3.41}$$

in its different parts. The evaluation proceeds straightforwardly, either by expansion of $a(t,\bar{t})$ and $b(\bar{t},t')$ according to (3.32) or by matrix multiplication using the structure shown above, and shall not be carried out explicitly. Instead we refer to [17] or [18] and only present the results in Tab. 3.2, that are known as Langreth rules. To write them in a compact way, we further introduce the

	$c(z,z') = \int_{\mathcal{C}} d\bar{t}\, a(t,\bar{t})\, b(\bar{t},t')$	$c(z,z') = a(t,t')\, b(t',t)$
$c^{>}(t,t')$	$a^{>} \circ b^{A} + a^{R} \circ b^{>} + a^{\rceil} \star b^{\lceil}$	$a^{>}\, b^{<}$
$c^{<}(t,t')$	$a^{<} \circ b^{A} + a^{R} \circ b^{<} + a^{\rceil} \star b^{\lceil}$	$a^{<}\, b^{>}$
$c^{\rceil}(\tau,t)$	$a^{R} \circ b^{\rceil} + a^{\rceil} \star b^{M}$	$a^{\rceil}\, b^{\lceil}$
$c^{\lceil}(t,\tau)$	$a^{\lceil} \circ b^{A} + a^{M} \star b^{\lceil}$	$a^{\lceil}\, b^{\rceil}$
$c^{M}(\tau,\tau')$	$a^{M} \star b^{M}$	$a^{M}\, b^{M}$
$c^{R}(t,t')$	$a^{R} \circ b^{R}$	$a^{R}\, b^{\gtrless} + a^{\gtrless}\, b^{A}$
$c^{A}(t,t')$	$a^{A} \circ b^{A}$	$a^{A}\, b^{\gtrless} + a^{\gtrless}\, b^{R}$

Table 3.1.: *Langreth rules for the determination of the contour parts of integral and product of two Keldysh functions. The latter one is needed for the determination of the polarization in the GW approximation.*

following short-hand notation

$$\big[\, a \circ b \,\big](t,t') \;\equiv\; \int_{t_0}^{\infty} d\bar{t}\; a(t,\bar{t})\, b(\bar{t},t') \tag{3.42}$$

$$\big[\, a \star b \,\big](t,t') \;\equiv\; -i \int_{t_0}^{t_0 - i\beta} d\bar{\tau}\; a(t,\bar{\tau})\, b(\bar{\tau},t') \tag{3.43}$$

The Langreth rules are crucial for the derivation of the equations of motion of the subordinated functions in the next section.

3.3. The Keldysh/Kadanoff-Baym equations

The Keldysh/Kadanoff-Baym equations are the equations of motion for the nonequilibrium Green function on the Keldysh-contour. The starting point for their derivation is the Heisenberg equation for the field operators

$$\begin{aligned} i\,\partial_t\, \Psi(1) \;&=\; \Big[\Psi(1), \hat{H}(t)\Big] \\ &=\; h(1)\,\Psi(1) \,+\, \int d2\; \Psi^{\dagger}(2)\; w(1,2)\; \Psi(2)\Psi(1)\,, \qquad (3.44) \\ i\,\partial_t\, \Psi^{\dagger}(1) \;&=\; \Big[\Psi^{\dagger}(1), \hat{H}(t)\Big] \qquad (3.45) \\ &=\; -h(1)\,\Psi^{\dagger}(1) \,-\, \int d2\; \Psi^{\dagger}(2)\; w(1,2)\; \Psi(2)\Psi^{\dagger}(1)\,. \qquad (3.46) \end{aligned}$$

The second equalities are obtained after the insertion of (3.12) and the evaluation of the arising commutators. Why don't we solve these equations but go on to the Green functions, whose definition is that more involved? Well, even though these equations appear to be very simple in their mean-field structure, they are not feasible - one has to remember that they contain the whole many-body problem. Thus we have to rely on averaged quantities, for which the three-operator product on the right-hand side can be approximated. However, the expectation value of a field operator is normally zero, as states corresponding to different particle numbers in Fock space

are orthogonal.[8] Following the strategy of averaging, the one-body Green function is the first non-vanishing expectation value of a product of field operators.
To derive the equation of motion for the Green function, we multiply (3.44) by $\Psi^\dagger(2)$ and (3.45) by $\Psi(2)$, apply the time-ordering operator to both equations and evaluate the ensemble average. The interchange of the differential operator and the time-ordering operator thereby produces an additional contour delta function [8]. This results in the Keldysh/Kadanoff-Baym equations (KKBE), that were derived by Leo Kadanoff and Gordon Baym and independently by Leonid Keldysh.[9]

$$\{i\,\partial_{t_1} - h(1)\}\; G(1,2) \;=\; \delta_{\mathcal{C}}(1-2) \pm i \int_{\mathcal{C}} d3\; W(1-3)\; G_{12}(13,23^+)\,, \tag{3.47}$$

$$\{-i\,\partial_{t_2} - h(2)\}\; G(1,2) \;=\; \delta_{\mathcal{C}}(1-2) \pm i \int_{\mathcal{C}} d3\; W(2-3)\; G_{12}(13,23^+)\,. \tag{3.48}$$

They appear as a coupled pair of adjoint first order integro-differential equations, that have to be solved simultaneously to satisfy the symmetry condition (3.65). The two-particle Green function under the (collision) integrals on the right hand sides indicates a general structure in many-body physics, for instance also found in BBGKY theory for the solution of the Liouville equation, namely that the equations are not closed, but only mark the first terms in the so-called Martin-Schwinger hierarchy. The full solution at last would involve the N-body Green function and again correspond to a solution of the full many-body problem. Thus the hierarchy has to be truncated at a certain stage, where an approximate Green function must be inserted. However, in this work we follow the common approach and decouple the hierarchy at the first level by introducing the self-energy Σ:

$$\pm i \int_{\mathcal{C}} d3\; W(1-3)\; G_{12}(13,23^+) \;:=\; \int_{\mathcal{C}} d3\; \Sigma[G](1,3)\; G(3,2)\,. \tag{3.49}$$

Through this definition, the N-particle problem has been mapped on an effective single-particle potential, that is a functional of the one-body Green function. The fundamental problem of course is thereby only displaced, and in the next chapter we will focus on the common approximations to the self energy. The KKBE then transform to [10]

$$\{i\,\partial_{t_1} - h(1)\}\; G(1,2) \;=\; \delta_{\mathcal{C}}(1-2) \;+\; \int_{\mathcal{C}} d3\; \Sigma[G](1,3)\; G(3,2)\,, \tag{3.50}$$

$$\{-i\,\partial_{t_2} - h(2)\}\; G(1,2) \;=\; \delta_{\mathcal{C}}(1-2) \;+\; \int_{\mathcal{C}} d3\; G(1,3)\; \Sigma[G](3,2)\,. \tag{3.51}$$

It is possible to write down a formal solution of these equations [16],

$$\begin{aligned} G^{\gtrless}(1,2) \;=\; & \int d\mathbf{x}_3\, d\mathbf{x}_4\; G^R(1,x_3t_1)\, G^{\gtrless}(x_3,x_4;t_0)\, G^R(x_4t_0,2) \;+ \\ & \int_{t_0}^{\infty} d3 \int_{t_0}^{\infty} d4\; G^R(1,3)\, \Sigma^{\gtrless}(3,4)\, G^A(4,2)\,, \end{aligned} \tag{3.52}$$

[8] Yet for special systems, e.g. Bose-Einstein condensates, there exist approximations, where the addition/removal of one particle nearly leads to the same state.

[9] Kadanoff and Baym derived their equations for the correlation functions $G^{\gtrless}$, while Keldysh considered the equivalent formulation in terms of the function $G_K = G^> + G^<$ [10].

[10] More precisely, in the second equation one should introduce the adjoint self-energy. However, it can be shown, that Σ is hermitian. In [9] this is done for initial equilibrium correlations, and with somewhat harder analysis in [19] for arbitrary initial correlations. In the latter work also the question of existence of a suitable self-energy term is faced.

where for the moment we disregarded the influence of initial correlations.[11] Neglecting the second integral term yields a scheme for the approximate solution of the KKBE, that is known as the "generalized Kadanoff-Baym ansatz". Thereby it is sufficient to evolve G^R and G^A only in a single time component, what saves a lot of complexity. The numerical algorithm presented in chapter 9 however solves the full KKBE (what corresponds to a determination of the G^R and G^A as well as Σ in (3.52)).

3.3.1. Basis representation

The equations (3.50) and (3.51) are very hard to treat numerically. For example, for a three-dimensional spin-polarized system the Green function is an eight-dimensional quantity, that even for small numbers of gridpoints exceeds the memory capacities of most computers. Besides, if we consider the difficulties in the solution of the three-dimensional single-particle Schrödinger equation, the attack seems hopeless. A way around this difficulty is to expand all quantities in an arbitrary orthonormal single-particle basis $\{\varphi_k\}$, that should be as complete as possible.[12]

$$G(1,2) \;=\; \sum_{ij} G_{ij}(t_1,t_2)\;\varphi_i(\mathbf{x}_1)\,\varphi_j^*(\mathbf{x}_2)\,, \tag{3.53}$$

$$\Sigma(1,2) \;=\; \sum_{ij} \Sigma_{ij}(t_1,t_2)\;\varphi_i(\mathbf{x}_1)\,\varphi_j^*(\mathbf{x}_2)\,. \tag{3.54}$$

After insertion of this expansion into (3.50) and (3.51) and spatial integration, the KKBE transform to the following matrix equations

$$\{i\,\partial_{t_1} - \mathbf{h}(t_1)\}\;\mathbf{G}(t_1,t_2) \;=\; \delta_C(t_1-t_2) \;+\; \int_{\mathcal{C}} d3\;\mathbf{\Sigma}(t_1,t_3)\;\mathbf{G}(t_3,t_2)\,, \tag{3.55}$$

$$\{-i\,\partial_{t_2} - \mathbf{h}(t_2)\}\;\mathbf{G}(t_1,t_2) \;=\; \delta_C(t_1-t_2) \;+\; \int_{\mathcal{C}} d3\;\mathbf{G}(t_1,t_3)\;\mathbf{\Sigma}(t_3,t_2)\,. \tag{3.56}$$

From here, the KKBE for the subordinated quantities are easily derived via the Langreth rules, Fig. 3.2. Using the same short-hand notation we obtain the (horrible) set of equations we are

[11] The reference considers the Green function only on the real time axis. However, a respective term that incorporates the complex part is probably easily derived.

[12] This will turn out to be not the universal approach as it seems. It is actually even harder to reach completeness in basis representation than in coordinate space. Here a general physical principle holds: "the complexity of the full problem is conserved". The basis representation thus only marks a suitable way to characterize the equilibrium state, while the excited states are often not adequately described. However, it is still the only feasible method.

going to attack numerically in chapter 9.

$$\Big\{i\,\partial_{t_1} - \mathbf{h}(t_1)\Big\}\,\mathbf{G}^{\gtrless}(t_1,t_2) \;=\; \Big[\,\mathbf{\Sigma}^{R}\circ\mathbf{G}^{\gtrless} + \mathbf{\Sigma}^{\gtrless}\circ\mathbf{G}^{A} + \mathbf{\Sigma}^{\rceil}\star\mathbf{G}^{\lceil}\,\Big](t_1,t_2) \;=\; \mathbf{I}_1^{\gtrless}(t_1,t_2)\,, \tag{3.57}$$

$$\mathbf{G}^{\gtrless}(t_1,t_2)\,\Big\{-i\,\partial_{t_2} - \mathbf{h}(t_2)\Big\} \;=\; \Big[\,\mathbf{G}^{R}\circ\mathbf{\Sigma}^{\gtrless} + \mathbf{G}^{\gtrless}\circ\mathbf{\Sigma}^{A} + \mathbf{G}^{\rceil}\star\mathbf{\Sigma}^{\lceil}\,\Big](t_1,t_2) \;=\; \mathbf{I}_2^{\gtrless}(t_1,t_2)\,, \tag{3.58}$$

$$\Big\{i\,\partial_{t_1} - \mathbf{h}(t_1)\Big\}\,\mathbf{G}^{\rceil}(t_1,t_2) \;=\; \Big[\,\mathbf{\Sigma}^{R}\circ\mathbf{G}^{\rceil} + \mathbf{\Sigma}^{\rceil}\star\mathbf{G}^{M}\,\Big](t_1,t_2) \;=\; \mathbf{I}^{\rceil}(t_1,t_2)\,, \tag{3.59}$$

$$\mathbf{G}^{\lceil}(t_1,t_2)\,\Big\{-i\,\partial_{t_2} - \mathbf{h}(t_2)\Big\} \;=\; \Big[\,\mathbf{G}^{\lceil}\circ\mathbf{\Sigma}^{A} + \mathbf{G}^{M}\star\mathbf{\Sigma}^{\lceil}\,\Big](t_1,t_2) \;=\; \mathbf{I}^{\lceil}(t_1,t_2)\,, \tag{3.60}$$

$$\Big\{-\partial_{\tau_1} - \mathbf{h}(t_0)\Big\}\,\mathbf{G}^{M}(\tau_1,\tau_2) \;=\; i\delta(\tau_1-\tau_2) + \Big[\,\mathbf{\Sigma}^{M}\star\mathbf{G}^{M}\,\Big](\tau_1,\tau_2) \;=\; \mathbf{I}^{M}(\tau_1,\tau_2)\,, \tag{3.61}$$

$$\mathbf{G}^{M}(\tau_1,\tau_2)\,\Big\{\partial_{\tau_2} - \mathbf{h}(t_0)\Big\} \;=\; i\delta(\tau_1-\tau_2) + \Big[\,\mathbf{\Sigma}^{M}\star\mathbf{G}^{M}\,\Big](\tau_1,\tau_2) \;=\; \mathbf{I}^{M}(\tau_1,\tau_2)\,. \tag{3.62}$$

As any (integro-)differential equation, the KKBE must be supplied with initial and/or boundary conditions. In our case, we have a boundary condition on the imaginary branch, where the solution is found self-consistently, and initial conditions for the nonequilibrium Green functions, that are propagated in real time. The boundary condition, called Kubo-Martin-Schwinger condition, is easily derived from (3.30) by means of the cyclic invariance of the trace.

$$G(x_1\,t_0,2) \;=\; \pm G(x_1\,t_0 - i\beta,2)\,, \tag{3.63}$$

$$G(1,x_2\,t_0) \;=\; \pm G(1,x_2\,t_0 - i\beta)\,. \tag{3.64}$$

Furthermore, directly from the definition we obtain the boundary condition on the time-diagonal $G^{>}(\mathbf{x}_1 t,\mathbf{x}_2 t) = G^{<}(\mathbf{x}_1 t,\mathbf{x}_2 t) - i\delta(\mathbf{x}_1-\mathbf{x}_2)$ as well as the important symmetry

$$G^{\gtrless}(1,2) = -[G^{\gtrless}(2,1)]^{\dagger}\,, \tag{3.65}$$

which later will save us a lot of work. The initial conditions to the Eqs. (3.57-3.60) can in principle be chosen arbitrarily. Within this work we chose to propagate the equilibrium solution from the Dyson equation, though more general initial correlations can be supposed, see Ref. [19].

3.3.2. Equilibrium Dyson equation

The equations (3.61) and (3.62), which determine the finite temperature Matsubara Green function $G^{M}(1,2)$, are usually referred to as the Dyson equations. However, it is inconvenient to consider them in this particular form. Instead, we can take advantage of the fact that the imaginary branch Keldysh functions $G^{M}(1,2)$ and $\Sigma^{M}(1,2)$ only depend on the difference between their time-arguments $-i\tau_1$ and $-i\tau_2$. We therefore define real functions according to

$$G_{ij}^{M}(\tau_1-\tau_2) \;:=\; -i\,G_{ij}^{M}(-i\tau_1,-i\tau_2) \tag{3.66}$$

$$\Sigma_{ij}^{M}(\tau_1-\tau_2) \;:=\; -i\,\Sigma_{ij}^{M}(-i\tau_1,-i\tau_2) \tag{3.67}$$

where without loss of generality we have assumed $t_0 = 0$. Further we define the relative time $\tau := \tau_1 - \tau_2$, and after addition of (3.61) and (3.62) and the use of the anti-periodicity condition

(3.63), we obtain the usual Dyson equation in its differential form

$$\left\{-\partial_\tau - \mathbf{h}^0\right\} \mathbf{G}^M(\tau) \;=\; \delta(\tau) \;+\; \int_0^\beta d\bar{\tau}\; \mathbf{\Sigma}^M(\tau - \bar{\tau})\, \mathbf{G}^M(\bar{\tau})\,. \tag{3.68}$$

To encounter the respective integral form, we expose the origin of the Green function's denotation and the relationship to its relatives known from classical physics. Therefore let $\mathbf{G}^0$ be the solution of the undisturbed Dyson equation

$$\left\{-\partial_\tau - \mathbf{h}^0\right\} \mathbf{G}^0(\tau) \;=\; \delta(\tau) \tag{3.69}$$

Then by insertion one easily proves, that

$$\mathbf{G}^M(\tau) \;=\; \mathbf{G}^0(\tau) \;+\; \int_0^\beta d\tau_1 \int_0^\beta d\tau_2\; \mathbf{G}^0(\tau - \tau_1)\, \mathbf{\Sigma}^M(\tau_1 - \tau_2)\, \mathbf{G}^M(\tau_2) \tag{3.70}$$

is a solution to (3.68), and at the same time it is the convenient form for the numerical treatment in chapter 8. However, there we don't start from the undisturbed but from the Hartree-Fock Green function, whose equation of motion is similar to (3.69) but also incorporates the Hartree-Fock self-energy, $\mathbf{h}^0 \to \mathbf{h}^0 + \mathbf{\Sigma}^0$.

4. Conserving approximations for the self-energy

The decoupling of the Martin-Schwinger hierarchy (3.47,3.48) is a crucial step in the previous chapter and in addition an exact one. It maps the whole many-body problem onto a single-particle quantity, the self-energy, which includes all the interaction as well as the memory of the system in a non-local external potential. The question that immediately arises is how to find the right self-energy, and the a priori answer comes equally fast: The right – meaning the exact – self-energy is unobtainable, as this would amount to an exact solution of the many-body problem.[1] However, the great advantage of the NEGF-formalism is that we know how it could be reached in principle, namely through the perturbation expansion of the Green function. The exact solution is obtained by taking all perturbation terms into account, while the way to derive approximations is to neglect certain – almost all – of these expansion terms, that are visualized by means of Feynman diagrams, and translate the remaining into a self-energy expression.
The thus achieved approximation of course has to be physically reasonable, which means that it has to fulfill the fundamental conservation laws, such as particle- or energy conservation or the continuity equation

$$\frac{\partial n(\mathbf{r})}{\partial t} + \operatorname{div} \mathbf{j}(\mathbf{r}, t) \;=\; 0 \; . \tag{4.1}$$

Baym showed in 1962 [20], that only so called Φ-derivable self-energies lead to conserving approximations. Φ is a generating functional, that yields the self-energy by a functional derivative with respect to the Green function

$$\Sigma[G] \;=\; \frac{\delta \Phi[G]}{\delta G} \, . \tag{4.2}$$

In this mainly numerical work we skip the proof of the previous statement as well as the derivation of a self-consistent scheme to derive these conserving approximations and refer to the original literature and the fine review [21]. Instead, we focus on the three most common approximations and motivate them through their diagrammatic representation. These are the Hartree-Fock, the second Born and the GW approximation. Other more sophisticated approximations such as the T-matrix or vertex corrections to GW anyway are numerically not yet feasible within our approach.

[1] Even for few-particle systems, for that the Schrödinger equation is exactly solvable - see chapter 7 - one cannot manage to determine the exact self-energy perturbatively.

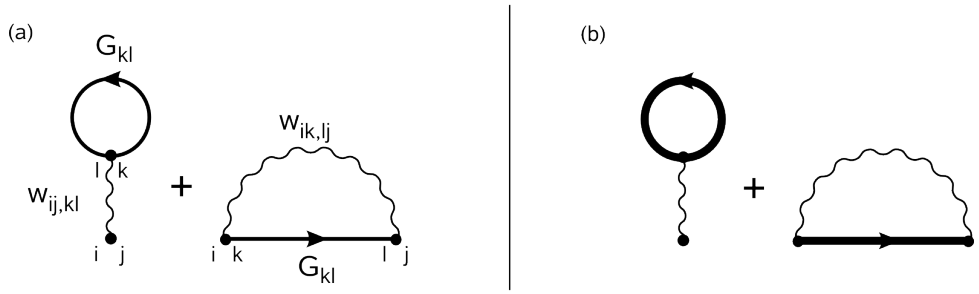

Figure 4.1.: *(a) The Hartree (left) and exchange term in diagrammatic representation, from which the analytical self-energy expression can be easily determined. (b) Full and consistent Hartree-Fock approximation that treats the background as fully interacting. The thick lines stand for the exact Green function.*

4.1. Hartree-Fock

The Hartree-Fock approximation is the first and easiest correction to the noninteracting Green function. It incorporates the two first-order diagrams in the perturbation expansion that account for the mean-field interaction, i.e. each particle is assumed to move in a one-body potential generated by the average interaction with all the other particles. In Fig. 4.1, the corresponding (single-particle) diagrams are shown, and the analytical expression can be readily identified:

$$\Sigma^{HF}_{ij}(t,t') \;=\; \sum_{kl} \left(\sigma\, w_{ij,kl} \pm w_{ik,lj} \right) G_{kl}(t,t^+)\,. \tag{4.3}$$

As throughout in this work, the upper sign corresponds to bosons and the lower one to fermions, and σ is the factor arising from the spin-summation explained below, $\sigma = 1$ for spin-polarized and $\sigma = 2$ for spin-restricted calculations. Note that in the Hartree diagram the delta-function is produced by the closed fermion loop, whose two vertices are identical and thus are situated at the same time. However, by convention the vertex (l) to that the Green function is pointing is situated at an infinitesimally later time, hence the GF agrees with the density matrix. This also holds for the exchange diagram, whose two vertices due to the interaction line are also at the same time. The interaction part of the Fock matrix, that we will encounter in chapter 6, has exactly the same structure as the Hartree-Fock self-energy.

A very ostensive derivation can also be given by the equivalent perturbation expansion of the two-particle Green function, which at first order is approximated as a product of two one-particle GFs [8]

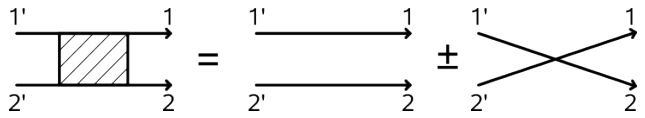

$$G_{12}(12,1'2') \;=\; G(1,1')\,G(2,2') \,\pm\, G(1,2')\,G(2,1')\,. \tag{4.4}$$

This terminates the Martin-Schwinger hierarchy at the first stage and yields closed equations (3.47) and (3.48) for the one-particle Green function.

We close with a remark we will return to in the next section: Actually the Hartree-Fock approximation is inconsistent – just like any other finite expansion – as it treats the background as noninteracting [11]. Yet the full Hartree-Fock self-energy in a consistent way is given in Fig. 4.1 (b), where the reference Green functions are replaced by the fully interacting Green functions.

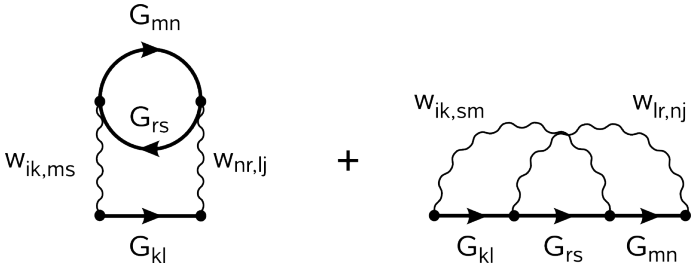

Figure 4.2.: *The diagrams taken into account by the second Born approximation. These are only two of the six proper second order diagrams, since the other four are already incorporated in Fig. 4.1 (b). As they only describe a change in the background, they are neglected.*

Spin-summation

By means of the computation of the Hartree-Fock self-energy, we give an example how the future spin-summation factors are obtained. The assumption here is that there occurs no interaction with the particle spin, except for the intrinsic Pauli exclusion. The interaction matrix elements (3.5) then become diagonal in the spin-product space

$$w_{ij,kl}^{\alpha\beta,\gamma\delta} \;=\; \delta_{\alpha\beta}\,\delta_{\gamma\delta}\;w_{ij,kl}\,, \tag{4.5}$$

and for the self-energy (4.3) we achieve (time variables are suppressed for simplicity)

$$\Sigma_{ij}^{\alpha\beta} \;=\; \sum_{kl}\sum_{\gamma\delta}\Big[\,\delta_{\alpha\beta}\,\delta_{\gamma\delta}\,w_{ij,kl} \;\pm\; \delta_{\alpha\gamma}\,\delta_{\beta\delta}\,w_{ik,lj}\,\Big]\,G_{kl}^{\gamma\delta} \tag{4.6}$$

$$\;=\; \sum_{kl} w_{ij,kl}\Big[\sum_{\gamma} G_{kl}^{\gamma\gamma}\,\Big] \;\pm\, w_{ik,lj}\,G_{kl}^{\alpha\beta}\,. \tag{4.7}$$

A spin-restricted treatment now implies $G_{ij}^{\uparrow\uparrow} = G_{ij}^{\downarrow\downarrow}$, and for a spin-independent external potential we have $G_{ij}^{\alpha\beta} \;=\; \delta_{\alpha\beta}\,G_{ij}$ (a particle can not change its spin-projection). Thus spin-restricted systems can be described by a Green function of only one particle – and therefore in the same way as in the spin-polarized case – if direct interaction terms and macroscopic observables are furnished by a factor of two.

4.2. Second Born approximation

With similar arguments than in the Hartree-Fock case, one can also derive the second Born approximation. At first we have the diagrammatic representation shown in Fig. 4.2, that consists of two of the ten second order Feynman diagrams. Why only two and why these ? Well, from the other eight second order diagrams the four improper[2] cancel with respect to the linked cluster theorem [11]. The remaining four diagrams are of the Hartree-Fock type, i.e. they are incorporated in Fig. 4.1 (b), and thus may be neglected, as they only describe a change in the background mean-field and not a direct interaction with the considered Green function. From the two selected

[2] An improper diagram decays in two separated diagrams if a Green function line is removed. A proper diagram does not.

second Born diagrams we can directly obtain the corresponding analytical expression

$$\Sigma_{ij}^{2ndBorn}(t,t') \;=\; \sum_{klmnrs} w_{ik,ms}(\sigma\; w_{rn,lj} \pm w_{rl,nj})\; G_{kl}(t,t')\; G_{mn}(t,t')\; G_{rs}(t',t)\,. \tag{4.8}$$

Note that because the interaction is local in time, in the exchange diagram the first and third vertex and the second and fourth vertex are each at the same time. Hence, if the first and third Green function are particle propagators, the intermediate is actually a hole propagator (and vice versa), what gives rise to interchanged time-indices.
We stop here. A further derivation in terms of the two-particle Green function is given in [8] and an analytical determination can be found in [9].

4.3. GW approximation

As seen before, the advantage of the NEGF formalism is that there exists a systematic perturbation expansion of the Green function, visualized by means of Feynman diagrams. However, it is already very hard to include third order diagrams in the explicit way above, and even if one could manage this, there is no need for them to converge.[3] So the best one can do is to sum up diagrams of one or a few special types to infinite order, what can also have a great impact on the convergence – an infinite set of diverging diagrams can be convergent [22]. One systematic approach to this strategy was given by Lars Hedin in a seminal paper [23] from 1965, where he invented an (in principle) exact self-consistent set of equations for the determination of the self-energy, the "Hedin equations"

$$\Sigma(1,2) \;=\; i\int_{\mathcal{C}} G(1,3)\; W(1^{+},4)\; \Gamma(32,4)\; d3\; d4 \tag{4.9}$$

$$W(1,2) \;=\; w(1,2) + \int_{\mathcal{C}} W(1,3)\; P(3,4)\; v(4,2)\; d3\; d4\,, \tag{4.10}$$

$$P(1,2) \;=\; -i\int_{\mathcal{C}} G(2,3)\; G(4,2)\; \Gamma(34,1)\; d3\; d4\,, \tag{4.11}$$

$$\Gamma(12,3) \;=\; \delta(1,2)\delta(1,3) + \int_{\mathcal{C}} \frac{\delta\Sigma(1,2)}{\delta G(4,5)}\; G(4,6)\; G(7,5)\; \Gamma(67,3)\; d4\; d5\; d6\; d7\,. \tag{4.12}$$

The idea behind this lines is to account for a screening of the interaction in the quasi-particle picture. For instance, electrons tend to generate positively charged (polarized) regions, called Coulomb holes, that weaken the interaction with the other electrons. In the equations, P is called the polarization, Γ the vertex function and the screened interaction W obeys the Bethe-Salpeter equation. As always, exact schemes can not be solved exactly, and approximations are derived in terms of Γ. The GW approximation is obtained by neglecting the integral in the equation for Γ and it reads explicitly

$$\Sigma(1,2) \;=\; i\; G(1,2)\; W(1,2)\,, \tag{4.13}$$

$$W(1,2) \;=\; w(1,2) \;+\; \int_{\mathcal{C}} d3\; d4\; W(1,3)\; P(3,4)\; w(4,2)\,, \tag{4.14}$$

$$P(1,2) \;=\; -i\;\sigma\; G(1,2)\; G(2,1)\,. \tag{4.15}$$

[3] However, for the regularized Coulomb interaction we are going to apply for 1D-systems, the convergence is guaranteed by the screening parameter.

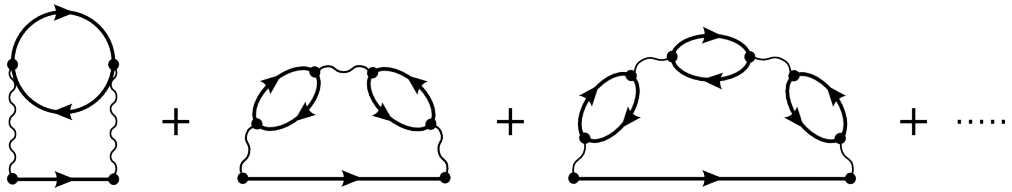

Figure 4.3.: *Diagrammatic representation of the GW-approximation.*

The polarization thereby is evaluated in the so called "Random Phase approximation" and models the propagation of a particle and a hole together through the system, see Fig. 4.4. This quasi-particle can have a much increased lifetime and on its way it can excite many other electron-hole pairs, what corresponds to iterations of the integral equation for W. The corresponding Feynman diagrams shown in Fig. 4.3 visualize this statement. For convenience, the eventual spin-factor σ has been absorbed in the polarization instead of writing it in the integral equation.

To treat the self energy in the same way as in the second Born case, i.e. divided in a singular Hartree-Fock part and a correlation part depending on two times, we define the non-singular part $\widetilde{W}$ of the screened interaction through

$$\widetilde{W}(1,2) \;=\; W(1,2) - w(1,2)\,. \tag{4.16}$$

Then we can write the correlation part of the self-energy as

$$\Sigma^{GW}(1,2) \;=\; i\; G(1,2)\; \widetilde{W}(1,2)\,, \tag{4.17}$$

while the integral equation for W transforms to

$$\widetilde{W}(1,2) \;=\; \int_{\mathcal{C}} d3\; d4\; w(1,3)\; P(3,4)\; w(4,2) \;+\; \int_{\mathcal{C}} d3\; d4\; \widetilde{W}(1,3)\; P(3,4)\; w(4,2)\,. \tag{4.18}$$

We are going to derive the basis representation of these equations.

4.3.1. Basis representation of the GW equations

We replace the Polarization function by its definition (4.15), expand each Green function according to (3.53) and use $v(4,2) = v(\mathbf{r}_4,\mathbf{r}_2)\delta(t_4 - t_2)$ to get

$$\begin{aligned}
&\widetilde{W}(\mathbf{r}_1 t_1, \mathbf{r}_2 t_2) \;= \\
&\int d\mathbf{r}_3 d\mathbf{r}_4\; \widetilde{W}(\mathbf{r}_1,\mathbf{r}_3)\; (-i) \sum_{ab} G_{ab}(t_3,t_4)\; \psi_a(\mathbf{r}_3)\psi_b^*(\mathbf{r}_4) \sum_{cd} G_{cd}(t_4,t_3)\; \psi_c(\mathbf{r}_4)\psi_d^*(\mathbf{r}_3)\; w(\mathbf{r}_4,\mathbf{r}_2) \;+ \\
&\int_{\mathcal{C}} dt_3 \int d\mathbf{r}_3 d\mathbf{r}_4 \widetilde{W}(\mathbf{r}_1 t_1, \mathbf{r}_3 t_3)(-i) \sum_{ab} G_{ab}(t_3,t_4)\psi_a(\mathbf{r}_3)\psi_b^*(\mathbf{r}_4) \sum_{cd} G_{cd}(t_4,t_3)\psi_c(\mathbf{r}_4)\psi_d^*(\mathbf{r}_3) w(\mathbf{r}_4,\mathbf{r}_2)\,.
\end{aligned} \tag{4.19}$$

Further we multiply by $\psi_i^*(\mathbf{r}_1)\psi_j(\mathbf{r}_1)\psi_k^*(\mathbf{r}_2)\psi_l(\mathbf{r}_2)$ and integrate over $\mathbf{r}_1$ and $\mathbf{r}_2$. For the left hand side similar to (3.5) we define

$$\widetilde{W}_{ij,kl}(t_1,t_2) \;:=\; \int\; d\mathbf{r}_1 d\mathbf{r}_2\; \psi_i^*(\mathbf{r}_1)\psi_j(\mathbf{r}_1)\; \widetilde{W}(\mathbf{r}_1 t_1, \mathbf{r}_2 t_2)\; \psi_k^*(\mathbf{r}_2)\psi_l(\mathbf{r}_2)\,, \tag{4.20}$$

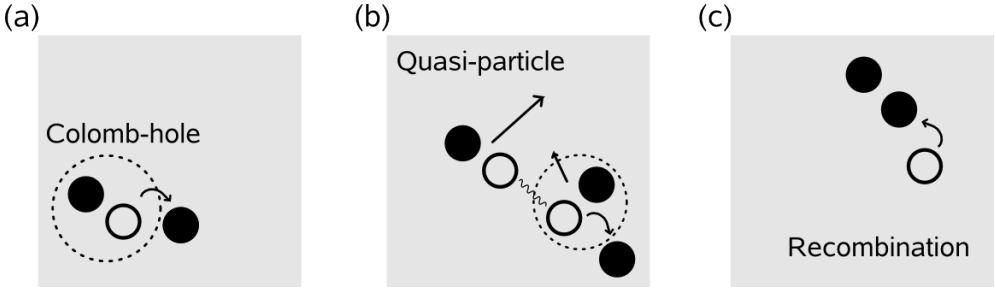

Figure 4.4.: *Sketch of the GW process [22]. (a) A particle polarizes the medium and forms a Coulomb-hole, that in GW is approximated by a particle-hole pair. (b) The quasi-particle propagates comparatively free through the system and probably excites some other particle-hole pairs. (c) After its lifetime the quasi-particle is destroyed by a recombination.*

while the second term on the right hand side becomes

$$\begin{aligned}
&\int d\mathbf{r}_1 d\mathbf{r}_2\ \psi_i^*(\mathbf{r}_1)\psi_j(\mathbf{r}_1)\ \psi_k^*(\mathbf{r}_2)\psi_l(\mathbf{r}_2) \int_{\mathcal{C}} dt_3 \int d\mathbf{r}_3 d\mathbf{r}_4\ \widetilde{W}(\mathbf{r}_1 t_1, \mathbf{r}_3 t_3) \\
&\qquad \cdot (-i) \sum_{ab} G_{ab}(t_3, t_2)\ \psi_a(\mathbf{r}_3)\psi_b^*(\mathbf{r}_4) \sum_{cd} G_{cd}(t_2, t_3)\ \psi_c(\mathbf{r}_4)\psi_d^*(\mathbf{r}_3)\ w(\mathbf{r}_4, \mathbf{r}_2) \\
&= \int_{\mathcal{C}} dt_3 \int d\mathbf{r}_1 d\mathbf{r}_3\ \psi_i^*(\mathbf{r}_1)\psi_j(\mathbf{r}_1)\ \widetilde{W}(\mathbf{r}_1 t_1, \mathbf{r}_3 t_3)\ \psi_d^*(\mathbf{r}_3)\psi_a(\mathbf{r}_3) \\
&\qquad \cdot (-i) \sum_{ab} G_{ab}(t_3, t_2)\ \sum_{cd} G_{cd}(t_2, t_3)\ \int d\mathbf{r}_2 d\mathbf{r}_4\ \psi_b^*(\mathbf{r}_4)\psi_c(\mathbf{r}_4)\ w(\mathbf{r}_4, \mathbf{r}_2)\ \psi_k^*(\mathbf{r}_2)\psi_l(\mathbf{r}_2) \\
&= \sum_{abcd} \int_{\mathcal{C}} dt_3\ \widetilde{W}_{ij,da}(t_1, t_3)\ (-i)\ G_{ab}(t_3, t_2) G_{cd}(t_2, t_3)\ w_{bc,kl} \\
&= \sum_{abcd} \int_{\mathcal{C}} dt_3\ \widetilde{W}_{ij,da}(t_1, t_3)\ P_{ab,cd}(t_3, t_2)\ w_{bc,kl}\,. \qquad (4.21)
\end{aligned}$$

After treating the first term on the right hand side in the same way, we obtain the basis representation of the integral equation for the non-singular part of the screened interaction

$$\widetilde{W}_{ij,kl}(t_1, t_2)\ -\ \sum_{abcd} \int_{\mathcal{C}} dt_3\ \widetilde{W}_{ij,da}(t_1, t_3)\ P_{ab,cd}(t_3, t_2)\ w_{bc,kl}\ =\ \sum_{abcd} w_{ij,da}\ P_{ab,cd}(t_1, t_2)\ w_{bc,kl}\,. \qquad (4.22)$$

Similarly, from (4.13) the GW self-energy evaluates to

$$\Sigma_{ij}^{GW}(t_1, t_2)\ =\ i \sum_{kl} G_{kl}(t_1, t_2)\ \widetilde{W}_{ik,lj}(t_1, t_2)\,. \qquad (4.23)$$

4.3.2. Equilibrium GW equations

We derive the Matsubara part of the equations given above, what implies that both time arguments are situated on the imaginary part $[t_0, t_0 - i\beta]$ of the Keldysh-Contour $\mathcal{C}$ and that the integration over the whole contour is restricted to this branch. By defining $\tau_k := i\, t_k$ and assuming

$t_0 = 0$ without loss of generality, we can rewrite equation (4.22):

$$\widetilde{W}_{ij,kl}(-i\tau_1, -i\tau_2) \; - \; \sum_{abcd} \int_0^\beta (-i)\, d\tau_3 \; \widetilde{W}_{ij,da}(-i\tau_1, -i\tau_3) \; P_{ab,cd}(-i\tau_3, -i\tau_2) \; w_{bc,kl} \\ = \; \sum_{abcd} w_{ij,da} \; P_{ab,cd}(-i\tau_1, -i\tau_2) \; w_{bc,kl} \, . \quad (4.24)$$

Further we introduce

$$\widetilde{W}^M_{ij,kl}(\tau_1 - \tau_2) \; := \; -i \, W_{ij,kl}(-i\tau_1, -i\tau_2) \quad (4.25)$$

$$P^M_{ij,kl}(\tau_1 - \tau_2) \; := \; -i \, P_{ij,kl}(-i\tau_1, -i\tau_2) \quad (4.26)$$

and the new variable $\tau := \tau_1 - \tau_2$, $\tau \in [-\beta, 0]$, to obtain

$$\begin{aligned} \widetilde{W}^M_{ij,kl}(\tau) \; &= \; \sum_{abcd} \int_0^\beta d\tau_3 \; \widetilde{W}^M_{ij,da}(\tau_1 - \tau_3) \; P^M_{ab,cd}(\tau_3 - \tau_2) \; w_{bc,kl} + \; \sum_{abcd} w_{ij,da} \; P^M_{ab,cd}(\tau) \; w_{bc,kl} \\ &= \; \sum_{abcd} \int_0^\beta d\tau_3 \; \widetilde{W}^M_{ij,da}(\tau_1 - \tau_3) \; P^M_{ab,cd}(\tau - (\tau_1 - \tau_3)) \; w_{bc,kl} + \; \sum_{abcd} w_{ij,da} \; P^M_{ab,cd}(\tau) \; w_{bc,kl} \, . \end{aligned}$$

Now we simply set $\tau_1 = 0$ (what is allowed since due to the (anti-)periodicity conditions any interval of length β contains the same information), introduce $\bar{\tau} = -\tau_3$ and interchange the boundaries to achieve the formula we are going to attack numerically in chapter 8:

$$\widetilde{W}^M_{ij,kl}(\tau) \; - \; \sum_{abcd} \int_{-\beta}^0 d\bar{\tau} \; \widetilde{W}^M_{ij,da}(\bar{\tau}) \; P^M_{ab,cd}(\tau - \bar{\tau}) \; w_{bc,kl} \; = \; \sum_{abcd} w_{ij,ad} \; P^M_{ab,cd}(\tau) \; w_{bc,kl} \, . \quad (4.27)$$

Finally, the polarization and the equilibrium self-energy evaluate to

$$P^M_{ij,kl}(\tau) \; = \; -\sigma \, G^M_{ij}(\tau) \, G^M_{kl}(\beta - \tau) \, , \quad (4.28)$$

$$\Sigma^{GW,M}(\tau) \; = \; - \sum_{kl} G^M_{kl}(\tau) \, W^M_{ik,lj}(\tau) \, . \quad (4.29)$$

Part II.

Numerical Implementation

5. Solution of the one-particle Schrödinger equation

In order to work out the influence of electron-correlation effects on the photoionization and to compare the NEGF-approach with the conventional procedure, we need to solve the one-particle Schrödinger equation, an issue that has been too widely studied in the literature to give an adequate and at the same time concise overview. In the following we will mainly apply the ideas summarized in [24].

5.1. Stationary Schrödinger equation

The general way to attack the stationary Schrödinger equation (2.1) is to rewrite the operator equation in a matrix equation by expanding it in a suitable basis, and afterward apply standard eigenvalue solvers - a scheme we will meet repeatedly in the present work. In coordinate representation, on which we will focus in this chapter, the basis consists of spatial eigenfunctions, which are Dirac delta functions on some chosen gridpoints.
For a given confinement the numerical solution of the stationary Schrödinger equation determines the eigenenergies and eigenfunctions on these chosen gridpoints, that serve as a natural orthonormal basis of the single-particle Hilbert-space. In our approach this does not only yield the starting point for the Hartree-Fock formalism, but also a reasonable initial condition for the time-propagation.

5.1.1. One dimensional case

The stationary one-dimensional Schrödinger equation in spatial coordinates of course reads

$$\left\{ -\frac{1}{2}\frac{\partial^2}{\partial x^2} + V(x) \right\} \Psi(x) = \epsilon \, \Psi(x) \,, \tag{5.1}$$

and is supplemented with the boundary condition $\Psi(x) \xrightarrow{x\to\infty} 0$.
Many procedures have been proposed for the numerical solution of this equation.[1] Here we will use a straightforward finite-difference method, that despite its simplicity yields very accurate solutions. Furthermore it has the advantage to be very easily extendible to higher dimensions.

As in most finite-difference methods in coordinate space, one at first chooses an equidistant spatial grid, $x_i,\ i = 1, .., N_x$, with boundaries $x_1 = a$ and $x_{N_x} = b$ and interpoint distance $h_x = (b-a)/(N_x - 1)$. Any function of x, e.g. $\Psi(x)$, then becomes a vector on this grid, and

[1] Among them are the imaginary time stepping method, the shooting and relaxation method, the Numerov method, Fourier-transform methods, wavelet methods and many more. The method used here has been found superior to the first two methods mentioned.

we set $\Psi_i = \Psi(x_i)$. Further, the boundary conditions on $\Psi(x)$ change to $\Psi(a) = \Psi_1 = 0$ and $\Psi(b) = \Psi_{N_x} = 0$. To yield physical results, the position of the boundaries should be chosen appropriately.[2]

Then the idea is to simply express also the Hamilton operator as a matrix on this grid and to diagonalize this matrix. Since the confinement is diagonal in coordinate space, we only have to discretize the operator of the second derivative, for what the well known formula

$$\left.\frac{\partial^2\Psi(x)}{\partial x^2}\right|_{x=x_i} \approx \frac{\Psi_{i+1} - 2\Psi_i + \Psi_{i-1}}{h_x^2} \quad , \quad i = 2, .., N_x - 1\,, \tag{5.2}$$

could be used. It is also valid for the endpoints, if we neglect boundary corrections and set all quantities outside the grid equal to zero, $\Psi_i = 0$ if $i < 1$ or $i > N_x$.

But we can do better by taking into account not only one grid point next to the point where the second derivative is applied, but r outer points. Then we obtain the similar formula

$$\left.\frac{\partial^2\Psi(x)}{\partial x^2}\right|_{x=x_i} \approx \frac{1}{h_x^2}\sum_{k=-r}^{r} c_k^{(r)}\,\Psi_{i+k}\,. \tag{5.3}$$

s To determine the coefficients $c_j^{(r)}$, we make a Taylor expansion of $\Psi(x + kh_x)$ and $\Psi(x - kh_x)$ up to order $2r + 1$ and add them to achieve the linear system ($k = 1, .., r$)

$$2\frac{(kh_x)^2}{2!}\Psi^{(2)}(x) + 2\frac{(kh_x)^4}{4!}\Psi^{(4)}(x) + ... + 2\frac{(kh_x)^{2r}}{(2r)!}\Psi^{(2r)}(x) = \Psi(x + kh_x) - 2\Psi(x) + \Psi(x - kh_x)\,. \tag{5.4}$$

By solving this system for $\Psi^{(2)}(x)$,[3] we obtain the coefficients for a chosen order r, that satisfy $c_k^{(r)} = c_{-k}^{(r)}$ due to the symmetry of the second derivative.[4]

r	**k=0**	1	2	3	4
1	-2	1			
2	$-\frac{5}{2}$	$\frac{4}{3}$	$-\frac{1}{12}$		
3	$-\frac{49}{18}$	$\frac{3}{2}$	$-\frac{3}{20}$	$\frac{1}{90}$	
4	$-\frac{205}{72}$	$\frac{8}{5}$	$-\frac{1}{5}$	$\frac{8}{315}$	$-\frac{1}{560}$

Table 5.1.: *The coefficients $c_k^{(r)}$ for $r \leq 4$ arising from (5.4).*

After this discretization of the operator of the second derivative, we can set up the Hamiltonian

[2] There also exist Green function methods to map the infinite system onto the finite grid, but since they are only applicable in 1D, they have not been implemented.

[3] Due to the linearity we can solve the system for each inhomogeneity separately, i.e. for $c_0^{(r)}$ we set the inhomogeneity $(-2, -2, .., -2)$, for $c_1^{(r)}$ $(1, 0, 0, .., 0)$ and so on. This gives the prefactor of each term Ψ_{i+k}, $k = 1, .., r$, in the sum (5.3).

[4] We can apply the same procedure to get the coefficients of the first derivative involving s grid points. In this way, numerical derivatives are computed in the code, mostly by using $s = 3$ or 4.

on the spatial grid

$$\mathbf{H} = -\frac{1}{2h_x^2}\begin{pmatrix} c_0^{(r)}-2h_x^2V_1 & c_1^{(r)} & \cdots & c_r^{(r)} & 0 & \cdots & & 0 \\ c_1^{(r)} & c_0^{(r)}-2h_x^2V_2 & c_1^{(r)} & \cdots & c_r^{(r)} & 0 & \cdots & 0 \\ \vdots & & \ddots & & & & & \vdots \\ \vdots & & & & & \ddots & & \vdots \\ 0 & \cdots & 0 & c_r^{(r)} & c_{r-1}^{(r)} & \cdots & c_0^{(r)}-2h_x^2V_{N_x} & c_1^{(r)} \\ 0 & & \cdots & 0 & c_r^{(r)} & c_{r-1}^{(r)} & \cdots & c_0^{(r)}-2h_x^2V_{N_x} \end{pmatrix}. \tag{5.5}$$

Then this bandmatrix is diagonalized, for $r > 1$ by use of the *Lapack* routine *dsbevx* and for $r = 1$ by *dstegr*, to yield the desired number $N_b \leq N_x$ of basisfunctions and related energies.

To increase the accuracy of the thus obtained wavefunctions, a further integer parameter q is introduced and the matrix is diagonalized on a grid with $q \cdot N_x$ nodes instead of N_x, what artificially reduces the interpoint spacing. The wavefunction is then set up with each q-th point of the eigenvector. This is instructive since in view on subsequent applications one is intended to keep the gridpoint number low, while the diagonalization is fast to accomplish, at least for tridiagonal matrices (i.e. $r = 1$).

5.1.2. Two-dimensional case

As mentioned above the extension to the two dimensional case (and to any higher dimension) is straightforward. One now has two spatial grids $x_i,\ i = 1,..,N_x$ and $y_j,\ j = 1,..,N_y$ and any function $\Psi(x,y)$ becomes a quantity with two indices $\Psi_{i,j} = \Psi(x_i, y_j)$ that is conveniently stored in a vector of dimension N_xN_y. The second derivate is evaluated at r_x/r_y outer points in x / y direction and the Hamiltonian becomes a $N_y \times N_y$ bandmatrix of $N_x \times N_x$ matrices

$$\mathbf{H} = \begin{pmatrix} \mathbf{A}_1 & \mathbf{C}_1^{(r_y)} & \cdots & \mathbf{C}_{r_y}^{(r_y)} & \\ \mathbf{C}_1^{(r_y)} & \mathbf{A}_2 & \mathbf{C}_1^{(r_y)} & \cdots & \mathbf{C}_{r_y}^{(r_y)} \\ \vdots & & & \ddots & \vdots \\ & \mathbf{C}_{r_y}^{(r_y)} & \cdots & \mathbf{C}_1^{(r_y)} & \mathbf{A}_{N_y} \end{pmatrix}, \tag{5.6}$$

where $\mathbf{C}_i^{(r_y)} = -\frac{c_i^{(r_y)}}{2h_y^2}\ \mathbf{I}_{N_x}$ is proportional to the unit matrix and

$$\mathbf{A_i} = \begin{pmatrix} \left(-\frac{c_0^{(r_x)}}{2h_x^2}-\frac{c_0^{(r_y)}}{2h_y^2}+V_{1,i}\right) & -\frac{c_1^{(r_x)}}{2h_x^2} & \cdots & -\frac{c_{r_x}^{(r_x)}}{2h_x^2} \\ -\frac{c_1^{(r_x)}}{2h_x^2} & \left(-\frac{c_0^{(r_x)}}{2h_x^2}-\frac{c_0^{(r_y)}}{2h_y^2}+V_{2,i}\right) & -\frac{c_1^{(r_x)}}{2h_x^2} & \cdots \quad -\frac{c_{r_x}^{(r_x)}}{2h_x^2} \\ \vdots & & \ddots & \vdots \end{pmatrix} \tag{5.7}$$

is a bandmatrix with the same structure as found in the previous section.
Since $\mathbf{H}$ is a sparse matrix, the direct diagonalization methods for dense matrices provided by *Lapack* are applicable only for small values of N_x and N_y ($\lesssim 10^2$). Thus another library has to be used that solves sparse eigenvalue problems iteratively, and after a comparison of the available codes the *Anasazi*-solver from the *Trilinos*-package [25] has been found suitable for its good structure and high performance.

5.1.3. Radial Schrödinger equation

In three dimensional central potentials, the Hamiltonian commutes with the square of the angular momentum operator, $[H, L^2] = 0$, leading to the ansatz

$$\psi_{nlm}(\mathbf{r}) \;=\; \frac{u_{nl}(r)}{r}\; \mathrm{Y}_{lm}(\theta, \varphi)\,, \tag{5.8}$$

where Y_{lm} is the spherical harmonic. The function u_{nl} satisfies the radial Schrödinger equation [26]

$$\left\{-\frac{1}{2\mu}\frac{d^2}{dr^2} + \frac{l(l+1)}{2\mu r^2} + V(r)\right\}\; u_{nl}(r) \;=\; \epsilon_{nl}\; u_{nl}(r) \tag{5.9}$$

and the normalization condition $\int u_{nl}(r)\; dr = 1$. μ is the reduced mass, that for atoms is normally set to one.

This equation is solved with the same method as in the one dimensional case, the only difference is that because of the singularity at the origin a small cutoff parameter is introduced to avoid a division by zero. Therefore, if $r = 0$ it is replaced by $r \approx 10^{-20}$. Unfortunately, for some potentials, e.g. the Coulomb potential, the magnitude of the first eigenvalue is then of the order -10^{20} and has to be neglected. In the code this is done automatically. For a more economical solution, one could also use a logarithmic grid, as it is for instance introduced in [13].
The obtained solutions are ordered by the quantum numbers (n_r, l, m), where n_r is the radial quantum number. This is also the intrinsic order of a numeric solution of (5.9), as for a given radial quantum number l the k-th eigenvector has k nodes (except the one at the origin), and thus $n_r = k$.

5.2. Time-dependent Schrödinger equation

Having obtained the stationary solutions, we can ask how they do evolve in time under an external perturbation. The essential technique in solving the time-dependent Schrödinger equation is to approximate the formal time-evolution operator

$$U(t, t_0) \;=\; T\, \mathrm{e}^{-i\int_{t_0}^{t} H(t')dt'}\,, \tag{5.10}$$

by dividing the time-span $[\,t_0, t\,]$ in $(N_t - 1)$ segments with duration Δt and assuming $H(t)$ to be constant therein.

$$U(t_{k+1}, t_k) \;\approx\; \mathrm{e}^{-iH(t+\frac{\Delta t}{2})\Delta t}\,, \qquad U(t, t_0) \;=\; \prod_{k=2}^{N_t} U(t_k, t_{k-1})\,. \tag{5.11}$$

The main problem is then to evaluate this expression and apply it to an initial state.

5.2.1. Generalized Crank-Nicolson scheme

Given the finite difference Hamiltonian (5.5), to evaluate (5.11) we have to calculate the matrix exponential, which is also a well-studied task.[5] One approximative method is to expand the exponential in a Taylor series up to first order around $t + \frac{\Delta t}{2}$ and simply apply it on $\psi(t)$ using matrix multiplication. This yields an explicit scheme that is, however, not very stable [27]. By demanding the Cayley formula

$$\left\{1 + iH\Delta t/2\right\}\, \psi(t + \Delta t) \;=\; \left\{1 - iH\Delta t/2\right\}\, \psi(t)\,, \tag{5.12}$$

we achieve an implicit and stable scheme named after Crank and Nicolson with accuracy $O(\Delta t^2)$. Since the right-hand side is known, $\psi(t + \Delta t)$ is found by solving a linear system of equations.

The generalization of this scheme up to arbitrary order can be obtained by reinterpreting the Cayley evolution operator

$$U(t + \Delta t, t) \;=\; \frac{1 - iH\Delta t/2}{1 + iH\Delta t/2} \tag{5.13}$$

as the [1/1] Padé-approximation of the exponential function. The [M/N] Padé-approximation of a function $f(z)$ around z_0 is an expansion in a rational function with polynomial order M in the numerator and N in the denominator

$$R(z) \;=\; \frac{a_0 + a_1 z + \cdots + a_M z^M}{1 + b_1 z + \cdots + b_N z^N}\,, \tag{5.14}$$

satisfying

$$R(z_0) \;=\; f(z_0) \qquad \text{and} \qquad \left.\frac{dR(z)}{dz}\right|_{z=z_0} = \left.\frac{df(z)}{dz}\right|_{z=z_0}\,. \tag{5.15}$$

These conditions give rise to a linear system of equations for the coefficients a_i and b_i [27]. The idea is then to extend (5.13) to the [M/M] Padé-approximation of the exponential function and factorize the polynomials

$$e^z \;=\; \frac{a_0 + a_1 z + \cdots + a_M z^M}{1 + b_1 z + \cdots + b_M z^M} \;=\; \prod_{s=1}^{M} \frac{1 - z/z_s^{(M)}}{1 + z/\overline{z}_s^{(M)}}\,, \tag{5.16}$$

where the roots $z_s^{(M)}$ of numerator and denominator are found to be complex conjugate to each other [24]. Instead of solving the linear system (5.15), the Padé approximation for the exponential can be obtained by a formula involving the confluent hypergeometric function [28]

$${}_1F1(-M, -2M, z) \;\stackrel{!}{=}\; 0 \tag{5.17}$$

We solve this equation with respect to z, which yields the roots $z_k^{(M)}$.[6] The values of some low order coefficients are displayed in Tab. 5.2. If we then set $z = -iH\Delta t$ and define

[5] Among the available methods are matrix decomposition, polynomial and ordinary differential equation methods.

[6] In the code this is done with the polynomial-solver from the library *gsl*.

M	s=0	1	2	3
1	$-2.0000 + i\ 0.0000$			
2	$-3.0000 + i\ 1.7321$	$-3.0000 - i\ 1.7321$		
3	$-4.6444 + i\ 0.0000$	$-3.6778 - i\ 3.5088$	$-3.6778 + i\ 3.5088$	
4	$-4.2076 + i\ 5.3148$	$-5.7924 + i\ 1.7345$	$-5.7924 - i\ 1.7345$	$-4.2076 - i\ 5.3148$

Table 5.2.: *The first coefficients $z_s^{(M)}$ from the factorization of the Padé-expansion of the exponential function.*

$$K_s^{(M)}(t) \;=\; \frac{1 - \frac{iH(t)\Delta t}{z_s^{(M)}}}{1 + \frac{iH(t)\Delta t}{\overline{z}_s^{(M)}}}\,, \tag{5.18}$$

we can write

$$\mathrm{e}^{-iH(t+\frac{\Delta t}{2})\Delta t} \approx \prod_{s=0}^{M} K_s^{(M)}(t + \Delta t/2)\,, \tag{5.19}$$

and thus

$$\psi(t + \Delta t) \approx \prod_{s=0}^{M} K_s^{(M)}(t + \Delta t/2)\ \psi(t)\,. \tag{5.20}$$

Since the operators $K_s^{(M)}$ commute (if they are all evaluated at the same time $t + \Delta t/2$), we can divide Δt into M substeps

$$\psi\left(t + \frac{(m+1)}{M}\Delta t\right) \approx K_s^{(M)}(t + \Delta t/2)\ \psi\left(t + \frac{m}{M}\Delta t\right)\ , \qquad m = 0, \cdots, M-1\,, \tag{5.21}$$

and solve each of these M equations with the same procedure as in the conventional Crank-Nicolson scheme, i.e. by solving a linear system of equations. As the Hamiltonian (5.5) is used, plus a diagonal term arising from an external disturbance, the coefficient matrix $\mathbf{1} + i\mathbf{H}\Delta t/\overline{z}_s^{(M)}$ of this system is a complex bandmatrix. In the code the solution is found with the *Lapack*-routine *zgbsv*.

In conclusion, we have derived a propagation scheme that is accurate in the order $O(\Delta t^M)$, so that in principle a much larger stepsize Δt can be chosen – at least for stationary or slowly varying external perturbations. One has to be careful though for highly oscillating fields, because there a larger stepsize may not represent the characteristic exactly. A possible way to amend this shortcoming is to include gradient corrections, as it is done e.g. in the Magnus expansion [29], but that has not been implemented in the code.

5.2.2. Split-Operator method

Another time-evolution scheme, the Split-Operator method, has been implemented, mostly to confirm the solutions obtained from the Generalized Crank-Nicolson scheme just mentioned and to compare their performance. The idea here is to apply the kinetic part T of the Hamiltonian in Fourier space, where it is diagonal, and equally the potential part V in position space. Application then means simply to perform a scalar multiplication in each component of the wavefunction-

vector. Thus it is an explicit scheme in contrast to the implicit CN-scheme, where a linear system must be solved.

The splitting scheme accurate to second order reads explicitly

$$\mathrm{e}^{-iH\Delta t} \;=\; \mathrm{e}^{-i(T+V)\Delta t} \;\approx\; \mathrm{e}^{-iV\Delta t/2}\,\mathrm{e}^{-iT\Delta t}\,\mathrm{e}^{-iV\Delta t/2}\,. \tag{5.22}$$

Thereby, the commutators arising from the Baker-Campbell-Hausdorff formula are neglected.

The application of this approximated time-evolution operator is simple: Since the exponential of a diagonal matrix is easily obtained by exponentiating the diagonal entries, we just have to multiply each component of the wavevector $\psi_i(t)$ with $\mathrm{e}^{-iV_i\Delta t/2}$. The resulting vector is then transformed into momentum space by a fast Fourier transform with respect to spatial coordinates, where the kinetic part is applied in the same way as the potential part.[7] Then after a transformation back into coordinate space the potential part is applied once again to yield the propagated wavefunction $\psi(t+\Delta t)$.

Beside this, also also a fourth-order scheme has been implemented. The splitting of the time-evolution operator there is given by [30]

$$\mathrm{e}^{-i\,(T+V)\,\Delta t} \;\approx\; \mathrm{e}^{-i\,\tilde{V}\,\Delta t/8}\,\mathrm{e}^{-i\,T\,\Delta t/3}\,\mathrm{e}^{-i\,V\,3\Delta t/8}\,\mathrm{e}^{-i\,T\,\Delta t/3}\,\mathrm{e}^{-i\,V\,3\Delta t/8}\,\mathrm{e}^{-i\,T\,\Delta t/3}\,\mathrm{e}^{-i\,\tilde{V}\,\Delta t/8}\,, \tag{5.23}$$

where $\tilde{V}$ now incorporates some contributions from the commutators

$$\tilde{V} \;=\; V + \frac{\Delta t^2}{48}\,[V,[T,V]]\,. \tag{5.24}$$

A straight forward calculation further gives

$$[V,[T,V]] \;=\; \sum_{i=1}^{d} |\nabla_i\, v(\mathbf{r})|^2\,. \tag{5.25}$$

The sum goes up to the dimension d and in the one-dimensional case ∇ is replaced by ∂/∂_x. The application of this scheme requires 6 FFT's and should be superior to the second order splitting in most of the times. The practical extension to higher dimensions is even more simple than in the Generalized-CN method – all we have to do is to use a higher dimensional FFT as it is available in the *fftw*-library.

5.3. Application

Higher-order derivatives

We check the influence of the higher-order derivation formulas in the diagonalization of the matrix (5.5). The considered system is a one-dimensional harmonic oscillator that is discretized by a grid-spacing of $\Delta x = 0.04$. In Fig. 5.1 (a), the total energies for different parameters r are tabulated up to the fiftieth basisfunction. Obviously, there is a great improvement for higher-order schemes and the best result is obtained with $r = 14$. However, the harmonic oscillator is known to be a

[7] In the code the Fourier transform is performed with help of the library *fftw*, that is able to treat arrays of arbitrary length and dimension with an $O(n\ log\ n)$-algorithm.

(a)

r	E_0	E_1	E_{49}
1	0.4987	1.4937	42.18
2	0.4999	1.4998	47.16
3	0.5	1.5	48.54
4	0.5	1.5	49.05
10	0.5	1.5	49.49
14	0.5	1.5	49.498
25	0.5013	1.5028	48.28

(b)

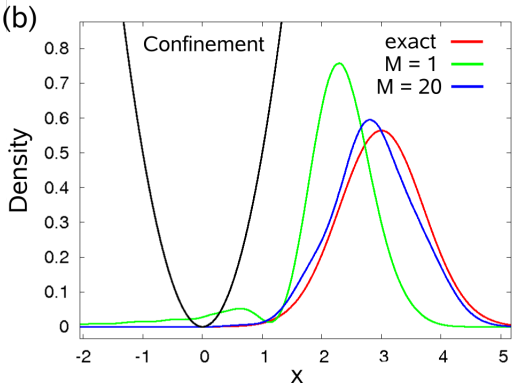

Figure 5.1.: *Comparison of the different-order schemes in the spatial diagonalization and time-evolution. (a) The total energies for the numbered basisfunctions in a 1D harmonic oscillator. (b) A displaced Gaussian wave package that oscillated 50 times ($T = 100\,\pi$) in the harmonic confinement. The number of time steps is chosen in such a way, that both evolutions require nearly the same computational effort. The higher order scheme with $M = 20$ is clearly superior to the Crank-Nicolson scheme with $M = 1$.*

very well-tempered system, so that for arbitrary confinements r should not be chosen that large, but rather between one and five.

Properties of the Generalized Crank-Nicolson method

We also investigate the influence of the parameter M, that denotes the order of the polynomials in the Padé approximation of the exponential. Here we only use $r = 1$, i.e. the discretization of the second derivative by formula (5.2), as it is numerically much more convenient to solve tridiagonal linear systems than banded ones. However, if we claim a higher accuracy for constant gridpoints – e.g. to avoid memory overflow – r should be set in between one and five.
Figure 5.1 (b) shows the evolution of a displaced Gaussian wave package in the harmonic oscillator, for which we know from the analytical solution that it oscillates by a frequency of $1/2\pi$. The initial state is centered at $x = 3$ and then evolved to time $T = 100\pi$, where it completes its fiftieth oscillation. The discretization of the spatial grid is $\Delta x = 0.0024$, and the respective number of time steps is chosen to require the same effort, i.e. $N_t = 20000$ for $M = 1$ and $N_t = 1000$ for $M = 20$. The result clearly reveals the advantage of the higher-order schemes that, especially in 2D calculations, can be used to significantly save time.

6. Roothaan-Hartree-Fock formalism

6.1. Overview

The Hartree-Fock- or self-consistent field method was invented by D.R. Hartree in 1928 and completed two years later by Fock and Slater, who independently pointed out that Hartree's approach was not correctly anti-symmetrized. They also showed how it could be derived from a variational principle applied to the simplest many-body wavefunction, a Slater determinant. However, the corresponding Hartree-Fock equations were not feasible until the beginning of the fifties, when C.C.J. Roothaan and G.G. Hall – again independently – introduced their basis representation.

Thereby the Hartree-Fock equations attain the form of a generalized eigenvalue problem, the Roothaan-Hall equations [7]

$$\mathbf{H}^{\mathrm{HF}}\ \mathbf{C} = \epsilon\ \mathbf{O}\ \mathbf{C}\,, \tag{6.1}$$

where $\mathbf{H}^{\mathrm{HF}}$ denotes the effective Hartree-Fock Hamiltonian or Fock matrix, $\mathbf{O}$ the overlap matrix and the solution $\mathbf{C}$ is the matrix of the expansion coefficients, that determine the Hartree-Fock orbitals $\{\psi_i\}$ as a linear combination of the chosen basis $\{\varphi_j\}$.

C.C. Roothaan[1]

$$\psi_i = \sum_j C_{ij}\ \varphi_j\,. \tag{6.2}$$

G.G. Hall[2]

The first decision one has to take is the selection of an appropriate basis. For quantum chemists this is right often the hardest part, as "probably there are as many basis sets as there are quantum chemists" [7]. However, most of these basis sets are specific to atoms and molecules, so that within this work only two basis sets from this large repertory are selected:

- **Natural orbitals (NO)**
  NOs designate the eigenfunctions of the single-particle Hamiltonian. Within this work they are calculated numerically by means of the procedures from Chapter 6. NOs are always usable, especially if the particle interaction is weak.
- **Slater-type orbitals (STO)**
  STOs are analytical basis functions specific to the Coulomb potential. They are similar to hydrogen eigenfunctions, but their radial part only depends on the principal quantum

[1] http://www.quantum-chemistry-history.com/Root_Dat/RevModPhys/RevModPh69.htm
[2] http://www.quantum-chemistry-history.com/Hall1.htm

number

$$\chi_{nlm}(\mathbf{r},\zeta) \;=\; \sqrt{\frac{(2\zeta)^{2n+1}}{(2n)!}}\; r^{n-1}\; \mathrm{e}^{-\zeta r}\; \mathrm{Y}_{lm}(\theta,\varphi)\,. \tag{6.3}$$

Y_{lm} are the spherical harmonics. In groundstate calculations, the parameter ζ is optimized with respect to the energy minimum.

Other often used basis sets are Gaussian type orbitals, also specific to molecules, and plane waves. Generally one can say that an analytical basis is superior to a numerical one. The reason for this is that there often exist closed formulas for the computation of the electron repulsion integrals, the bottleneck in SCF calculations. In addition, the possibility to introduce further parameters makes the basis more flexible, as the spanned Hilbert-subspace can be freely varied. Later we will show the drastic advantage of this flexibility.
Our use of the numerical NOs indeed is comfortable, but not optimal. Probably it would be better to expand the wavefunctions in an appropriate analytical basis, for instance plane waves, and solve the single particle Schrödinger equation by variation of the expansion coefficients, a procedure that is called "linear variation method".[3] This would eliminate the need for storage of the wavefunctions on the spatial grid points, what not only saves a lot of memory, but also gives the possibility to greatly enlarge the dimension of the grid – this is particularly interesting for ionization processes. In addition one can enjoy all the mentioned advantages of an analytical basis.

Before starting the SCF calculation, one also has to specify the treatment of the spin, for what again numerous methods exist:

- **Spin-polarized**
  In the first approach, we consider all electrons to have the same arbitrary spin, what leads to singly occupied orbitals in the fermionic case. While not covering the situation of real materials, the spin-polarized ansatz can be used as an easy model to investigate the underlying physical processes, especially because it has turned out to be numerically the most stable choice, see also the discussion in the following section.

- **Restricted Hartree-Fock (RHF)**
  The RHF ansatz models the simple picture one bears in mind, in which each spatial orbital is occupied by two electrons with opposite spin. It is the most common choice for Hartree-Fock calculations and often yields reasonable predictions for real materials.

- **Restricted open-shell Hartree-Fock (ROHF)**
  ROHF is an extension of RHF in which also open shells, i.e. singly occupied orbitals whose spins are assumed to be parallel, are added to the description. The corresponding equations have also been found by Roothaan in 1960 [31].

- **Unrestricted Hartree-Fock (UHF)**
  In contrast to RHF calculations, in UHF one assumes that each electron sits in its own spatial orbital. In basis representation this leads to a coupled system of two eigenvalue equations of the Roothaan-Hall form, that are called Pople-Nesbet equations [7]. The enlargement of the variational space will in general provide better ground-state energies, while the resulting

[3] Unfortunately this common idea only arose late during this work, when (after a lot of trials with the analytical basis sets provided here) the importance of an adapted basis became obvious. The implementation will be part of the future work.

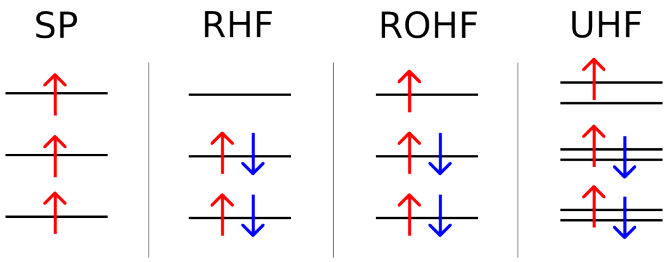

Figure 6.1.: *The usual types of treating the spin in (fermionic) single-determinant Hartree-Fock calculations.*

wavefunction, however, is not an eigenstate of $\mathbf{S}^2$. Thus an UHF calculation is often followed by appropriate projection techniques to restore the expected symmetries [4] [32].

In Fig. 6.1, a sketch of the enumerated types is shown. In this work we consider all of them, except for the ROHF method, but as an expansion basis for the Green function until now only the spin-polarized and spin-restricted cases are used. To cover both in the following mathematical formulation, in chapter 4 a parameter σ was introduced, which is set to one in the spin-polarized case and to two in RHF calculations. For bosonic particles in the absence of a spin-dependent disturbance or interaction, only the spin-polarized and the UHF approach are sensible, as bosons don't obey any restrictions in the possible occupation of one state.

6.2. Solution of the Roothaan-Hall equations

The Roothaan-Hartree-Fock method is a standard procedure described in many textbooks, e.g. [7], but almost all of them consider the zero-temperature case. We will explain a different, more physical approach to treat also finite temperatures by using thermodynamic ensembles [18].

As input to the Roothaan equations we need the electron integrals in the chosen basis, summarized in the following:

$$O_{ij} = \int d\mathbf{x}\ \varphi_i^*(\mathbf{x}))\varphi_j(\mathbf{x})\,, \tag{6.4}$$

$$h_{ij}^0 = \int d\mathbf{x}\ \varphi_i^*(\mathbf{x})\ \left\{-\frac{1}{2}\nabla^2 + v(\mathbf{r})\right\}\ \varphi_j(\mathbf{x})\,, \tag{6.5}$$

$$w_{ij,kl} = \iint d\mathbf{x}\ d\mathbf{x}'\ \varphi_i^*(\mathbf{x})\varphi_j(\mathbf{x})\ w(\mathbf{r},\mathbf{r}')\ \varphi_k^*(\mathbf{x}')\varphi_l(\mathbf{x}')\,. \tag{6.6}$$

$\mathbf{O}$ is the overlap-matrix, $\mathbf{h^0}$ the single-particle Hamiltonian and $\mathbf{w}$ denotes the two-electron (or electron repulsion) integrals. To compute the respective energies, also the kinetic and potential part of $\mathbf{h^0}$ should be determined. Further, an eventual spin dependence is suppressed in the variable $\mathbf{x}$ and integration leads to a delta function, as the operators are spin-independent and different spinfunctions are orthonormal.
As mentioned, the calculation of these integrals is a specific field on its own. In one dimension, we compute them by a simple numerical Simpson integration. Since the one-particle matrices for

[4] This has been liberally explained to us by one of the authors of the reference, Fabio Cavaliere, in a private talk at the FQMT 08 conference in Prague. He also pointed out the importance of symmetry-breaking processes in the Hartree-Fock procedure, see the following discussion on the convergence properties.

real orbitals are symmetric, only the upper triangular matrix has to be calculated. Furthermore, the two-electron integral $w_{ij,kl}$ is symmetric under exchange of $(ij) \rightarrow (ji)$, $(kl) \rightarrow (lk)$ as well as under interchange of the two blocks $(ij, kl) \rightarrow (kl, ij)$, which is why only one eighth of them have to be computed. Additionally, in Chapter 10 an approximation scheme is introduced to further reduce the computational effort of $\mathcal{O}(N_b^4/8)$.

Having obtained the input matrices, the practical computation proceeds as follows:

(i.) Calculate the Hamiltonian $\mathbf{H}^{\mathrm{HF}}$ (also called Fock matrix) given by

$$H_{ij}^{\mathrm{HF}} \;=\; h_{ij}^0 + \sum_{kl} (\sigma\; w_{ij,kl} \pm w_{ik,lj})\; \rho_{kl}\,, \tag{6.7}$$

the first time with an initial guess for the density matrix $\boldsymbol{\rho}$. The factor σ coming from the spin-summation is in the spin-polarized case $\sigma = 1$, while for RHF calculations $\sigma = 2$.

(ii.) Solve the generalized eigenvalue problem

$$\mathbf{H}^{\mathrm{HF}}\; \mathbf{C} \;=\; \epsilon\; \mathbf{O}\; \mathbf{C}\,, \tag{6.8}$$

requiring the orthonormalization $\mathbf{C}^\dagger\; \mathbf{O}\; \mathbf{C} = \mathbf{1}$. In the code this is done with the *Lapack* routine *dsygvd*, that performs a Cholesky decomposition of the matrix $\mathbf{O}$, transforms $\mathbf{H}^{HF}$ to the new basis and solves the resulting standard eigenvalue problem.

(iii.) Determine the new chemical potential μ by requiring the total number of particles N to be

$$N(\beta, \{\epsilon_k\}, \mu) \;=\; \sigma\; \sum_i n_i(\beta, \epsilon_i, \mu)\;, \qquad n_i(\beta, \epsilon_i, \mu) \;=\; \frac{1}{\mathrm{e}^{\beta(\epsilon_i - \mu)} \pm 1}\,, \tag{6.9}$$

where in the grand-canonical formalism the occupation number n_i is obtained either from the Bose/Einstein or the Fermi/Dirac distribution. In the RHF case, n_i is multiplied by two, as each orbital is doubly occupied. The root of the sum is found with the algorithms of the library *gsl*. For Bosons one has to narrow the search to the energy region lower than the first energy-eigenvalue to avoid numerical instabilities, since the chemical potential can not be larger than this value.

(iv.) Calculate the new density matrix ρ and the new total energy E_{tot} by

$$\rho_{ij} \;=\; \sum_k\; C_{ik}\; n_k\; C_{jk}^*\,, \tag{6.10}$$

$$E_{\mathrm{tot}} \;=\; \sigma\; \mathrm{Tr}\{\boldsymbol{\rho}\; \mathbf{h^0}\} + \frac{\sigma}{2}\; \mathrm{Tr}\{\boldsymbol{\rho}\; (\mathbf{H}^{\mathrm{HF}} - \mathbf{h^0})\}\,. \tag{6.11}$$

The first term in the expression for E_{tot} accounts for the single-particle contribution and the second term for the mean-field part. As always, the factor $\frac{1}{2}$ prevents a double-counting of the interaction. Further, if the density matrix is asked for information on the occupation numbers, the entries also have to be multiplied by σ.

(v.) Return to (i.) with the updated density matrix $\boldsymbol{\rho}$ as long as the total energy is changing, i.e as long as $|E_{\mathrm{tot}}^{(\nu)} - E_{\mathrm{tot}}^{(\nu-1)}| > \Delta E_{\mathrm{tot}}$. ν labels the iteration cycle and ΔE_{tot} is the claimed accuracy, usually chosen smaller than 10^{-10}. Alternatively one could question the averaged

convergence of the density matrix by

$$\Delta\rho = \frac{1}{N_b^2} \sum_{ij} \left| \rho_{ij}^{(\nu)} - \rho_{ij}^{(\nu-1)} \right| , \tag{6.12}$$

what turned out to be a more sensitive test, see the following discussion on convergence properties.

The convergence of this iteration scheme is not assured. Even if the total energy converges, the difference of two successive density matrices $\Delta\rho$ can remain large, what is caused by periodic changes. The convergence can sometimes be improved by introducing a damping-parameter α, with which the new density-matrix is obtained by an average with the one from the previous cycle

$$\boldsymbol{\rho}^{(\nu+1)} \;:=\; \alpha\, \boldsymbol{\rho}^{(\nu+1)} \;+\; (1-\alpha)\, \boldsymbol{\rho}^{(\nu)} . \tag{6.13}$$

However, even if both quantities converge, the result may not be the desired Hartree-Fock equilibrium state. For example, a restricted Hartree-Fock calculation for a two-dimensional isotropic harmonic oscillator does not necessarily lead to a radial-symmetric density distribution, see section 8.4. The only way around this problem is to restore the expected symmetry by applying certain symmetrizing procedures [32], which also bring correlation into the system, as the symmetrized densities are no longer described by a single Slater determinant.

6.2.1. Canonical ensemble

The extension of the above algorithm to the canonical ensemble is straightforward. All we have to do is to replace the grand-canonical expectation value of the mean particle number by its canonical counterpart

$$\langle n_i \rangle_{gc} \;\longrightarrow\; \langle n_i \rangle_{can} \tag{6.14}$$

As it is known from statistical physics, in the case of non-degenerate energy levels the canonical average can be achieved from the grand-canonical by discarding the chemical potential and restricting the sum over the Fock-space to a fixed particle number N [33]

$$\langle n_i \rangle_{can} \;=\; \frac{1}{Z_{can}} \sum_{n_1=0}^{1} \sum_{n_2=0}^{1} \cdots\; n_i \; \mathrm{e}^{-\beta \sum_{k=1}^{\infty} \epsilon_k n_k} \; \delta_{N, \sum_{k=1}^{\infty} n_k} . \tag{6.15}$$

In the bosonic case the summations are performed up to infinity instead of one, because each state can be occupied by an infinite number of bosons (yet regarding the Kronecker-delta, summation up to N is sufficient). As there is no analytical formula available like in the grand-canonical case, we have to attack the partition function and the mean particle number numerically. In the following the applied procedures are explained detail.

Recursion formulas

One recursion formula for the calculation of the partition function for noninteracting particles in the canonical ensemble is given by [34]

$$Z_N(\beta) = \frac{1}{N} \sum_{k=1}^{N} (\pm 1)^{k+1} \; Z_1(k\beta) \; Z_{N-k}(\beta) \; , \qquad Z_0(\beta) \equiv 1 \, , \tag{6.16}$$

where $Z_1(k\beta) = \sum_j \mathrm{e}^{-j\beta e_j}$ is the one-particle partition function at temperature $k\beta$.

The mean occupation of an orbital with energy ϵ_i is then obtained by

$$n_i(N,\beta) = \frac{1}{Z_N(\beta)} \sum_{k=1}^{N} (\pm 1)^{k+1} \; \mathrm{e}^{-k\beta\epsilon \; Z_{N-k}(\beta)} \, . \tag{6.17}$$

As the partition function grows exponentially with N, for larger particle numbers one should use multiple precision arithmetic [5] to avoid overflows.

Direct evaluation

Though the recursion formulas are clearly superior to the direct evaluation of (6.15), we will derive the latter one as well, not only since it was our first and straightforward approach, but also because it will be needed in the following chapter. Therefore we must specify all accessible states to a given particle number and – leaving out all zeros from the Kronecker delta – perform the sum (6.15) only over those states. In the following we will give the method to obtain all these states for a given particle number N and number of basis functions N_b in occupation number representation[6].

(i) **Bosonic case only: Integer partition of** N
To find the integer partition of N means to determine the set of integers that yield N when summed up. For example, the integer partition of 4 is $\Big\{\{4\},\{3,1\},\{2,2\},\{2,1,1\},\{1,1,1,1\}\Big\}$. For fermions only the simple partition $\{1,1,1,1\}$ is used.

(ii) **Cyclic permutation**
Each partition is written in the first components of a vector of length N_b and the other entries are padded with zeros. Then all cyclic permutations of each vector are found.

Let us consider an example: We want to find all states for $N = 3$ particles and $N_b = 4$ basis functions. For fermions we switch immediately to (ii) and get

$$(1,1,1,0) \quad (1,1,0,1) \quad (1,0,1,1) \quad (0,1,1,1)$$

[5] For example the gnu multi-precision library (GMP)

[6] Another algorithm is possible: Instead of relating particle numbers to states one can do the opposite and assign a state to each particle. This has been independently implemented by Martin Heimsoth to yield exactly the same results.

while for boson we first appoint the integer partition of 3, $\Big\{\{3\},\{2,1\},\{1,1,1\}\Big\}$, and permute each of these subsets

$$\begin{array}{cccc} (3,0,0,0) & (0,3,0,0) & (0,0,3,0) & (0,0,0,3) \\ (2,1,0,0) & (2,0,1,0) & (2,0,0,1) & (1,2,0,0) \quad \cdots \\ (1,1,1,0) & (1,1,0,1) & (1,0,1,1) & (0,1,1,1) \end{array}$$

Then the energy $\sum_{k=1}^{\infty} \epsilon_k n_k$ of each state is known and expression (6.15) can be evaluated. For comparison between the two ensembles see the figures in section 6.3.

6.2.2. Hartree-Fock orbital representation

Our primary aim in doing Hartree-Fock calculations is to obtain the orthonormal basis of Hartree-Fock orbitals, that shall be used to expand the Green function and perform "beyond mean-field" or correlated calculations. Though when switching to this new basis, any of the already calculated quantities needed in the following steps also have to be transformed. A general one-body operator in the new basis is given in terms of the old and the expansion coefficients $\mathbf{C}$ obtained from (6.8)

$$O_{ij}^{\mathrm{HF}} \;=\; \langle\psi_i|\hat{O}|\psi_j\rangle \;=\; \sum_{kl} C_{ki}^{*} C_{lj} \;\langle\varphi_k|\hat{O}|\varphi_l\rangle \;=\; \sum_{kl} C_{ki}^{*}\; O_{kl}\; C_{lj}\,. \tag{6.18}$$

For the single particle Hamiltonian, it is thereby convenient to subtract the chemical potential from the diagonal entries

$$\left(h_{ij}^{0}\right)^{\mathrm{HF}} \;=\; \sum_{kl} C_{ki}^{*}\; h_{kl}^{0}\; C_{lj} - \mu\;\delta_{ij}\,, \tag{6.19}$$

for reasons that are explained in Chapter 10. Another special case is the density matrix $\boldsymbol{\rho}$, which by definition transforms into a diagonal matrix containing the respective HFO occupation numbers. This property serves as a sensitive test for the correctness of the eigenvectors $\mathbf{C}$.
Furthermore, from (6.6) we obtain for the two-electron integrals in the new basis the expression

$$w_{ij,kl}^{\mathrm{HF}} \;=\; \sum_{abcd} \Big[A_{ai} A_{bj}^{*}\Big]^{*}\; w_{ab,cd}\; \left[A_{ck} A_{dl}^{*}\right]\,. \tag{6.20}$$

In the numerical execution for large basis sets it is indispensable to query for the size of $w_{ab,cd}$ and perform the loop over (ijkl) only if it exceeds a chosen cutoff parameter ($\sim 10^{-15}$ a.u.).

6.2.3. Unrestricted Hartree-Fock

The previous Hartree-Fock algorithm can handle spin-polarized as well as spin-restricted systems, and in the latter case the expected $\hat{S}^2$-symmetry is implicitly assumed. However, sometimes it is more instructive to enforce a UHF-state, that is no eigenstate of $\hat{S}^2$, e.g. if a better groundstate energy is needed or if the modeled molecule has an unequal number of particles with different spin. In particular, it is sensible if the RHF result has suffered a symmetry-breaking process [32] and symmetry-restoring operators are applied anyway.
The mathematical formulation as well as the numerical implementation are not more difficult than in the spin-polarized case. All we have to do is to assume two spin-polarized subsystems of different spin, that within each subsystem interact via the normal Hartree-Fock interaction

and in between both systems only through Hartree interaction. In addition, one obtains two density matrices and chemical potentials. The representation in a basis yields two coupled matrix equations for the expansion coefficients of species ↑ and ↓, that are called Pople-Nesbet equations [7]

$$\mathbf{H}^{\mathrm{UHF},\uparrow\downarrow}\ \mathbf{C}^{\uparrow\downarrow}\ =\ \epsilon^{\uparrow\downarrow}\ \mathbf{O}\ \mathbf{C}^{\uparrow\downarrow}\,. \tag{6.21}$$

Thereby the unrestricted Hartree-Fock Hamiltonian or the Fock matrix is given by

$$H_{ij}^{\mathrm{UHF},\uparrow\downarrow} =\ h_{ij}^{0} + \sum_{kl}(w_{ij,kl} \pm w_{ik,lj})\ \rho_{kl}^{\uparrow\downarrow}\ + \sum_{kl} w_{ij,kl}\ \rho_{kl}^{\downarrow\uparrow}\,. \tag{6.22}$$

If $N_\uparrow = N_\downarrow$, one should use different starting guesses for the two density matrices, unless the restricted HF result is desired. Even then, the iteration process can converge in the RHF result.

6.3. Application

Comparison between NO and STO calculations

By means of the example Helium, we show how the improved flexibility of analytical functions can lead to much better results. The NOs are given by (5.8), and the two-electron integrals are calculated by the formula from Appendix A. The formulas for the one-center electron integrals involving STOs, though straightforward to compute, are taken from [35], while the optimized coefficients are gained after a numerical minimization of the energy. For the minimization we use the "downhill simplex method" of Nelder and Meat [27] as implemented in the library *gsl*, that has the advantage that no derivatives are needed.
At first we tried the natural orbital basis, for which we collect the total energies of two different groundstate calculations ($\beta = 100$) in both ensembles. In the groundstate, the principle of Ritz holds, so the quality of a given result can immediately be valued. A denotation of the form $(9, 1)$ means, that all orbitals with $n_r \leq 9$, $l \leq 1$ and $-l \leq m \leq l$ are included. The results are

Helium	Basis	E_{tot}^{gc}	E_{tot}^{can}
NO	(5,0)	−2.8351	−2.8351
	(9,1)	−2.8354	−2.8354

Further we calculated the virial ratio, $E_{kin}/E_{tot} = -1.11$, that should be exactly minus one for atomic systems. One sees, that an augmentation of the basis does not necessarily lead to a better result.

Next, we inserted a basis of Slater type orbitals (STO) and optimized the coefficients with respect to the total energy. This time the corresponding notation (321) means that we used 3 s-functions, 2 p-functions, 1 d-function and so on. The variational space can be even more extended, if the principal quantum numbers are allowed to become non-integer. The calculations in which in addition to the to the exponents also the principal quantum numbers are optimized, are denoted by NISTO. We obtained the following results:

Helium	Basis	E_{tot}
STO	(1)	−2.84765625
NISTO	(1)	−2.854208497
STO	(222)	−2.861679996

Interestingly, one optimized Slater type orbital yields a better result than 30 basisfunctions in the (9,1,1) NO calculation. The result for the (222)-basis exactly agrees with the Hartree-Fock limit [36], the value which corresponds to a fictitious calculation with $N_b \to \infty$. Accordingly, the respective virial ratio is $E_{kin}/E_{tot} = -0.9999996$. The optimized parameters for the minimal basis sets (1) are given by

	ζ	n
STO	1.6875	$n \equiv 1$
NISTO	1.61172	0.955057

By comparing the optimized exponents ζ to the exponent of the first s-orbital obtained from the Schrödinger equation, which is proportional to e^{-2r}, we can guess why the STO calculations are that superior.
These results suggest an impressive saving in the number of basisfunctions on the HF level. For correlated calculations,however, one often needs larger basis sets to reach the limit of the respective approximation.

Minimization of analytical NO's

Recognizing the results from the last example, one can guess that any analytical basis can be improved by introducing additional parameters followed by a minimization of the (internal) energy in the zero-temperature case, respectively of the free energy for finite temperatures. In any case the basis gets more flexible and, as seen before, if a sensible choice is taken the HF-limit can be reached much earlier. As an example we extend the NOs of the one-dimensional harmonic oscillator by the parameter ζ in the following way:

$$\left(\frac{\Omega}{\pi}\right)^{\frac{1}{4}} \mathrm{H}_n(\sqrt{\Omega}\, x)\, \mathrm{e}^{-\frac{\Omega x^2}{2}} \quad \to \quad \left(\frac{\Omega\zeta}{\pi}\right)^{\frac{1}{4}} \mathrm{H}_n(\sqrt{\Omega\zeta}\, x)\, \mathrm{e}^{-\frac{\Omega\zeta x^2}{2}} \tag{6.23}$$

H are the Hermite polynomials and Ω is the trap frequency, that is formally able to vary for each eigenfunction.[7] To investigate this replacement, we need a (temporary) reference result from a spin-polarized, grand-canonical calculation within the standard basis:

$$N_b = 20\,, \quad N = 3 \quad \beta = 100\,, \quad \lambda = 1.0 \quad \to \quad E_{tot} = 6.61446 \tag{6.24}$$

Again the temperature is sufficiently low to model the groundstate, thus the Ritzian principle holds and lower energies imply a better approximation to the searched groundstate. The energies after minimization are

N_b	E_{before}	E_{min}
4	6.65984	6.61479
12	6.61461	6.61436

The minimized result for $N_b = 12$ is slightly better than the reference result. Further, the result for 4 basisfunctions is comparable to the reference and much better than the energy without

[7] Similarly to the STO calculations, also non-integer quantum numbers could be used, for instance through the expansion of Hermite polynomials in hypergeometric functions.

optimization. The optimized parameters for $N_b = 4$ read

$$\zeta_0 = 1.15858\,, \quad \zeta_1 = 1.11377\,, \quad \zeta_2 = 0.85686\,, \quad \zeta_3 = 1.03496\,, \tag{6.25}$$

and have to be compared to the pure NO basisfunctions with $\zeta_i \equiv 1$.
For $N_b = 12$ basisfunctions, the deviation between the energies before and after minimization is only small. This implies, that here the HF-limit is reached if a larger basis, for example $N_b = 30$ NOs, is used. Since in view on nonequilibrium calculations this is what we are going to do, in the further work only the pure NOs are used.
However, the approach of these extended basisfunctions could be sensible for a large number of particles $N \lesssim N_b$ or also for strong interaction, as the wavefunction differs more and more from the ideal case. Further it could be advantageous in the dynamic description of ionization: When the groundstate is adequately described by a few extended NOs, more continuum wavefunctions can be used.

Grandcanonical vs. canonical ensemble

While the results from canonical and grand-canonical groundstate calculations agree, for finite temperatures both approaches yield different results. As already indicated in [18], there by comparison of the total energies arising from canonical path-integral Monte Carlo simulations and grand-canonical Matsubara Green function results in second Born approximation, the canonical energies are lower than the grand-canonical. Here we investigate the occurring ensemble differences more consistently within one method and explain the reason for this behavior.
Figure 6.3 shows the total energies for different coupling parameters, that are found to deviate the most in the region between $\beta \approx 0.5$ and $\beta \approx 4.0$. For β larger than five, both ensembles yield the same groundstate result, as the orbital occupation is identical - the first N orbitals are fully occupied and all others are empty. We also reveal, that for a larger λ the beginning of the deviation shifts to lower inverse temperatures.

The empirical explanation of this behavior is given in terms of the densities, see Fig. 6.2. For large β, the system is in its groundstate and the densities correspond to the the distribution which minimizes the energy. For larger coupling parameters, the peaks get more localized as the system approaches the Wigner crystallization regime. When the system is warmed up from the groundstate, the particles gain kinetic energy and turn to wash out the optimal distribution, until for very high temperatures, when all other energy contributions are negligible, the distribution in both ensembles becomes a Maxwellian. Now in the intermediate region, the ensembles show their difference: The canonical ensemble densities are more localized than the ones in the grand-canonical ensemble, that are correspondingly broader and more washed out. This implies, that the kinetic energy and particle-interaction energy in the grand-canonical ensemble are increased. At the same time those orbitals, that were fully occupied in the groundstate, for finite temperatures have a smaller occupation in the grand-canonical ensemble, while for the formerly unoccupied states it is vice versa. This behavior is shown in Fig. 6.4.

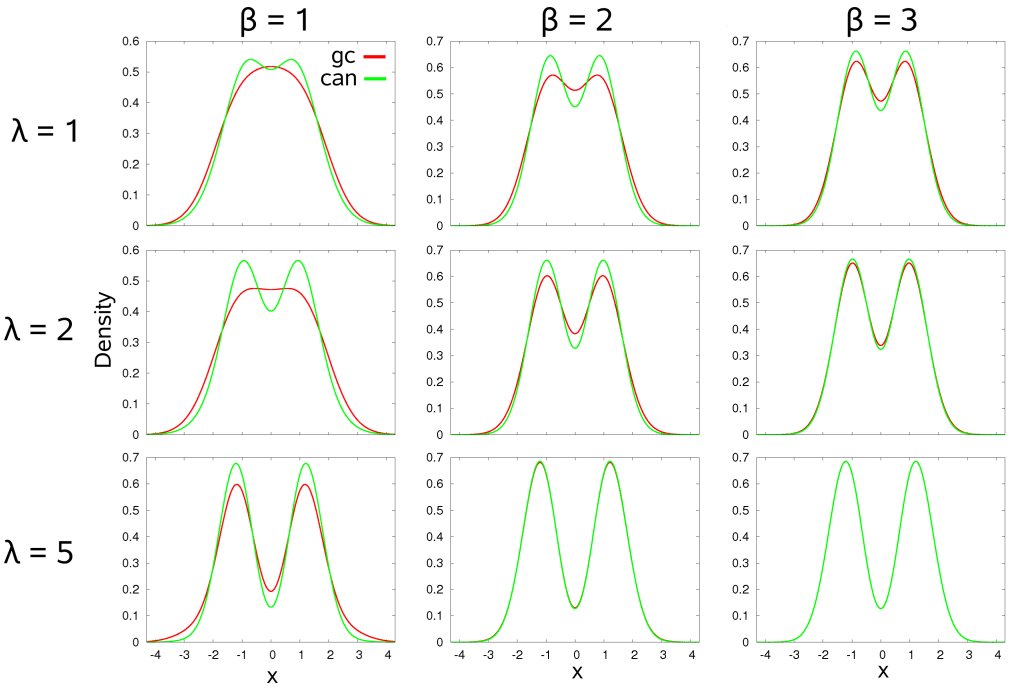

Figure 6.2.: *The Hartree-Fock densities for $N = 2$ particles in both ensembles for different inverse temperatures and coupling parameters.*

Figure 6.3: *Dependence of the total energies on the inverse temperature for $N = 2$ spin-polarized particles in a 1D harmonic oscillator. Compared are the results from canonical and grand-canonical calculations. As can be seen, for higher temperatures the canonical energy is found to be lower than its grand-canonical counterpart.*

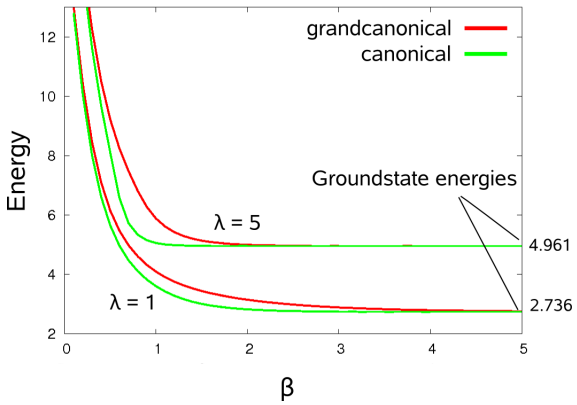

Spin-restricted vs. spin-polarized

Finally, we show the Hartree-Fock results arising from the different treatments of the spin as collected in section 7.1. We consider $N = 4$ particles in the 1D harmonic oscillator with $N_b = 15$, $\beta = 50$ and $\lambda = 1$. In Fig. 6.5 (a), we compare the densities from spin-polarized and spin-restricted calculations. In the spin-polarized case, we can resolve the four particles, while the RHF result rather resembles the densities for $N = 2$, Fig. 6.2.
In Fig. 6.5 (b) the UHF results are compared to those from RHF, and as expected they appear less symmetric. The green curve shows the spin-density, $\rho^S(x) = \rho^{\uparrow}(x) - \rho^{\downarrow}(x)$, that yields the spatially resolved expectation value of the spin.
The three total energy values are $E_{sp} = 12.076$, $E_{\mathrm{RHF}} = 11.932$ and $E_{\mathrm{UHF}} = 11.661$.

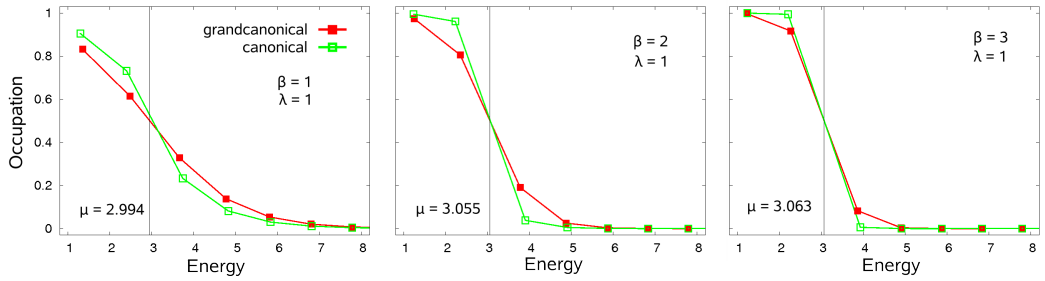

Figure 6.4.: *Occupation numbers in the two ensembles for different inverse temperatures,* $\lambda = 1$.

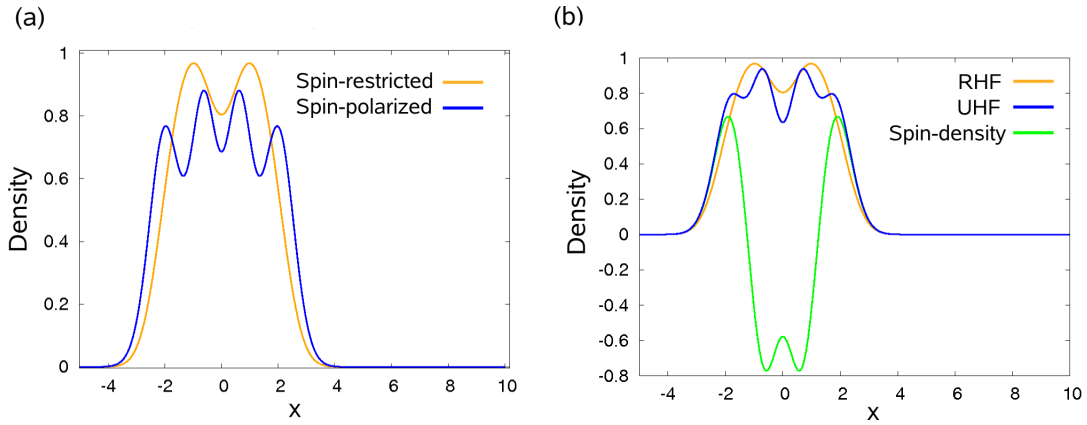

Figure 6.5.: *The densities from the different spin-methods for* $N = 4$ *particles,* $\lambda = 1$, $\beta = 50$. *(a) Comparison between spin-restricted and spin-polarized densities. (b) Restricted HF, unrestricted HF and spin density.*

7. Configuration Interaction

Before encountering the numerics of the Green function, let us consider an approach that is much more straightforward. Configuration Interaction or Exact Diagonalization designates a formalism, in which the many-body Schrödinger equation is solved exactly. Our aim behind implementing this method is mainly to provide a reference, against that the results from the approximate NEGF approach can be checked. To this end, only very basic implementations are used and almost the whole literature available in physics and quantum chemistry – such as [37] or [7] to name a few – has been neglected.

7.1. Full Configuration Interaction

As is well known from quantum mechanics, the N-particle wavefunction is an element of the space of (anti-)symmetrized wavefunctions $\mathcal{H}_N^{\pm}$, which is a subspace of the direct product of N one-particle Hilbert spaces. An (anti-)symmetrized wavefunction is thus composed of orbitals $\{\varphi_k\}$ of a one-particle Hilbert space, and a basis of $\mathcal{H}_N^{\pm}$ is given by all of these wavefunctions, that are conveniently described in the occupation representation by infinite vectors. In numerical calculations, of course, we have to restrict ourselves to a finite basis. This is naturally obtained if only a restricted number of orbitals is taken into account. It leads directly to the occupation vectors derived in section 6.2.1.

The idea is to represent the full Hamiltonian in second quantization

$$\hat{H} = \sum_{ij} h^0_{ij}\ \hat{a}^\dagger_i \hat{a}_j \ + \ \frac{1}{2} \sum_{ijkl}\ w_{il,kj}\ \hat{a}^\dagger_i \hat{a}^\dagger_j \hat{a}_k \hat{a}_l \,. \tag{7.1}$$

Note that the interaction matrix element is rearranged to the "normal" appearance in order to use our definition (6.6).
Further we calculate the matrix elements of $\hat{H}$ in the basis of the occupation vectors, which is very easily done since the action of the creators and annihilators on a basis state is well known.

$$H_{n,n'} \ = \ \langle\ \mathbf{n}\ |\ \hat{H}\ |\ \mathbf{n'}\ \rangle \ = \ \langle\ n_1\ n_2 \cdots\ |\ \hat{H}\ |\ \cdots n'_2\ n'_1\ \rangle\ . \tag{7.2}$$

Then, all one has to do is to diagonalize this matrix to obtain the many body groundstate as well as the excited states:

$$\mathbf{H} \ = \ \mathbf{A}\ \mathbf{E}\ \mathbf{A}^\dagger \,. \tag{7.3}$$

The diagonal matrix $\mathbf{E}$ contains the eigenvalues of $\mathbf{H}$ and the unitary matrix $\mathbf{A}$ the respective eigenvectors.

However, this easy command is in practice only feasible for small numbers of particles and basis-functions, because the size of the basis and thus the dimension of the Eigenvalue problem grows

very rapidly when increasing them. More precisely, for Fermions the number of occupation vectors is $\binom{N_b}{N}$.
For a reduction of the problem, any symmetry of the Hamiltonian can be used. If $\hat{H}$ commutes with an hermitian operator $\hat{O}$, it becomes decomposed in blocks and has to be diagonalized only in the respective subspaces. As the diagonalization effort (of dense $n \times n$ matrices) grows with $O(n^3)$, this can yield a well reduction.

In the code, for diagonalization again the *Lapack* library is used. An extension to the *Anasazi* sparse solver package as used in section 6.2. could be implemented straightforwardly and should be advisable when higher dimensions than one are considered.

7.2. Density matrix and natural orbitals

Once the Hamiltonian is diagonalized, it is very easy to calculate expectation values of an (arbitrary-particle) operator $\hat{O}$, either by averaging over the wavefunction or within the canonical ensemble. Since the first alternative is common, we will focus only on the ensemble case. The expectation value there is achieved by taking the trace of the product with the canonical density operator $\hat{\varrho}$

$$\begin{aligned} \langle\, \hat{O} \,\rangle_{can} &= \mathrm{Tr}\, (\hat{O}\, \hat{\varrho}) = \frac{1}{Z}\, \mathrm{Tr}\, (\hat{O}\, \mathrm{e}^{-\beta \hat{H}}) = \frac{1}{Z} \sum_n \langle\, \mathbf{n} \mid \hat{O}\, \mathrm{e}^{-\beta \hat{H}} \mid \mathbf{n} \,\rangle \\ &= \frac{1}{Z} \sum_{n,n'} \langle\, \mathbf{n} \mid \hat{O} \mid \mathbf{n}' \,\rangle \langle\, \mathbf{n}' \mid \mathrm{e}^{-\beta \hat{H}} \mid \mathbf{n} \,\rangle\,. \end{aligned} \tag{7.4}$$

The latter factor is known from the diagonalization

$$\begin{aligned} \langle\, \mathbf{n}' \mid \mathrm{e}^{-\beta \hat{H}} \mid \mathbf{n} \,\rangle &= \sum_{i,j} \langle\, \mathbf{n}' \mid \psi_i \,\rangle \langle\, \psi_i \mid \mathrm{e}^{-\beta \hat{H}} \mid \psi_j \,\rangle \langle\, \psi_j \mid \mathbf{n} \,\rangle \\ &= \sum_{i,j} \langle\, \mathbf{n}' \mid \psi_i \,\rangle\, \mathrm{e}^{-\beta E_i}\, \delta_{ij}\, \langle\, \psi_j \mid \mathbf{n} \,\rangle \\ &= \sum_{i} \langle\, \mathbf{n}' \mid \psi_i \,\rangle\, \mathrm{e}^{-\beta E_i}\, \langle\, \psi_i \mid \mathbf{n} \,\rangle \\ &= \sum_{i} A_{n',i}\, \mathrm{e}^{-\beta E_i}\, A^*_{n,i}\,. \end{aligned} \tag{7.5}$$

Of special importance is the expectation value of two field operators that yields the density matrix (which is to say the lesser Green function at equal times)

$$\rho_{ij} = \langle\, \hat{a}_i^\dagger\, \hat{a}_j \,\rangle\,. \tag{7.6}$$

With it, we can calculate the generalized density

$$\rho(x, x') = \sum_{ij} \rho_{ij}\, \varphi_i(x) \varphi_j^*(x')\,, \tag{7.7}$$

and by diagonalizing the density matrix, $\boldsymbol{\rho} = \mathbf{B}\,\mathbf{d}\,\mathbf{B}^\dagger$, we get the natural orbitals $\{\chi_i\}$ and their respective occupation:

$$\chi_i(x) \;=\; \sum_j B_{ij}\;\varphi_j(x)\,. \tag{7.8}$$

These could serve as a possible basis to expand the Green function in, but no real advantage would be gained by applying an approximation scheme to an exact basis. Alternatively, we could treat only some of the lowest states by CI and complete them by Hartree-Fock states. To get an orthonormal basis, the overlap matrix of this new basis can be diagonalized and the orbitals can be transformed to the orthonormal basis.

7.3. Time evolution

The time evolution of a many-body state is governed by the Schrödinger equation

$$i\frac{\partial}{\partial t}\;\mid\psi\,\rangle\,(t) \;=\; \hat{H}(t)\;\mid\psi\,\rangle\,(t)\,. \tag{7.9}$$

The time-dependent wavefunction is given as an expansion in the basis of occupation vectors with time-dependent coefficients,

$$\mid\psi\,\rangle\,(t) \;=\; \sum_{n'} c_{n'}(t)\mid\mathbf{n}'\,\rangle\;. \tag{7.10}$$

We insert this into Eq. (7.9), insert a unity operator in between the right-hand side and project the whole on $\langle\,\mathbf{n}\mid$ to get

$$\sum_{n'}\langle\,\mathbf{n}\mid\dot{c}_{n'}(t)\mid\mathbf{n}'\,\rangle \;=\; \sum_{n',n''}\langle\,\mathbf{n}\mid\hat{H}(t)\mid\mathbf{n}''\,\rangle\,\langle\,\mathbf{n}''\mid c_{n'}(t)\mid\mathbf{n}'\,\rangle \tag{7.11}$$

$$\longrightarrow\qquad \dot{c}_n(t) \;=\; \sum_{n'} H_{n,n'}(t)\;c_{n'}(t)\,, \tag{7.12}$$

or, in matrix form,

$$\dot{\mathbf{c}}(t) \;=\; \mathbf{H}(t)\;\mathbf{c}(t)\,. \tag{7.13}$$

The solution of this equation is

$$\mathbf{c}(t) \;=\; \mathbf{U}(t,t_0)\;\mathbf{c}(t_0)\,, \tag{7.14}$$

with the time-evolution operator $\mathbf{U}(t,t_0)$ as given in chapter 5. We again approximate it by a product of piecewise constant operators

$$\mathbf{U}(t+\Delta t,t) \;\approx\; \mathrm{e}^{-i\mathbf{H}(t+\Delta t/2)\Delta t}\,, \tag{7.15}$$

which can be computed with any of the methods given in section 5.2. Also an exact determination of $\mathbf{U}$ is possible (and would have been in 5.2.), if a repeated diagonalization is feasible. To this

end, we perform the same calculation as in (7.5) to obtain

$$U_{ij}(t+\Delta t,t) = \sum_k A_{i,k}\ \mathrm{e}^{-iE_k(t+\Delta t/2)\Delta t}\ A^*_{j,k}\,. \tag{7.16}$$

The time-dependence of expectation values can be either achieved by average over the wave-function or in the canonical ensemble. In the canonical ensemble, the expectation values can be computed by employing the cyclic invariance of the trace

$$\begin{aligned} \langle\ \hat{O}_H(t)\ \rangle &= \mathrm{Tr}\ (\ \hat{O}_H(t)\ \hat{\varrho}(t_0)\ ) \\ &= \mathrm{Tr}\ (\ \hat{U}(t_0,t)\ \hat{O}(t)\ \hat{U}(t,t_0)\ \hat{\varrho}(t_0)\ ) \\ &= \mathrm{Tr}\ (\ \hat{O}(t)\ \hat{U}(t,t_0)\ \hat{\varrho}(t_0)\ \hat{U}(t_0,t)\ )\,, \end{aligned} \tag{7.17}$$

i.e. by a trace of the product of $\mathbf{O}(t)$ and the time-dependent density-operator matrix

$$\boldsymbol{\varrho}(t) \ = \ \mathbf{U}(t,t_0)\ \boldsymbol{\varrho}(t_0)\ \mathbf{U}^\dagger(t,t_0)\,. \tag{7.18}$$

7.4. Application

Comparison with PIMC

For a one-dimensional quantum-dot, we compare the total energies of canonical Hartree-Fock and Configuration Interaction calculations with those arising from path integral Monte Carlo simulations, which are also set in the canonical ensemble. The PIMC results are taken from [18], where they were obtained with a program of Alexei Filinov. The HF and CI energies show a clear trend. The poor agreement with PIMC could be caused by the screening parameter in the Coulomb interaction. However, it is unclear why the approximately linear trend (that is also predicted by perturbation theory) for small λ is overestimated by PIMC. Primarily at larger λ, the CI and PIMC results become similar.

N	λ	HF	CI	PIMC
3	0.0	1.5671	1.5671	[1.5671]
	0.3	1.7792	1.7887	1.8287
	0.6	1.9808	1.9997	1.9749
	0.9	2.1740	2.2011	2.1908
	1.2	2.3607	2.3941	2.3878
	1.5	2.5423	2.5793	2.5769
4	0.0	2.0507	2.0507	[2.0507]
	0.5	2.5652	2.5756	2.8
	1.0	3.0443	3.0623	3.0375
	1.5	3.4966	3.5171	3.5077
	2.0	3.9277	3.9449	3.9385

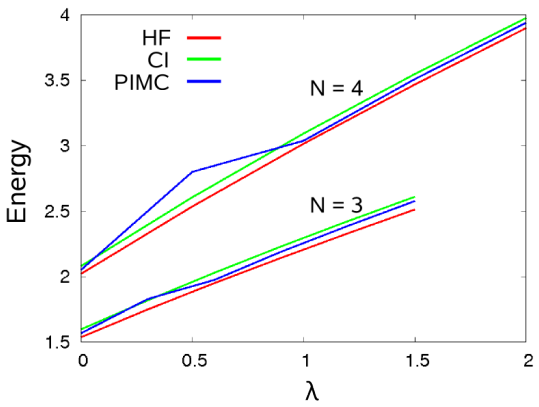

Figure 7.1.: *Comparison of the total energies of a 1D harmonic oscillator arising from the different canonical methods for $N_b = 15$ and $\beta = 2$. For the ideal systems, the energies in brackets were analytically computed [18]. In the graphic, for clarity the CI curves were shifted by 0.03 and the HF curves by -0.03.*

8. Dyson equation

The Dyson equation, invented 1948 by Freeman Dyson, has become a standard tool for the investigation of the correlated equilibrium state in terms of Green functions. In fact, the approach was feasible already in the late sixties and since then has been applied to almost all models of equilibrium many-body physics. The reason for this unusually easy access is the convolution structure of the Dyson equation, which in frequency space transforms into a simple multiplication. The Green function as well as the self-energies are thus obtained as solutions of algebraic equations – and not of integral equations. However, we will face the task of finding the Green function in time space, as this yields a natural starting point for the time-evolution in the next chapter. The numerical implementation explained below mainly follows the work of Nils Erik Dahlen, Robert van Leeuwen and Adrian Stan, who have presented self-consistent solutions of the Dyson equation in second Born and GW approximation a few years ago, see Refs. [38] and [39]. For GW, however, they did not publish their numerical method, wherefore the corresponding algorithm in this work has been independently derived.

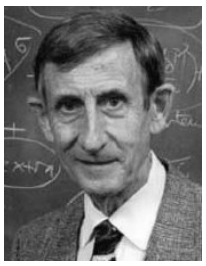

F. Dyson[1]

8.1. Self-consistent solution

Solution of the integral equation

In the following, a procedure for the self-consistent solution of the Dyson equation in integral form is derived. Let us recall its basis representation from section 3.3.2,

$$\mathbf{G}^M(\tau) \;=\; \mathbf{G}^0(\tau) \;+\; \int_0^\beta d\tau_1 \int_0^\beta d\tau_2 \; \mathbf{G}^0(\tau-\tau_1)\left[\mathbf{\Sigma}^M(\tau_1-\tau_2) - \delta(\tau_1-\tau_2)\;\mathbf{\Sigma}^0\right]\mathbf{G}^M(\tau_2) \tag{8.1}$$

$$\;=\; \mathbf{G}^0(\tau) \;+\; \int_0^\beta d\tau_1 \int_0^\beta d\tau_2 \; \mathbf{G}^0(\tau-\tau_1)\;\mathbf{\Sigma}^{\mathrm{corr}}(\tau_1-\tau_2)\;\mathbf{G}^M(\tau_2)\,. \tag{8.2}$$

The self-consistent solution is found by an iteration procedure starting from the solution of the uncorrelated Dyson equation. We choose to start from the Hartree-Fock solution, which is why the undisturbed Green function in the interval $[-\beta, 0]$ is set up by the Hartree-Fock orbital energies and occupation numbers

$$G^0_{ij}(\tau) \;=\; \delta_{ij}\; n_i\; \mathrm{e}^{-(\epsilon_i-\mu)\tau} \;=\; \frac{\delta_{ij}}{\mathrm{e}^{(\beta+\tau)(\epsilon_i-\mu)} \pm \mathrm{e}^{\tau(\epsilon_i-\mu)}}\,. \tag{8.3}$$

The HF-Green function is diagonal since it does not contain any correlation contributions. One could also start from a correlated Green function[2], which requires a slight modification of the

[1] `http://img167.imageshack.us/img167/6613/dysonpx4.jpg`

[2] This is e.g. done in [40] in frequency space, where T-matrix calculations are performed starting from a Green function in GW approximation.

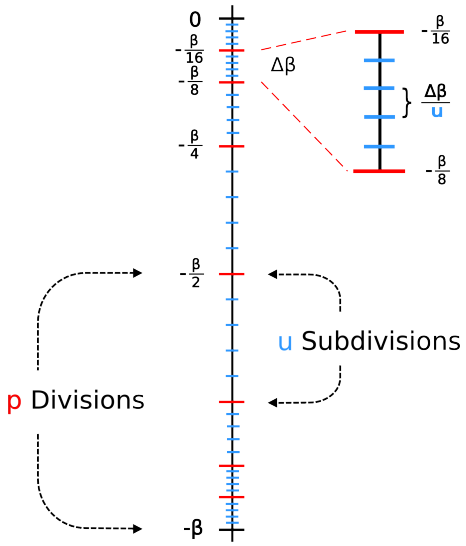

Figure 8.1: ***Uniform power mesh (UPM)*** *on which the Matsubara Green function and self-energy is represented. First the interval* $[-\beta, 0]$ *is divided in* $2p$ *divisions scaling by powers of two, then each one is subdivided into* u *equally spaced segments. Thus the total number of grid points is* $N_\tau = 2pu + 1$*, being dense around the end points. In the graphic the UPM is visualized for p=4 and u=5.*

following algorithm. The shift of the HF-energies by the chemical potential again is not necessary, but introduced consistent to (6.19). It causes the undisturbed Green function G^0_{ii} at $\tau = 0^-$ to be close to one if the averaged occupation of the orbital i is close to one and zero if it is close to zero. Because of the anti-periodicity of the Green function, at $\tau = -\beta$ it is the other way round. Hence, the slope of the time dependent matrix elements is large at $\tau = 0^-$ for occupied orbitals and at $\tau = -\beta$ for unoccupied ones.
To represent the Green function in an economical way we use a special grid, that is dense around the endpoints of the interval and sparse in the middle. It is called "Uniform power mesh" (UPM) and its properties can be seen in Fig. 8.1. The drawback of this saving is that the well known and easy integral formulas for equidistant grids can not be applied. Further, care must be taken when evaluating quantities at differences of grid points $\Delta\tau = \tau_1 - \tau_2$, since it does not necessarily correspond to an existing point on the grid. To this end, interpolations should be used when computing quantities at $\Delta\tau$.[3]

The Dyson equation in basis representation is an integral equation of the second Fredholm type [27] with the peculiarity, that it involves discrete matrices rather than single continuous functions. However, the solution method we use, the Nystrom method [27], is not affected thereof. It provides the conversion of an integral equation into a linear system of equations. As a first step we approximate the integral by an appropriate quadrature rule on N_τ gridpoints

$$\int_a^b f(s)\, ds \;=\; \sum_{q=0}^{N-1} \nu^{(q)} f(s^{(q)})\,. \tag{8.4}$$

Reference [27] recommends Gaussian integration for that, and one could really think about representing the quantities on the imaginary axis at the abscissas of the Laguerre integration, which has the weight function e^{-x} similar to the undisturbed Green function. This could further reduce the number of needed gridpoints. However, for the present approach we skip that since we already invented an appropriate mesh, whereupon for most of the times we will use the generalized trapezoidal rule. Here, the abscissas are the UPM grid-points and the (positive) weights are given

[3] In the code, the interpolation routines from the *gsl*-library are used, which provide linear,cubic and Akima spline interpolation.

by

$$\nu^{(q)} = \frac{1}{2} \cdot \begin{cases} \tau^{(0)} - \tau^{(1)} & \text{for } q = 0 \\ \tau^{(N_\tau-2)} - \tau^{(N_\tau-1)} & \text{for } q = N_\tau - 1 \\ \tau^{(q-1)} - \tau^{(q+1)} & \text{otherwise} \end{cases} \qquad \Big[\text{ Trapezoidal } \Big] . \tag{8.5}$$

Also, a generalized Simpson rule has been attempted, which in reference [41] is referred to as "Brun's rule". Again the abscissas are the (odd number of) UPM points and the weights read

$$\nu^{(q)} = \frac{1}{6} \cdot \begin{cases} 3\tau^{(0)} - 4\tau^{(1)} + \tau^{(2)} & \text{for } q = 0 \\ -3\tau^{(N_\tau-3)} + 4\tau^{(N_\tau-2)} - \tau^{(N_\tau-1)} & \text{for } q = N_\tau - 1 \\ -\tau^{(q-2)} + 4\tau^{(q-1)} - 4\tau^{(q+1)} + \tau^{(q+2)} & \text{for } q \text{ even} \\ -4\tau^{(q-1)} + 4\tau^{(q+1)} & \text{for } q \text{ odd} \end{cases} \qquad \Big[\text{ Simpson } \Big] . \tag{8.6}$$

If we apply these discretization schemes to the Dyson equation (8.1) and use $G^0_{ij}(\tau) =: \delta_{ij} G^0_i(\tau)$ we obtain [18]

$$\begin{aligned} &\delta_{ij} G^0_i(\tau^{(p)}) \\ &= G^M_{ij}(\tau^{(p)}) + \sum_k \int_0^\beta d\tau_2 \left[\int_0^\beta d\tau_1 \; G^0_i(\tau^{(p)} - (\tau_1 - \beta)) \; \Sigma^c_{ik}(\tau_1 - \tau_2) \right] G^M_{kj}(\tau_2) \\ &= G^M_{ij}(\tau^{(p)}) + \sum_k \in^0_{-\beta} d\tau_2 \left[\int_0^\beta d\tau_1 \; G^0_i(\tau^{(p)} - (\tau_1 - \beta)) \; \Sigma^c_{ik}(\tau_1 - (\tau_2 + \beta)) \right] G^M_{kj}(\tau_2 + \beta) \\ &\approx G^M_{ij}(\tau^{(p)}) - \sum_k \sum_{q=0}^{N_\tau - 1} \nu^{(q)} \left[\int_0^\beta d\tau_1 \; G^0_i(\tau^{(p)} - (\tau_1 - \beta)) \; \Sigma^c_{ik}(\tau_1 - (\tau^{(q)} + \beta)) \right] G^M_{kj}(\tau^{(q)}) \\ &= \sum_k \sum_{q=0}^{N_\tau - 1} \Big[\delta_{ik}\delta_{pq} \; - \; \nu^{(q)} F_{ik}(\tau_p, \tau_q) \Big] \, G^M_{kj}(\tau^{(q)}) \, . \end{aligned} \tag{8.7}$$

In the last step the convolution integrals $F_{ij}(\cdot, \cdot)$ have been defined, whose evaluation proceeds in the same way as before:

$$\begin{aligned} F_{ij}(\tau^{(p)}, \tau^{(q)}) \; &:= \; \int_0^\beta d\tau_1 \; G^0_i(\tau^{(p)} - (\tau_1 - \beta)) \; \Sigma^c_{ij}(\tau_1 - (\tau_2 + \beta)) \\ &= \; \int_{-\beta}^0 d\tau \; G^0_i(\tau^{(p)} - \tau) \; \Big[\Sigma^{\text{corr}}_{ij}(\tau - \tau^{(q)}) + \delta(\tau - \tau^{(q)}) \; \Big(\Sigma^{\text{HF}}_{ij} - \Sigma^0_{ij} \Big) \Big] \\ &= \; G^0_i(\tau^{(p)} - \tau^{(q)}) \Big(\Sigma^{\text{HF}}_{ij} - \Sigma^0_{ij} \Big) + \int_{-\beta}^0 d\tau \; G^0_i(\tau^{(p)} - \tau) \; \Sigma^{\text{corr}}_{ij}(\tau - \tau^{(q)}) \\ &\approx \; G^0_i(\tau^{(p)} - \tau^{(q)}) \Big(\Sigma^{\text{HF}}_{ij} - \Sigma^0_{ij} \Big) + \sum_{s=0}^{N_\tau - 1} \nu^{(s)} \; G^0_i(\tau^{(p)} - \tau^{(s)}) \; \Sigma^{\text{corr}}_{ij}(\tau^{(s)} - \tau^{(q)}) \, . \end{aligned} \tag{8.8}$$

Equation (8.7) is already the linear system aimed to receive. By defining

$$A_{(ip),(kq)} = \delta_{ik}\delta_{pq} - \nu^{(q)} F_{ik}(\tau^{(p)}, \tau^{(q)}) , \tag{8.9}$$

$$x^{(j)}_{(kq)} = G^M_{kj}(\tau^{(q)}) , \tag{8.10}$$

$$b^{(j)}_{(ip)} = \delta_{ij} G^0_{ij}(\tau^{(p)}) , \tag{8.11}$$

we can present it in the standard form

$$\mathbf{A} \cdot \mathbf{x}^{(j)} = \mathbf{b}^{(j)} , \qquad \sum_{kq} A_{(kq),(ip)} \; x^{(j)}_{(kq)} = \; b^{(j)}_{(ip)} . \tag{8.12}$$

In the code this linear system is solved with the Lapack routine *dgesv*.

Algorithm

The self-consistent solution of the Dyson equation proceeds in the following steps:

(i.) Set up the reference Green function $\mathbf{G}^0$ on the UPM.

(ii.) Calculate the self-energy in the chosen approximation as explained in the following section.

(iii.) Compute the convolution-integrals, set up the linear system (8.12) and solve it.

(iv.) Return to (ii.) unless the Green function has not converged, i.e. unless the averaged deviation δ between two successive cycles counted by ν,

$$\delta = \frac{1}{N_b^2 N_\tau} \sum_{p=0}^{N_\tau - 1} \sum_{ij} \left| G^{M,(\nu)}_{ij}(\tau^{(p)}) - G^{M,(\nu-1)}_{ij}(\tau^{(p)}) \right| , \tag{8.13}$$

is smaller than a chosen value. Typically, we choose δ in between 10^{-5} and 10^{-10}.

At each cycle also the following quantities are calculated:

- **Energies** – from reference [18]

$$E_{\text{single}} = \sigma \; \text{Tr} \left\{ \mathbf{h}^0 \mathbf{G}^M(0^-) \right\} + \mu N , \tag{8.14}$$

$$E_{\text{HF}} = \frac{\sigma}{2} \; \text{Tr} \left\{ \mathbf{\Sigma}^{\text{HF}} \mathbf{G}^M(0^-) \right\} , \tag{8.15}$$

$$E_{\text{corr}} = -\frac{\sigma}{2} \int_{-\beta}^{0} d\tau \; \text{Tr} \left\{ \mathbf{\Sigma}^{\text{corr}}(\tau) \mathbf{G}^M(-\beta - \tau) \right\} . \tag{8.16}$$

  The kinetic and potential energy as well are calculated by a trace over the density matrix $\mathbf{G}^M(0^-)$, where the contribution from the chemical potential is counted in the potential part.

- **Symmetry** – yields a test for the accuracy of the calculated Green function:

$$\text{Sym} = \frac{2}{N_b(N_b - 1)} \frac{1}{N_\tau} \sum_{p=0}^{N_\tau - 1} \sum_{i<j} \left| G^M_{ij}(\tau^{(p)}) - G^M_{ji}(\tau^{(p)}) \right| . \tag{8.17}$$

In addition, the particle number is determined as the trace of the density matrix $G_{ij}^{M}(0^{-})$. Roughly speaking, it should not deviate more than one percent from the chosen particle number N. However, in the grand-canonical ensemble especially for high temperatures and strong interactions – where correlation becomes more important – the procedure can naturally become unstable with regard to N. A way out would be to adjust the chemical potential, that during the whole algorithm is fixed to the HF value. Unfortunately, there is no easy way to do so unless one works in frequency space, where the relation

$$\int A(\omega)d\omega = N, \quad \text{with} \qquad A(\omega) \;=\; G(\omega)f(\omega,\mu) \tag{8.18}$$

can be used.

8.2. Calculation of the self-energies

Now, as the general solution of Dyson's equation has been recapitulated, we focus on the calculation of the most important ingredient, the self-energy.

Hartree-Fock approximation

The Hartree-Fock self-energy is local in time $\Sigma_{ij}^{\mathrm{HF}}(\tau) = \delta(\tau)\Sigma_{ij}^{\mathrm{HF}}$ and equals the mean-field part of the Fock matrix (6.7)

$$\Sigma_{ij}^{\mathrm{HF}} \;=\; \sum_{kl}(\sigma\; w_{ij,kl} \pm w_{ik,lj})\; G_{kl}^{M}(0^{-}) \tag{8.19}$$

The reference self-energy $\mathbf{\Sigma}^{0}$ is evaluated in the same way with $\mathbf{G}^{M}(0^{-})$ replaced by the reference Green function $\mathbf{G}^{0}(0^{-})$, which equals the Hartree-Fock density matrix $\boldsymbol{\rho}^{HF}$ in our case.

Second Born approximation

The formula for the Second Born self-energy is easily obtained by a transformation of (4.1) to the imaginary branch

$$\Sigma_{ij}^{2ndBorn}(\tau) \;=\; \sum_{klmnrs} w_{ik,ms}(\sigma\; w_{lj,rn} \pm w_{nj,rl})\; G_{kl}^{M}(\tau)\; G_{mn}^{M}(\tau)\; G_{rs}^{M}(\beta-\tau) \tag{8.20}$$

As always, $\sigma = 1$ for the spin-polarized case and $\sigma = 2$ in the RHF case.

Though straightforward and very easy to implement, in second Born approximation the determination of the self-energy takes most of the time. It is therefore instructive to introduce a cutoff-parameter and perform the sum only if the absolute value of the Green function is bigger than this cutoff. By reordering the summation we could also query the two-electron integrals for their magnitude. The cutoff-parameter is usually chosen between 10^{-4} to 10^{-10} to yield a remarkable gain in speed while merely changing the final result.

Another idea that came up was to perform the six summations in (8.20) with Monte-Carlo integration. It would have the advantage that any higher order Feynman diagram, whose direct calculation until now would be too demanding, could be included since Monte-Carlo scales only

linearly with the dimension of the summation. Unfortunately, the first tests succeeded only for the Hartree-Fock approximation, while the second Born self-energy was underestimated by many orders of magnitude. The reason for this is the highly oscillating behavior of the integrand, which causes the importance sampling to fail. However, it could be possible to find an adequate ordering scheme to diminish these oscillations.

GW approximation

Let us recall the basis representation of the integral equation for the non-singular part of the screened interaction $\widetilde{W}$ (4.22)

$$\widetilde{W}_{ij,kl}(\tau) \; - \sum_{abcd} \int_{-\beta}^{0} d\bar{\tau} \; \widetilde{W}_{ij,da}(\bar{\tau}) \; P_{ab,cd}(\tau - \bar{\tau}) \; w_{bc,kl} \; = \sum_{abcd} w_{ij,ad} \; P_{ab,cd}(\tau) \; w_{bc,kl} \tag{8.21}$$

For solving this equation we could proceed the same way as above in the Dyson equation and we have done so, but the problem here is the increased numerical effort due to the four indices of the two-particle quantities. We had to solve N_b^2 times a linear system of equations of dimension $N_b^2 N_\tau \times N_b^2 N_\tau$, so that only a small number of basis functions were accessible.

The idea to improve this scheme is to represent the integral equation in an appropriate basis. First, we mention that any two particle quantity is defined in a basis of generally non-orthogonal product states

$$\begin{aligned} w_{ij,kl} \; &= \iint d\mathbf{x} \; d\mathbf{x}' \; \underbrace{\phi_i^*(\mathbf{x}) \; \phi_j(\mathbf{x})} \; w(\mathbf{r},\mathbf{r}') \; \underbrace{\phi_k^*(\mathbf{x}') \; \phi_l(\mathbf{x}')} \\ &= \iint d\mathbf{x} \; d\mathbf{x}' \qquad \psi_{Q1}(\mathbf{x}) \quad w(\mathbf{r},\mathbf{r}') \qquad \psi_{Q2}(\mathbf{x}') \\ &=: \; w_{Q1,Q2} \, , \end{aligned} \tag{8.22}$$

and can also be represented as a one-particle quantity in the product basis $\{\psi_Q\} = \{\phi_i \phi_j\}$.

We will transform the integral equation to the basis, in which the bare Coulomb interaction is diagonal.[4] Therefore, we diagonalize the matrix $\mathbf{w}$, what is possible since it is symmetric, and write it as the matrix product

$$\mathbf{w} = \mathbf{U} \; \hat{\mathbf{w}} \; \mathbf{U}^T \, , \tag{8.23}$$

where the diagonal matrix $\hat{\mathbf{w}}$ contains the eigenvalues and the orthogonal matrix $\mathbf{U}$ the respective eigenvectors. We will denote each quantity represented in the new basis with a hat.

We rearrange the indices of the polarization $P_{ab,cd} \longrightarrow \bar{P}_{da,bc}$ and write (8.21) as

$$\widetilde{W}_{Q1,Q2}(\tau) \; - \sum_{Q3,Q4} \int_{-\beta}^{0} d\bar{\tau} \; \widetilde{W}_{Q1,Q3}(\bar{\tau}) \; \bar{P}_{Q3,Q4}(\tau - \bar{\tau}) \; w_{Q4,Q2} \; = \sum_{Q3,Q4} w_{Q1,Q3} \; \bar{P}_{Q3,Q4}(\tau) \; w_{Q4,Q2} \, , \tag{8.24}$$

where $Q1 = (ij)$, $Q2 = (kl)$, $Q3 = (da)$, $Q4 = (bc)$. This equation is transformed to the new basis by applying $\mathbf{U}$ from the right, $\mathbf{U}^T$ from the left and inserting $\mathbf{U}\mathbf{U}^T = \mathbf{1}$ in between each

[4] The motivation for a change of the basis came from Robert van Leeuwen and Adrian Stan during their stay at Kiel in may 2008. Yet they use another basis in which the overlap matrix is diagonal, i.e. an orthonormal basis.

matrices:

$$\widehat{\widetilde{W}}_{Q1,Q2}(\tau) \;-\; \sum_{Q3} \int_{-\beta}^{0} d\bar{\tau}\; \widehat{\widetilde{W}}_{Q1,Q3}(\bar{\tau})\; \hat{\tilde{P}}_{Q3,Q2}(\tau-\bar{\tau})\; \hat{w}_{Q2,Q2} \;=\; \hat{w}_{Q1,Q1}\; \hat{\tilde{P}}_{Q1,Q2}(\tau)\; \hat{w}_{Q2,Q2} \tag{8.25}$$

Note that one summation on the left hand side and both summations on the right hand side vanish due to the diagonality of $\hat{\mathbf{w}}$. This saves time when computing the coefficients and inhomogenities of the linear system we are going to set up.

We insert $\widehat{\widetilde{W}}_{Q1,Q2}$ under the integral and approximate it by a suitable quadrature rule, e.g. (8.5),

$$\sum_{Q3} \sum_{q=1}^{N_\tau} \Big[\delta_{Q2,Q3}\; \delta_{p,q} \;-\; \nu^{(q)} \hat{\tilde{P}}_{Q3,Q2}(\tau^{(p)}-\tau^{(q)})\; \hat{w}_{Q2}\Big]\; \widehat{\widetilde{W}}_{Q1,Q3}(\tau^{(q)}) \;=\; \hat{w}_{Q1}\; \hat{\tilde{P}}_{Q1,Q2}(\tau^{(p)})\; \hat{w}_{Q2}\,, \tag{8.26}$$

to get the form of a linear system of equations:

$$\sum_{Q3} \sum_{q=1}^{N_\tau} A^{(Q2,p)}_{(Q3,q)}\; x^{(Q1)}_{(Q3,q)} \;=\; b^{(Q1,Q2,p)} \tag{8.27}$$

with

$$A^{(Q2,p)}_{(Q3,q)} \;=\; \delta_{Q2,Q3}\; \delta_{p,q} \;-\; \nu^{(q)} \hat{\tilde{P}}_{Q3,Q2}(\tau^{(p)}-\tau^{(q)})\; \hat{w}_{Q2}\,, \tag{8.28}$$

$$b^{(Q1,Q2,p)} \;=\; \hat{w}_{Q1}\; \hat{\tilde{P}}_{Q1,Q2}(\tau^{(p)})\; \hat{w}_{Q2}\,, \tag{8.29}$$

$$x^{(Q1)}_{(Q3,q)} \;=\; \widehat{\widetilde{W}}_{Q1,Q3}(\tau^{(q)})\,. \tag{8.30}$$

After solving this linear system we transform $\widehat{\widetilde{\mathbf{W}}}$ back to the original basis, set up the self-energy according to (4.23) and solve the Dyson equation.
Another word has to be said about the evaluation of the polarizabilty at differences of grid points. In the original basis we could simply use the symmetry properties of the Green function as already applied in the solution of the Dyson equation. In the transformed basis this is no longer possible, since in the product basis the index-rearranged polarizability can not be represented as a product of Green functions. Thus we have to interpolate it directly, where the relation

$$\hat{\tilde{P}}_{Q1,Q2}(\tau) \;=\; \hat{\tilde{P}}_{Q2,Q1}(\beta-\tau) \tag{8.31}$$

is used to relate the values on the positive imaginary branch to that interpolated on the negative.

Up to this point, computing time is saved in the calculation of the coefficients and the inhomogeneities, but even more time is lost by transforming the polarization $\bar{\mathbf{P}}$ to the new basis and the screened interaction $\widehat{\widetilde{\mathbf{W}}}$ back ($\mathbf{w}$ has to be diagonalized only once). Nevertheless, the dimension of the linear system is still the same as in equation (8.21). So why do we proceed in this way?
The answer is that in the new basis an approximation can be very easily derived. Let us consider again (8.25). If w_{Q1} is smaller than a chosen value, we can directly set $W_{Q1,Q2} = 0$. Further, if w_{Q2} gets small, we can set the inhomogeneity equal to 0 and solve the homogeneous system only once. This yields a remarkable reduction of the size of the linear system and additionally time is saved in the transformation to the new basis. In Fig. 8.2 the approximation scheme is visualized

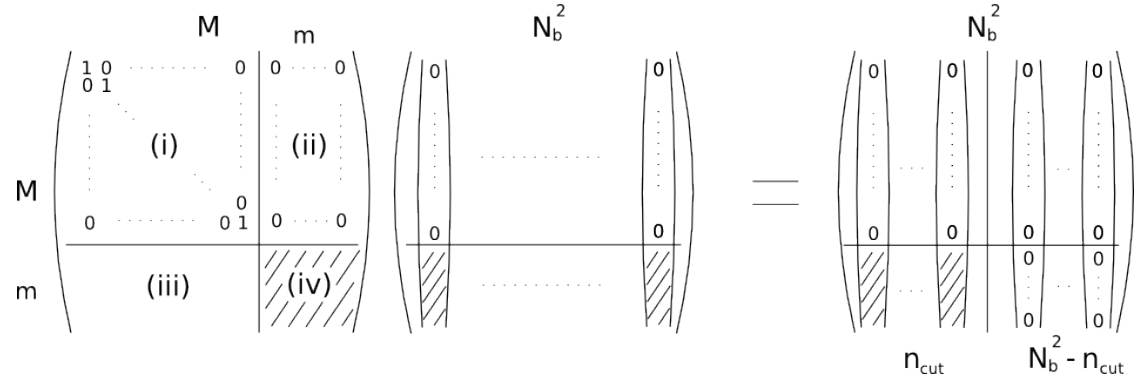

Figure 8.2.: *Approximation scheme for the solution of the linear system of equations* $\mathbf{A} \cdot \mathbf{x} = \mathbf{b}$ *for the screened interaction. The dimension of the primary system is* $M = N_b^2 N_\tau$ *and it has to be solved for* N_b^2 *inhomogenities. After choosing a cutoff parameter, all non-diagonal elements of the submatrices (i) and (ii) and the first* $M - m$ *elements of the inhomogenities vanish and a system (iv) of dimension* $m = n_{cut} N_\tau$ *remains, that has to be solved* n_{cut} *times plus one time for the homogeneous system. The submatrix (iii) is non-zero, but as the first equations fix the first* $M - m$ *components of the solution to zero it has not to be evaluated.*

and further explained. In Tab. 8.1, the saving for the NO basis functions of the 1D harmonic oscillator is shown and right aside, in Tab. 8.2 the remarkable dependence of the total energy on the cutoff parameter is examined.

In summary, we have derived a scheme that avoids the calculation of many small matrix elements in the screened interaction and thus considerably shortens the calculations. It is able to replace semi-empirical approximation schemes, as e.g. the one used in [42] to study quantum transport.

N_b	N_b^2	cutoff	n_{cut}	$\hat{\approx} N_b$
15	225	10^{-15}	112	11
15	225	10^{-5}	29	5
25	625	10^{-15}	317	18
25	625	10^{-5}	49	7

Table 8.1.: *Saving for the 1D harmonic oscillator for different cutoff-parameters. The last column gives the number of basis functions, on which the full system given by the first column is roughly mapped.*

cutoff	n_{cut}	E_{tot}
0 (full GW)	64	3.0077
0.01	22	3.0077
0.1	18	3.0079
0.5	8	3.0176
1.5	3	3.0762
$\to \infty$ (HF)	0	3.1627

Table 8.2.: *Total energy for different cutoff-parameters for two particles in a two-dimensional harmonic oscillator with* $N_b = 8$ *NOs at* $\beta = 50$ *and* $\lambda = 1.0$ *and UPM parameters* $p = 10$ *and* $u = 3$. *The energy deviates from the exact result at larger cutoffs than* 0.1. *Even with very few basis functions GW yields reasonable results.*

8.3. Ionization energies from the Extended Koopmans theorem

In the introduction we promised that the Green function formalism also provides us ionization energies and electron affinities. Yet earlier, on Hartree-Fock level, we already have access to these quantities. The general approach is thereby the same: Given the equilibrium Green function or

the Hartree-Fock energies of a N-particle system, try to gather information on the energies of a $N \pm 1$ particle state. The difference yields the removal energy or the electron affinity.

At first, let us have a look at the Koopmans theorem [7]. It states that the energy needed to ionize a particle is simply the negative of its Hartree-Fock orbital energy that is assumed to be negative. Similarly, the energy to add a further particle to an unoccupied level is also given by the negative HF-energy of this orbital that now has a positive energy. The assumption made here is that the HF-orbitals of the $N \pm 1$-particle state are identical to those of the N-particle state, which results in neglecting orbital relaxation effects ("frozen orbital approximation"). In addition, it does not account for correlation effects. Fortunately, both effects often cancel, so that the Koopmans theorem often yields good results for the ionization energy. However, the results for electron affinities are usually poor. In the following, we will concentrate on ionization.
The Koopmans theorem in the presented form and also its extended version below are at first only applicable to confinements, whose bound states have negative energy and whose scattering states have positive energy – like the Coulomb potential or the adjusted box potential. For any other confinement, such as the harmonical oscillator, one must choose an energy point, that shall mark the crossing from bound to continuum states. Although this principle is only natural – model atoms can always be ionized – it is not clear at which value this energy should be chosen. In the best case one can adjust it to experiments or to predictions of more advanced models.

Let us turn to the extended Koopmans theorem as described in Refs. [43]. We define a $N-1$ particle state $|\xi_i^{N-1}\rangle = \int d\mathbf{x}\, u_i^*(\mathbf{x})\, \hat{\Psi}(x)\, |\Phi_0^N\rangle$, where $|\Phi_0^N\rangle$ is the groundstate wavefunction. Thus the following result is restricted to the zero-temperature case. The function $u_i(\mathbf{x})$ is determined by requiring that $\langle \xi_i^{N-1}|\hat{H}|\xi_i^{N-1}\rangle$ is stationary with respect to variations in $u_i(\mathbf{x})$, with the constraint that $|\xi_i^{N-1}\rangle$ is normalized. After a straightforward calculation we obtain

$$\begin{aligned} 0 &= \frac{\delta}{\delta u^*(\mathbf{x}_1)} \left[\langle \xi_i^{N-1}|\hat{H}|\xi_i^{N-1}\rangle - \lambda_i \langle \xi_i^{N-1}|\xi_i^{N-1}\rangle \right] \\ &= \int d\mathbf{x}\; u(x) \left[-\langle \Phi_0^N|\hat{\Psi}^\dagger(\mathbf{x}) \Big[\hat{\Psi}(\mathbf{x}_1), \hat{H}\Big]|\Phi_0^N\rangle - (\lambda_i - E_0^N + \mu N)\, \rho(\mathbf{x}_1, \mathbf{x}) \right] . \end{aligned} \tag{8.32}$$

The function $\rho(\mathbf{x}, \mathbf{x}')$ is the generalized density obtained from the equilibrium Green function by $\rho(\mathbf{x}, \mathbf{x}') = G^M(\mathbf{x}, \mathbf{x}', 0^-)$.

We can now use the fact that the operator in the finite temperature formalism have the time-dependence $\hat{\Psi}(\mathbf{x}, \tau) = e^{\hat{H}\tau} \hat{\Psi}(\mathbf{x}) e^{-\hat{H}\tau}$ and that $-\partial_\tau \Psi(\mathbf{x}, \tau)\Big|_{\tau=0^-} = [\Psi(\mathbf{x}), \hat{H}]$ to write

$$\begin{aligned} -\partial_\tau G^M(\mathbf{x}_1, \mathbf{x}, \tau)\Big|_{\tau=0^-} &= -\partial_\tau \left\langle \Phi_0^N|\hat{\Psi}^\dagger(\mathbf{x})\, \hat{\Psi}(\mathbf{x}_1, \tau)|\Phi_0^N\right\rangle \Big|_{\tau=0^-} \\ &= \langle \Phi_0^N|\hat{\Psi}^\dagger(\mathbf{x}) \Big[\hat{\Psi}(\mathbf{x}_1, \tau), \hat{H}\Big]|\Phi_0^N\rangle \equiv \Delta(\mathbf{x}_1, \mathbf{x}) . \end{aligned} \tag{8.33}$$

Using this definition we can rewrite (8.32) according to

$$\int d\mathbf{x}\; \Delta(\mathbf{x}_1, \mathbf{x})\, u(\mathbf{x}) = -(\lambda_i - E_0^N + \mu N) \int d\mathbf{x}\; \rho(\mathbf{x}_1, \mathbf{x})\, u(\mathbf{x}) \tag{8.34}$$

$$= -\tilde{\lambda}_i \int d\mathbf{x}\; \rho(\mathbf{x}_1, \mathbf{x})\, u(\mathbf{x}) . \tag{8.35}$$

If we now interpret the states $|\xi^{N-1}\rangle$ as approximations to the $N-1$ particle eigenstates $|\Phi_i^{N-1}\rangle$, and the λ_i as approximations to the eigenvalues $E_i^{N-1} - \mu(N-1)$, the eigenvalues $\tilde{\lambda}_i$ of the

generalized eigenvalue problem (8.34) become

$$\tilde{\lambda}_i \;=\; -(E_i^{N-1} - E_0^N) - \mu\,. \tag{8.36}$$

Thus the ionization potentials, that determine the energy needed to remove a particle from the state i, are given by $(E_i^{N-1} - E_0^N) = \lambda_i - \mu$. When the Hartree-Fock Green function is inserted, the scheme reduces to the normal Koopmans theorem and reproduces the HF-energy eigenvalues.

In basis representation Eq. (8.34) transforms into a matrix equation.

$$\Delta\, u \;=\; \rho\, u\, \tilde{\lambda}\,, \tag{8.37}$$

where

$$\rho_{ij} \;=\; G_{ij}^M(0^-)\,, \tag{8.38}$$

$$\Delta_{ij} \;=\; -\partial_\tau\, G^M(\tau)\Big|_{\tau=0^-}\,. \tag{8.39}$$

In the code the derivative is found numerically using a spline interpolation as it is available in the library *gsl*. This can be also used as a valid test for the sufficiency of the UPM discretization. If the grid is too sparse, the eigenvalues from the extended Koopmans theorem applied to the HF Green function deviate from the HF orbital energies. Alternatively, Δ can be obtained from the Dyson equation

$$\Delta \;=\; -\partial_\tau\, \mathbf{G}^M(\tau)\Big|_{\tau=0^-} \;=\; \mathbf{h}\,\mathbf{G}^M(0^-) \;+\; \int_0^\beta d\bar{\tau}\; \mathbf{\Sigma}(\tau-\tau')\,G(\tau')\Big|_{\tau=0^-}\,. \tag{8.40}$$

8.4. Application

Convergence behavior

The self-consistent Matsubara Green function depends on several quantities. The most important thereby is the number of basis functions – especially in view of later nonequilibrium calculations – that should be of course appropriate to model the analytical form of the Green function. Another general quantity in 1D calculations is the screening parameter α in the Coulomb interaction,

$$w(x,x') \;=\; \frac{\lambda}{\sqrt{(x-x')^2+\alpha^2}} \tag{8.41}$$

At first glance, one could say that results should be independent of α and that the screened interaction should be near the "real" Coulomb interaction, i.e $\alpha = 0$. However, in a 1D calculation this is not physically reasonable, as a small α does not allow the particles to pass each other. More theoretically, the sense of this particular interaction should be clarified, since it is in general not meaningful just to change the dimension of a certain interaction, as is done here by conversion of the 3D Coulomb interaction (remember that the 3D Coulomb interaction originates from the solution of the Poisson equation, which in 1D is given by $|x|$). However, our intention by performing 1D calculations is to model real systems, and in this view the introduced interaction term should be reasonable.
The third considered quantity is the cutoff-parameter explained in section 8.2, that is indispens-

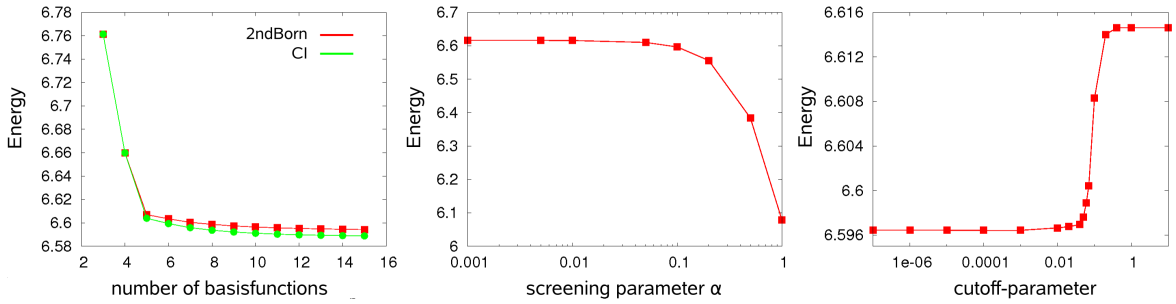

Figure 8.3.: *Convergence properties of the Dyson equation, considered are the total energies of $N = 2$ particles in a one-dimensional harmonic confinement, the UPM parameters are $p = 20$ and $u = 6$. (a) Total energy against the number of basisfunctions. (b) Convergence in dependence of the screening parameter α in the Coulomb interaction. (c) Convergence in dependence of the cutoff-parameter.*

able in doing second Born calculations. The convergence behavior of all these parameters on the second Born level is examined in Fig. 8.3.

Equilibrium properties of quantum dots

The investigations of quantum dots and quantum well heterostructures has attained a great interest in theoretical physics and nanotechnology. The difference to bulk semiconductors is the confinement that traps the particles. This confinement can be approximated by a harmonic oscillator potential [44]. The main concern of the actual theoretical description thereby lies on the transport properties under action of external fields. Here we will focus on the equilibrium properties of two- and three-dimensional quantum dots in the groundstate, whereby our intention is not to provide large tabulars (they may already exist, except for GW), but rather to test the introduced methods in higher dimensions and to show their interplay and relative differences.
In Tab. 8.3 we present the groundstate total energies for a two dimensional quantum dot with $N = 2$ particles. Due to the Ritzian principle, all the methods yield a lower energy than Hartree-Fock, except for $\lambda = 1$, where the unrestricted Hartree-Fock procedure converges to the restricted solution. This may be avoided if further initial density matrices are tested. The benchmark results are given by Configuration Interaction. Second Born approaches the exact solution and for $\lambda = 1$ it is able to account for 88% of the correlation energy, being defined as the difference between HF and CI. GW underestimates the exact solution, indicating a trend that has already been found in [39].
The three-dimensional quantum dot, whose electron integrals were calculated by the formulas in Appendix A, shows a similar trend, see Tab. 8.4. However, there the GW result behaves as favored and stays beyond the one from CI. We may explain the reason for the different behavior of GW in 2D and 3D. Obviously, in lower dimensions the screening gets stronger – mention the one dimensional case, where it is set up on a line – what results in an underestimated interaction

λ	RHF	UHF	2ndBorn	GW	CI
1	3.162	3.162	3.030	2.964	3.012
2	4.185	4.034	3.792	3.630	3.732

Table 8.3.: *Total energies of $N = 2$ spin-restricted electrons trapped in a two-dimensional quantum dot at $\beta = 50$. As basisfunctions we use again $N_b = 25$ NOs and the self-energy cutoff parameter is 10^{-5}. The electron integrals were calculated by Karsten Balzer.*

λ	RHF	UHF	2ndBorn	GW	CI
1	3.769	3.769	3.743	3.735	3.731
2	4.495	4.495	4.424	4.406	4.360

Table 8.4.: *Total energies of $N = 2$ spin-restricted electrons in a three-dimensional quantum dot at $\beta = 50$. As basis functions we use again $N_b = 16$ NOs, where the highest radial quantum number is $n_r = 3$ and the angular momentum number $l \leq 1$. The self-energy cutoff parameter is again is 10^{-5}.*

energy. By taking the real Coulomb interaction, that is yielded as the solution of Poisson's equation in the respective dimension, this effect is likely to disappear.

Symmetry breaking of Hartree-Fock

The Hartree-Fock method is known to break the symmetry, see Ref. [32] and references therein. As mentioned before, this may result in a non radial-symmetric density, even if the Hamiltonian is invariant under rotations. At the example of the two-dimensional isotropic quantum dot, we show this unpleasant behavior. We consider $N = 4$ spin-restricted particles and the small number of $N_b = 10$ basisfunctions – CI is hard. For this case, we compare the Hartree-Fock density to the one arising from a CI calculation in Fig. 8.4. As predicted, the Hartree-Fock density has suffered a symmetry breaking, while CI yield an almost symmetric result. The slight deviations are probably caused by the small basis.
We also tried to obtain the densities in second Born and GW approximation. It is an open question, if the Random Phase approximation may cure the loss of symmetry (while we don't think it can). Unfortunately, none of the two methods converged, what may also be caused by the unphysical input from Hartree-Fock.

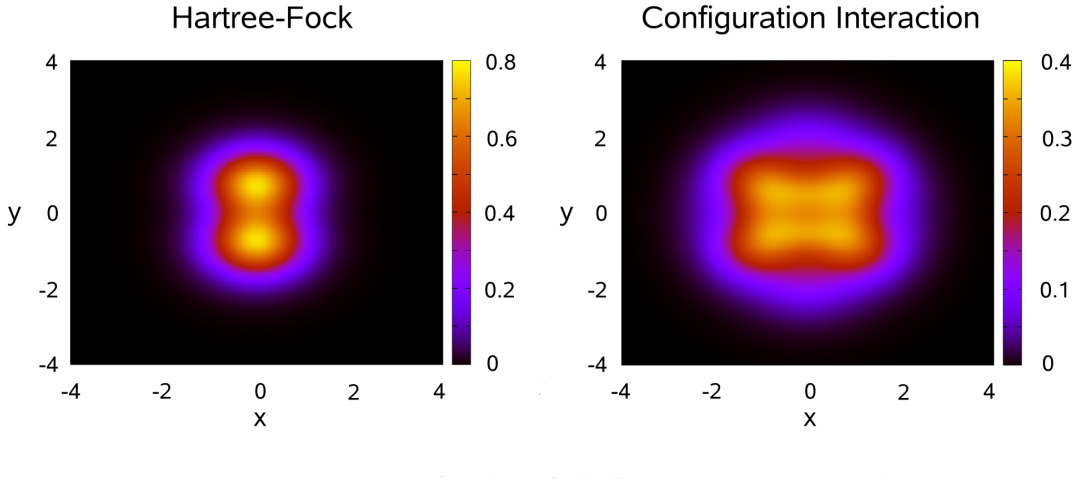

Figure 8.4.: *Example for a symmetry breaking in the Hartree-Fock method. Plotted are the densities for $N = 4$ spin-restricted particles in a two-dimensional quantum dot with $N_b = 10$ basisfunctions. The slight deviations from the symmetry in the Configuration Interaction method is likely to be caused by the small basis.*

9. Keldysh/Kadanoff-Baym equations

While the approach of Dyson's equation has a long history in physics and quantum chemistry, the time propagation of the so obtained initial state is a relatively unexplored topic. In fact, there are only a few existing codes, that solve the Kadanoff-Baym equations on the two-time plane, i.e. without further approximation schemes such as the Kadanoff-Baym ansatz [10]. For an overview see Ref. [16]. Among them is the first code from Danielewicz and a code from Bonitz and Semkat, which considers homogeneous systems [45] in a basis of plane waves, that are propagated only on the real part of the Keldysh contour, while the initial state is assumed to be either uncorrelated or furnished with certain initial correlations. Another one, of which our code is a descendant, has been recently implemented by Dahlen, van Leeuwen and Stan, see Refs. [46] and [47]. It is designed to treat inhomogeneous systems in coordinate space, that are initially in thermal equilibrium. The hopeless complexity of the Green function – as a four- to eight-dimensional quantity dependent on two spatial and two time variables – there is faced by an expansion in a basis, which in our case consists of Hartree-Fock orbitals.
In the following we recapitulate the numerical implementation in a similar way than in [18] and augment it by some slight extensions.


Leo Kadanoff [1]

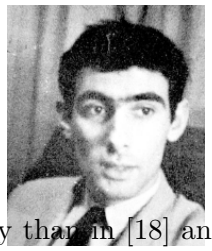
Gordon Baym[1]

9.1. Time-propagation of the NEGFs

The solution of the Keldysh/Kadanoff-Baym equations in basis representation, Eqs. (3.57-3.60), implies a determination of each nonequilibrium Green function on its respective two-time plane. By using the symmetry properties found in chapter 3, $\mathbf{G}^{\lessgtr}(t,t') = -[\mathbf{G}^{\lessgtr}(t',t)]^{\dagger}$, and the boundary condition on the time-diagonal, $\mathbf{G}^{>}(t,t) = -i + \mathbf{G}^{<}(t,t)$, we are able to restrict $\mathbf{G}^{<}(t,t')$ to the triangular $t \leq t'$ and $\mathbf{G}^{>}(t,t')$ to the region $t > t'$. As for the equilibrium Green function in the Dyson equation, we choose the lesser function to be represented on the time-diagonal, because it agrees with the density matrix. With these symmetry properties we can rewrite the equations of motions in the form

$$i\,\partial_t\,\mathbf{G}^{>}(t,t') \;=\; \mathbf{h}(t)\,\mathbf{G}^{>}(t,t') \;+\; \mathbf{I}_1^{>}(t,t')\,, \tag{9.1}$$

$$-i\,\partial_t\,\mathbf{G}^{<}(t',t) \;=\; \mathbf{G}^{<}(t',t)\,\mathbf{h}(t) \;+\; \mathbf{I}_2^{<}(t',t)\,, \tag{9.2}$$

$$i\,\partial_t\,\mathbf{G}^{\rceil}(t,-i\tau) \;=\; \mathbf{h}(t)\,\mathbf{G}^{\rceil}(t,-i\tau) \;+\; \mathbf{I}^{\rceil}(t,-i\tau)\,, \tag{9.3}$$

$$-i\,\partial_t\,\mathbf{G}^{\lceil}(-i\tau,t) \;=\; \mathbf{h}(t)\,\mathbf{G}^{\lceil}(-i\tau,t) \;+\; \mathbf{I}^{\lceil}(-i\tau,t)\,, \tag{9.4}$$

where $\mathbf{h}(t) = \mathbf{h}^0(t) + \mathbf{\Sigma}^{\mathrm{HF}}(t)$ is the time-dependent Hartree-Fock Hamiltonian, a sum of the external potential and the mean-field contribution. As for any integro-differential equation, we

[1] The pictures show them at the time of the invention of their equations in 1961, and are taken from "Progress in non-equilibrium Green's functions" edited by M. Bonitz and D. Semkat.

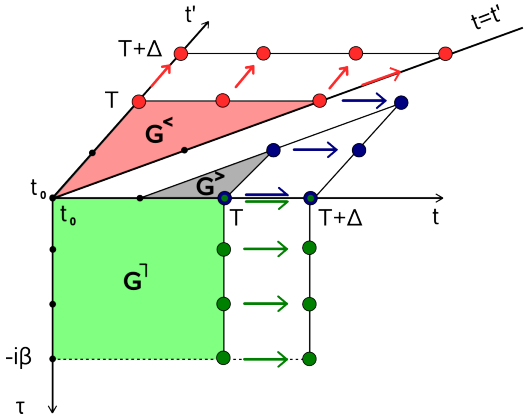

Figure 9.1: *Visualization of the time stepping $T \to T + \Delta$. Due to symmetry relations $G^<$ must only be propagated on the upper (red) triangle, $G^>$ on the lower (blue) triangle and $G^⌉$ as well as $G^⌈$ (hidden in the picture) has to be stored on the whole (green) rectangle.*

have to specify the system's initial state at the time t_0. For notational clarity, we temporarily assume $t_0 = 0$ without loss of generality, what leads to the following initial conditions:

$$\mathbf{G}^{>}(0,0) \;=\; i\,\mathbf{G}^{M}(0^{-})\,, \qquad \mathbf{G}^{>}(0,0) \;=\; i\,\mathbf{G}^{M}(0^{+}) \;=\; -i\,\mathbf{G}^{M}(-\beta)\,, \tag{9.5}$$

$$\mathbf{G}^{⌉}(0,-i\tau) \;=\; i\,\mathbf{G}^{M}(-\tau)\,, \qquad \mathbf{G}^{⌈}(-i\tau,0) \;=\; i\,\mathbf{G}^{M}(\tau) \;=\; -i\,\mathbf{G}^{M}(\tau-\beta)\,. \tag{9.6}$$

Furthermore, the collision terms on the right-hand sides, that account for the memory or – sounding more important – for the non-Markovian behavior, are given like in (3.57-3.60):

$$\begin{aligned}\mathbf{I}_1^{>}(t,t') \;=\; &\int_{t_0}^{t} d\bar{t}\,\Big[\mathbf{\Sigma}^{>}(t,\bar{t}) - \mathbf{\Sigma}^{<}(t,\bar{t})\Big]\,\mathbf{G}^{>}(\bar{t},t') + \int_{t_0}^{t'} d\bar{t}\,\mathbf{\Sigma}^{>}(t,\bar{t})\,\Big[\mathbf{G}^{<}(\bar{t},t') - \mathbf{G}^{>}(\bar{t},t')\Big] \\ &- i\int_0^{\beta} d\bar{\tau}\;\mathbf{\Sigma}^{⌉}(t,-i\bar{\tau})\,\mathbf{G}^{⌈}(-i\bar{\tau},t')\,,\end{aligned} \tag{9.7}$$

$$\begin{aligned}\mathbf{I}_2^{<}(t',t) \;=\; &\int_{t_0}^{t'} d\bar{t}\,\Big[\mathbf{G}^{>}(t',\bar{t}) - \mathbf{G}^{<}(t',\bar{t})\Big]\,\mathbf{\Sigma}^{<}(\bar{t},t) + \int_{t_0}^{t} d\bar{t}\,\mathbf{G}^{<}(t',\bar{t})\,\Big[\mathbf{\Sigma}^{<}(\bar{t},t) - \mathbf{\Sigma}^{>}(\bar{t},t)\Big] \\ &- i\int_0^{\beta} d\bar{\tau}\;\mathbf{G}^{⌉}(t',-i\bar{\tau})\,\mathbf{\Sigma}^{⌈}(-i\bar{\tau},t)\,,\end{aligned} \tag{9.8}$$

$$\mathbf{I}^{⌉}(t,-i\tau) \;=\; \int_{t_0}^{t} d\bar{t}\,\Big[\mathbf{\Sigma}^{>}(t,\bar{t}) - \mathbf{\Sigma}^{<}(t,\bar{t})\Big]\,\mathbf{G}^{⌉}(\bar{t},-i\tau) + \int_0^{\beta} d\bar{\tau}\;\mathbf{\Sigma}^{⌉}(t,-i\bar{\tau})\,\mathbf{G}^{M}(\bar{\tau}-\tau)\,, \tag{9.9}$$

$$\mathbf{I}^{⌈}(-i\tau,t) \;=\; \int_{t_0}^{t} d\bar{t}\;\mathbf{G}^{⌈}(-i\tau,\bar{t})\,\Big[\mathbf{\Sigma}^{<}(\bar{t},t) - \mathbf{\Sigma}^{>}(\bar{t},t)\Big] + \int_0^{\beta} d\bar{\tau}\;\mathbf{G}^{M}(\tau-\bar{\tau})\,\mathbf{\Sigma}^{⌈}(-i\bar{\tau},t)\,. \tag{9.10}$$

They obey the following symmetry properties

$$\mathbf{I}^{\gtrless}(t,t') \;=\; -\Big[\mathbf{I}^{\gtrless}(t',t)\Big]^{\dagger}\,, \qquad \mathbf{I}^{⌈}(-i\tau,t) \;=\; \Big[\mathbf{I}^{⌉}(t,-i(\beta-\tau))\Big]^{\dagger}\,. \tag{9.11}$$

To solve the KKBEs (9.1-9.4) numerically, we introduce an equally spaced two-dimensional time grid with temporal width Δ. As derived by N.E. Dahlen and Robert van Leeuwen and explained in detail in the appendix of [18], the NEGFs – assumed to be fully known on the square $t, t' \leq T$

– are propagated according to the following set of discrete matrix equations

$$\mathbf{G}^{>}(T+\Delta,t') \;=\; \mathbf{U}(\Delta)\,\mathbf{G}^{>}(T,t') \;-\; \mathbf{V}(\Delta)\,\mathbf{I}_1^{>}(t')\,, \tag{9.12}$$

$$\mathbf{G}^{<}(t',T+\Delta) \;=\; \mathbf{G}^{<}(t',T)\,\mathbf{U}(\Delta) \;-\; \mathbf{V}(\Delta)\,\mathbf{I}_2^{<}(t')\,, \tag{9.13}$$

$$\mathbf{G}^{<}(T+\Delta,T+\Delta) \;=\; \mathbf{U}(\Delta)\,\left[\mathbf{G}^{<}(T,T) \;+\; \sum_{n=0}^{\infty}\mathbf{C}^{(n)}\right]\,\mathbf{U}^{\dagger}(\Delta)\,. \tag{9.14}$$

For the mixed functions we extract

$$\mathbf{G}^{\rceil}(T+\Delta,-i\tau') \;=\; \mathbf{U}(\Delta)\,\mathbf{G}^{\rceil}(T,-i\tau') \;-\; \mathbf{V}(\Delta)\,\mathbf{I}^{\rceil}(T,-i\tau')\,, \tag{9.15}$$

$$\mathbf{G}^{\lceil}(-i\tau,T+\Delta) \;=\; \mathbf{U}(\Delta)\,\mathbf{G}^{\lceil}(-i\tau,T) \;-\; \mathbf{V}(\Delta)\,\mathbf{I}^{\lceil}(-i\tau,T)\,. \tag{9.16}$$

The introduced time-evolution operators are thereby defined in terms of the Hamiltonian $\mathbf{h}$ at time T through

$$\mathbf{U}(\Delta) \;=\; \mathrm{e}^{-i\,\mathbf{h}\,\Delta}\,, \qquad \mathbf{V}(\Delta) \;=\; \frac{1}{\mathbf{h}}\left(1-\mathrm{e}^{-i\,\mathbf{h}\,\Delta}\right)\,, \tag{9.17}$$

and are calculated as in (7.5) by diagonalization of $\mathbf{h}$. The matrices $\mathbf{C}^{(n)}$ recursively are given by the commutator

$$\mathbf{C}^{(n)} \;=\; \frac{i\,\Delta}{n+1}\Big[\,\mathbf{h}\,,\,\mathbf{C}^{(n-1)}\,\Big], \qquad \mathbf{C}^{(0)} \;=\; -i\,\mathbf{I}_{12}^{<}\,\Delta\,, \tag{9.18}$$

where the recursion scheme of course has to be truncated at a finite value n_{max}, chosen in a way that the result converges. The matrix $\mathbf{I}_{12}^{<}$ in the time-interval $T \le t,t' \le T+\Delta$ is approximated by

$$\mathbf{I}_{12}^{<} \;\approx\; \mathbf{I}_1^{>}(t,t') - \mathbf{I}_2^{<}(t,t')\,. \tag{9.19}$$

Furthermore, in Eqs. (9.12-9.16) for $T \le t,t' \le T+\Delta$ we have approximated the right hand sides through

$$\mathbf{I}_1^{>}(t,t') \approx \mathbf{I}_1^{>}(t')\,, \qquad \mathbf{I}_2^{<}(t',t) \approx \mathbf{I}_2^{<}(t')\,, \tag{9.20}$$

$$\mathbf{I}^{\rceil}(t,-i\tau) \approx \mathbf{I}^{\rceil}(-i\tau)\,, \qquad \mathbf{I}^{\lceil}(-i\tau,t) \approx \mathbf{I}_2^{\lceil}(-i\tau)\,, \tag{9.21}$$

which in addition has the numerical advantage, that the collision integrals as well as the self-energies can be implemented as one-dimensional arrays in time.

9.1.1. Scheme of the numerical solution

Let us summarize the steps to propagate the Green functions by a single time-step from T to $T+\Delta$:

(i.) Calculate the single-particle Hamiltonian $\mathbf{h}^0$, the Hartree-Fock self-energy $\mathbf{\Sigma}^{HF}$ and the effective Hamiltonian $\mathbf{h} = \mathbf{h}^0 + \mathbf{\Sigma}^{HF}$ at time T.

(ii.) Calculate all two-time self-energies $\left\{\mathbf{\Sigma}^{>},\mathbf{\Sigma}^{<},\mathbf{\Sigma}^{\rceil},\mathbf{\Sigma}^{\lceil}\right\}$ and the collision integrals $\left\{\mathbf{I}_1^{>},\mathbf{I}_2^{<},\mathbf{I}^{\rceil}\right\}$ for $t_0 \le t \le T$, respectively for $-\beta \le \tau \le 0$. The integral $\mathbf{I}^{\lceil}$ is obtained by the symmetry property (9.11). All quantities are implemented as one-dimensional arrays in time.

(iii.) Set up the time-evolution matrices $\mathbf{U}$ and $\mathbf{V}$ as well as the commutators $\mathbf{C}_{12}$ and propagate the Green functions as instructed by Eqs. (9.12-9.16).

This scheme corresponds to the **Euler method** for the solution of an ordinary differential equation and its error is of the order $\mathcal{O}(\Delta^2)$. To achieve higher-order propagation schemes, we can borrow any of the methods known from the numerics of differential equations. We will restrict us to two explicit schemes, one of second order known as the Heun method and the classical fourth-order Runge-Kutta scheme.
In the **Heun method**, that is also known as the second-order Runge-Kutta scheme, at first the Green function is propagated one time-step by the Euler method, where again the density-matrix and all collision integrals are calculated. Then all matrices at both timepoints are averaged, and the Green function is propagated once again with the corrected quantities. By using generalized integration routines as explained in the next method, also another second-order scheme, known as the "midpoint"-rule is possible. There the first trial Green function is only propagated by $\Delta/2$ instead of a whole time step Δ.
The **fourth-order Runge-Kutta** (RK4) scheme works similar, except that the Green functions are propagated four times. At first all Green functions are propagated by $\Delta/2$, where the density matrix and the collision integrals are calculated. With them the Green functions are propagated again from T to $T + \Delta/2$. After a renewed computation of both quantities the Green function is propagated the whole time step from T to $T + \Delta$, where the density matrix and the collision integrals are calculated the fourth time. Having obtained these four density matrices and sets of collision integrals, we average them with the following weigths

$$\boldsymbol{\rho}(T) := \frac{1}{6}\,\boldsymbol{\rho}_1(T) + \frac{1}{3}\,\boldsymbol{\rho}_2(T+\Delta/2) + \frac{1}{3}\,\boldsymbol{\rho}_3(T+\Delta/2) + \frac{1}{6}\,\boldsymbol{\rho}_4(T+\Delta) \tag{9.22}$$

to obtain the final density matrix and collision integrals. These are used to propagate the Green function at time T towards $T+\Delta$. To calculate the collision integrals at intermediate time points, one needs generalized sum rules such as (8.5) or spline-integration, as it is available in the *gsl*-library.
The way of transferring ODE solution methods to our matrix equations has become clear now. All we have to do is to replace the right-hand sides by the density matrix and the collision integrals. With this recipe, the methods above, implemented only for equidistant time-steps, also could

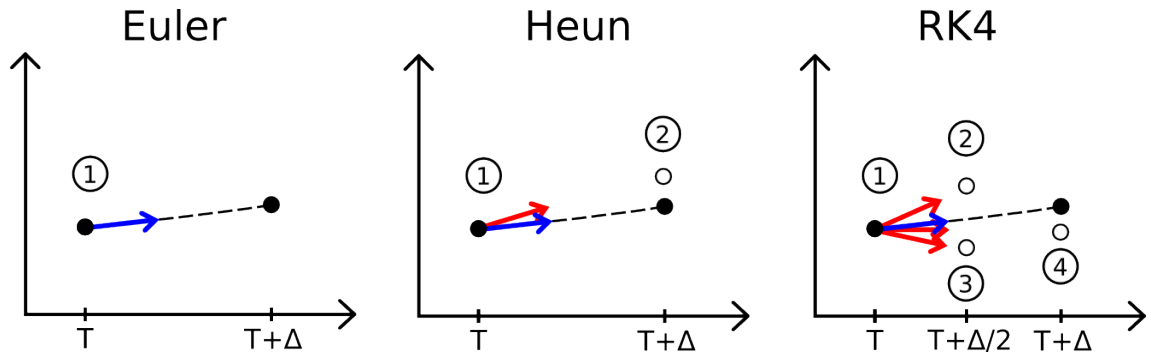

Figure 9.2.: *Explicit solution methods for ordinary differential equations as explained in the text. Filled dots represent final Green function values, while open dots indicate the intermediate trial Green functions. Blue arrows represent the final derivative and red ones the trials, where the derivatives here are replaced by the density matrix and the collision integrals.*

be easily extended to an adaptive stepsize control [27]. Furthermore, other more sophisticated ODE integrators, such as predictor-corrector or Burlisch-Stoer methods could be superior to our approach and should be tried.

9.1.2. Time-dependent energies

The different energies already collected in (8.14-8.16) for the thermal equilibrium state, in nonequilibrium take an explicit time-dependence. Thereby, all single-particle energies (potential and kinetic energy) and the Hartree-Fock energy follow from the time-dependent complex density matrix $\boldsymbol{\rho}(t)$ given by the lesser correlation function at equal time-arguments

$$\rho_{ij}(t) \;=\; \pm i\, G^{<}_{ij}(t,t)\,. \tag{9.23}$$

As discussed below, the computation of the correlation energy is somewhat more difficult. If the system is not disturbed by some additional time-dependent potential, the total energy and all contributing energies are conserved, the verification of which is an essential test for the numerics and furthermore controls the time-step length Δ. In summary:

(i) **Single-particle energy** with the time-dependent Hamiltonian $\mathbf{h}(t) = \mathbf{t}(t) + \mathbf{v}(t)$:

$$E_{Single}(t) \;=\; \mathfrak{Re}\; \sigma\, \mathrm{Tr}\left\{\mathbf{h}(t)\,\boldsymbol{\rho}(t)\right\} \;+\; \mu N\,. \tag{9.24}$$

Remember that $\sigma = 1$ for spin-polarized particles and $\sigma = 2$ for spin-restricted ones.

(ii) **Hartree-Fock energy**, given by a similar expression than in chapter 6:

$$E_{HF}(t) \;=\; \mathfrak{Re}\; \frac{\sigma}{2}\, \mathrm{Tr}\left\{\boldsymbol{\Sigma}^{HF}(t)\,\boldsymbol{\rho}(t)\right\}. \tag{9.25}$$

(iii) **Correlation energy** as given in reference [46]:

$$E_{corr}(t) \;=\; \mathfrak{Im}\; \frac{\sigma}{2} \int_{\mathcal{C}} d\bar{t}\; \mathrm{Tr}\left\{\boldsymbol{\Sigma}(t,\bar{t})\,\mathbf{G}(\bar{t},t^{+})\right\} \;=\; \mathfrak{Im}\; \frac{\sigma}{2}\; \mathrm{Tr}\left\{\mathbf{I}^{>}_{1}(t,t)\right\}. \tag{9.26}$$

(iv) **Field energy**: For an arbitrary external potential $\mathbf{v}_{ext}(t)$, there is in general no way to monitor the energy that is transferred to the system. Nevertheless, as we only consider dipole fields, $\mathbf{v}_{ext}(t) = -\mathcal{E}(t)\mathbf{x}$, the energy expression is well known from classical electrodynamics – this would also be the case for higher multipole terms:

$$E_{field}(t) \;=\; \int_{t_0}^{t} d\bar{t}\;\; \langle x(t)\rangle\;\; \partial_{\bar{t}}\mathcal{E}(t)\,. \tag{9.27}$$

The spin-factor is contained in the averaging.

9.1.3. Self-energy contributions

In the following we collect the self-energy expressions needed in the solution of the Kadanoff-Baym equations. The time-dependent GW approximation due to lack of time has not been implemented yet, though the general strategy of attack has already been established in Ref. [10], there without the mixed functions that account for initial correlations.

Hartree-Fock approximation

In the Hartree-Fock approximation the self-energy is approximated by the singular part of (3.32) on the Keldysh-Contour, while the other components are set to zero. Thus all collision integrals are zero as well and the set of equations (9.12-9.16) can be solved without great efforts. The self-energy evaluates to

$$\Sigma_{ij}^{HF}(t) \;=\; \sum_{kl}(\,\sigma\, w_{ij,kl} \pm w_{ik,lj})\; G_{kl}^{<}(t,t)\,. \tag{9.28}$$

In addition, the spectral properties of the system are known analytically, so that the Green function can be propagated on the time-diagonal only, what effectively yields a scheme for the density matrix. In contrast to correlated calculations, this saves a lot of time, while in most systems it yields a well approximation for the exact results.

Second Born approximation

The second Born self-energies are easily calculated from (4.1) together with Langreth rules for products of Keldysh contour functions, Fig. 3.2. Without any further derivation, we only present the formulas:

$$\Sigma_{ij}^{\gtrless}(t,t') \;=\; \sum_{klmnrs} w_{ik,ms}(\,\sigma\, w_{lj,rn} \pm w_{nj,rl})\; G_{kl}^{\gtrless}(t,t')\; G_{mn}^{\gtrless}(t,t')\; G_{rs}^{\lessgtr}(t',t)\,, \tag{9.29}$$

$$\Sigma_{ij}^{\rceil}(t,-i\tau) \;=\; \sum_{klmnrs} w_{ik,ms}(\,\sigma\, w_{lj,rn} \pm w_{nj,rl})\; G_{kl}^{\rceil}(t,-i\tau)\; G_{mn}^{\rceil}(t,-i\tau)\; G_{rs}^{\lceil}(-i\tau,t)\,, \tag{9.30}$$

$$\Sigma_{ij}^{\lceil}(-i\tau,t) \;=\; \sum_{klmnrs} w_{ik,ms}(\,\sigma\, w_{lj,rn} \pm w_{nj,rl})\; G_{kl}^{\lceil}(-i\tau,t)\; G_{mn}^{\lceil}(-i\tau,t)\; G_{rs}^{\rceil}(t,-i\tau)\,. \tag{9.31}$$

The implementation is done in the same way as in the equilibrium case, see the discussion after Eq. (8.20).

9.2. Application

Energy conservation, current densities and the continuity equation

To estimate the quality of the presented algorithm, we propagate the NEGF for the 1D harmonic oscillator system and monitor the energy conservation. As mentioned above, for an unexcited system, all equilibrium energy contributions have to remain constant, while for a system under external perturbation at least the total energy – field plus particle – should not change.

Given the NEGF, we have access to the time-dependence of every one-body quantity, such as the one-particle density and current density. Since the density matrix is obtained as the equal-time limit of the lesser Green function, the time-dependent generalized density is obtained by transferring the density matrix back to spatial representation

$$\rho(x,x',t) \;=\; \sum_{ij}\rho_{ij}(t)\;\psi_i^*(x)\,\psi_j(x')\,. \tag{9.32}$$

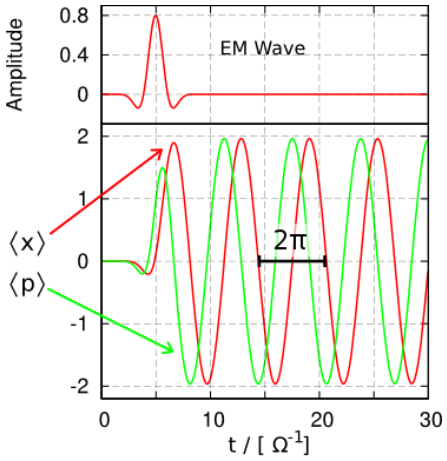

Figure 9.3: *Time-dependent expectation values of position and momentum for $N = 2$ particles in a 1D quantum dot. The system is excited by an electromagnetic wave with amplitude $E_0 = 0.8$, frequency $\omega = 1.4$ and a Gaussian envelope with $t_{mid} = 5$ and $\Delta t = 1.0$ and is propagated $N_t = 400$ time-steps in Hartree-Fock approximation. After the pulse, the density profile oscillates rigidly with the trap frequency.*

Similarly, the generalized current density is given by

$$\rho(p, p', t) \;=\; \sum_{ij} \rho_{ij}(t)\; \psi_i^*(p)\, \psi_j(p')\,, \tag{9.33}$$

where $\psi_i(p)$ denote the Fourier transformed HF basisfunction, that are again obtained by the aid of the library *fftw*. The corresponding densities then agree with the diagonal entries

$$n(x,t) \;=\; \rho(x,x,t), \qquad n(p,t) \;=\; \rho(p,p,t) \tag{9.34}$$

In Fig. 9.4, we plotted the densities for an excited 1D harmonic oscillator, and in Fig. 9.3 the corresponding expectation values are shown. The spatial density profile thereby does not change its relative form, but oscillates as a whole. After the action of the pulse, the particles oscillate with the trap frequency. This is a special case of a general theorem given in [48], which states that a system under action of an external dipole field whose self-energies are obtained within conserving approximation fulfills the Kohn-theorem, i.e. the center of mass oscillates like a single-particle. Moreover this result is independent of the considered interaction type.
Furthermore in Fig. 9.5 (a), we show the differences in the occupation numbers (and therefore in all other observables) that arise from the different methods. As one can see the Hartree-Fock and second Born results agree almost perfectly, while the deviation from CI is likely to be caused by the different orders in the propagation schemes. Finally, in Fig. 9.5 (b) the energy conservation in second Born approximation is proved.

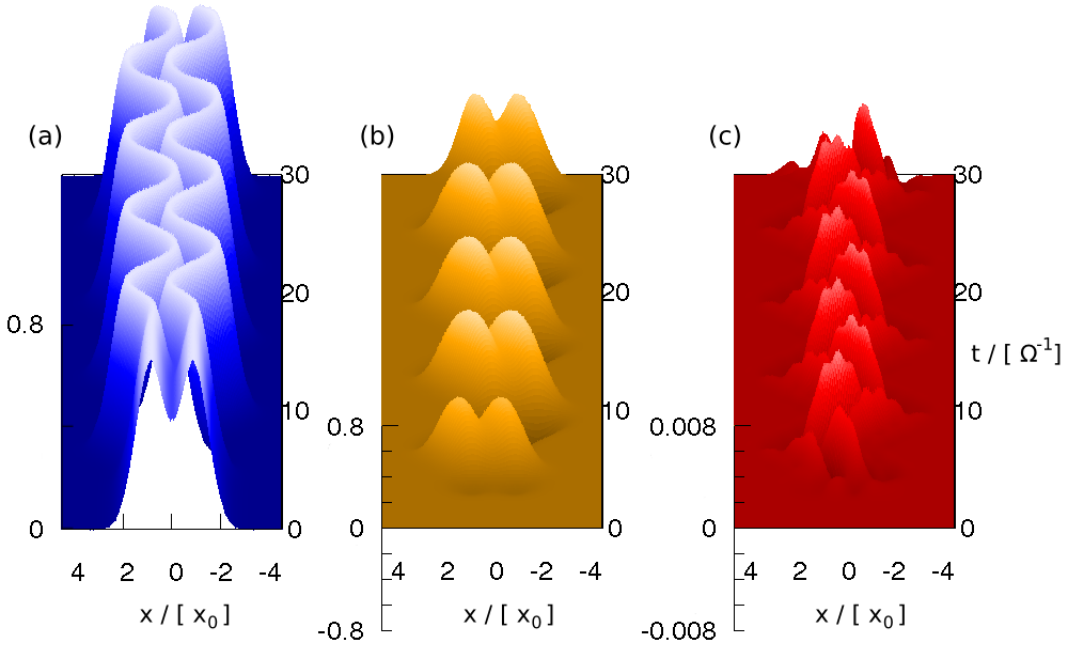

Figure 9.4.: *Time-dependent Hartree-Fock approximation for $N = 2$ particles in a 1D quantum dot excited by the wave shown in Fig. 9.3. (a) Time-dependent density. (b) Current density. (c) Validity of the continuity equation. Note that the z-axis in comparison to the densities is scaled by a factor 100.*

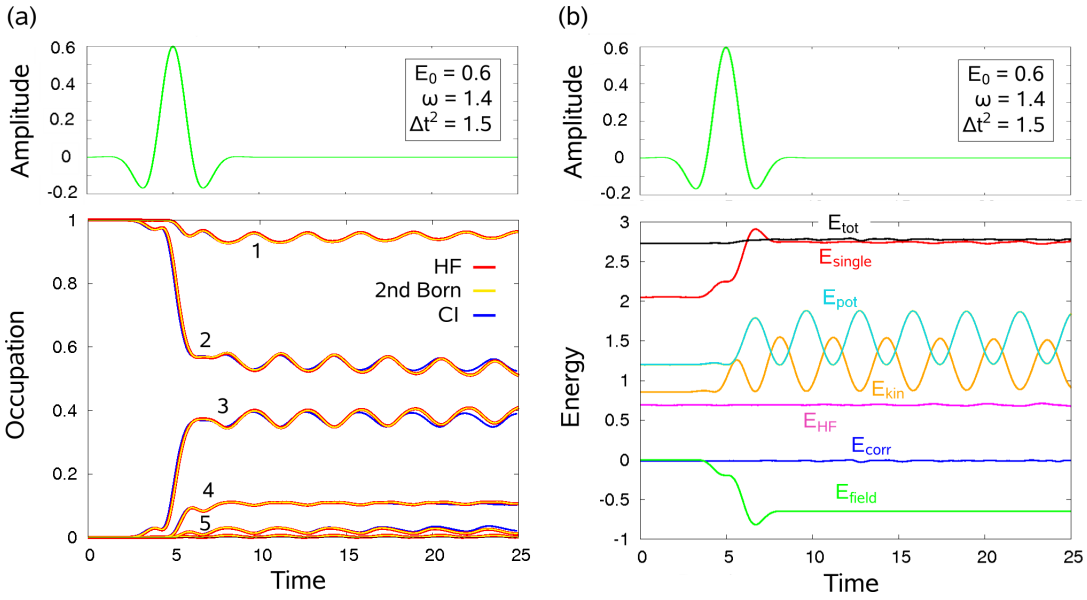

Figure 9.5.: *Excitation of $N = 2$ particles in the harmonic oscillator, $\beta = 50$, $\lambda = 1$. The system is propagated $N_t = 250$ time steps with the Heun method for HF and second Born and with the presented first-order scheme for CI. (a) Comparison of the occupation numbers from HF, second Born and CI calculations. The deviation between second Born and CI probably is caused by the different order schemes in the solution methods. (b) Time-dependent energies in second Born approximation. Due to the Kohn-theorem the density is unchanged, so HF and correlation energy should stay constant.*

Part III.

Results

10. Equilibrium properties

Until here, the NEGF formalism has been provided on a very general level and exercised on a basic confinement model, the harmonic oscillator. We are now able to apply it to nearly any system with spin-independent interaction, that allows for an expansion in a basis. In particular the problems related to the dimensionality of the system - as they would appear in spatial representation - are reduced to the task of calculating the electron integrals.
In this last part of the thesis, we will focus on the main subject of this work, ionization processes. After introduction of the general model, we determine the correlated equilibrium state for different model atoms, what will yield us a lot of information about ionization properties. Due to the moderate basis size needed in equilibrium, we consider also the three-dimensional case.

10.1. The model

The general model we consider consists of a model atom and the surrounding continuum, see Fig. 10.1 (a). Though the model atom in principle can be represented by an arbitrary confinement – the Born-Oppenheimer approximation is implied – most of the times we consider the easiest choice, the finite box potential and some times also a regularized Coulomb potential. The particles thereby will be treaten in both fashions, spin-polarized and spin-restricted, where at least for real systems the latter one is the more natural choice.
More interesting is the question of modelling the continuum adequately. The first approach is a simple infinite box, whose eigenfunctions resemble the real and imaginary part of plane waves, except for the influence of the atom. It meets the basic requirements to a continuum up to the boundaries, namely that a propagating wavepacket is not scattered. The width of the continuum box directly determines the density of states and therefore the resolution of the continuum, and given a number of basisfunctions, it also fixes the highest energy level. These competing attributes must be chosen appropriately and in dependence on the aim of the simulation, a question that will be faced later. In Fig. 10.1 (b)-(e) some other possible types of model continua plus their restrictions and advantages are shown.
Though the model will be a good approximation to all one-dimensional systems and maybe also to radial-symmetric two- and three-dimensional states, the investigation of characteristic higher dimensional properties - such as angular momentum, polarized waves or the influence of the magnetic field - of course is denied.

10.2. Correlated equilibrium state

The equilibrium state is found in Hartree-Fock, second Born and GW approximation. As earlier, we also present the unrestricted HF results and CI benchmark calculations. Due to avoid a thermal ionization, in all calculations the groundstate is considered, i.e. the inverse temperature is set sufficiently large, $\beta = 50$.

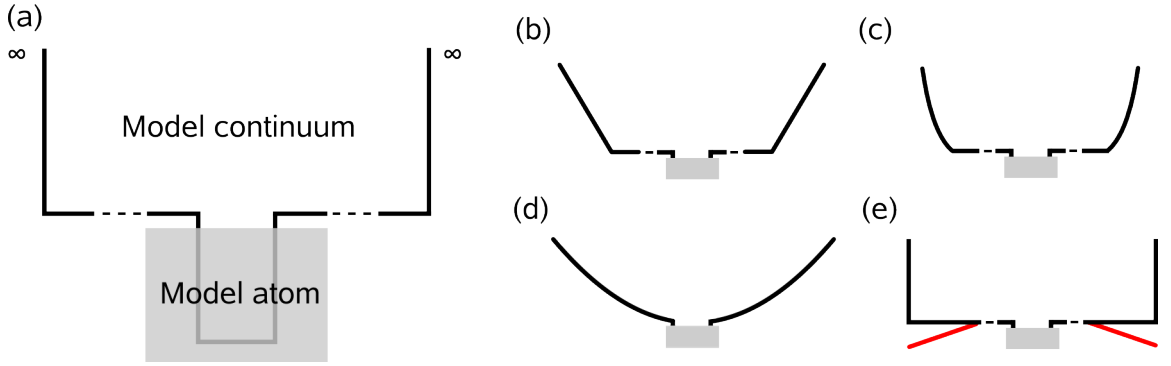

Figure 10.1.: *Some selected continuum models and their characteristics. (a) The basic model. In one dimension the energy distance grows quadratically and thus the density of states decreases as $E^{-1/2}$. (b) To modify the DOS, f.i. to decrease the resolution for low energies and improve it for high, the boundaries can be adjusted. (c) Constant potential plus harmonic oscillator. Yields equidistant spacing for upper energy levels. (d) Harmonic oscillator continuum. Yields an equidistant energy spacing also for lower continuum levels, but back-scattering of ionized particles. (e) Basic model plus complex (optical) linear potential. Absorbs the ionized particle to avoid reflections at the boundaries. However, there is also a re-scattering at the crossing.*

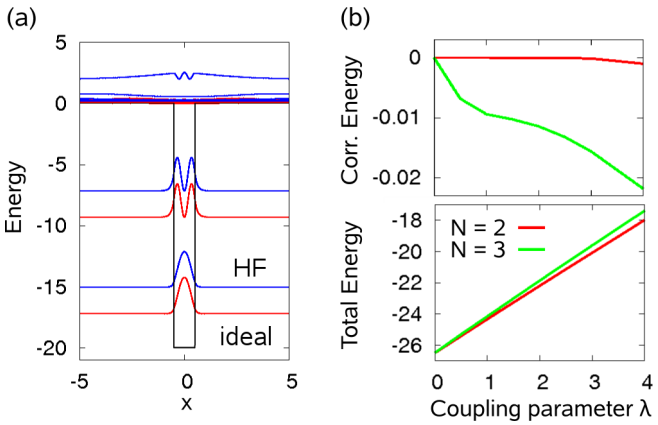

Figure 10.2: *(a) The one-dimensional finite-box model and its first ten eigenfunctions. The box has a width of $a = 1$ and a depth of $V_0 = -20$, the continuum boundaries are at $b = 20$. The red curves show the ideal basis functions and the green curve the Hartree-Fock basis. Mention, that in the HF basis the highest state is actually the third bound state, that is shifted in the continuum. (b) Total and correlation energies of the groundstate, plotted against the coupling parameter. For the box model, we can neglect the correlation contributions to the energy.*

One-dimensional box model atom

The most basic choice for the model atom is given by a finite box, see Fig. 10.2 (a). The full confinement then is determined by three parameters: The box width a, its depth V_0 as well as the width b of the continuum box. The reason for this easy choice is the assumption, that the physical properties found for the box potential are also valid for many other types of potentials.

In the following, we do not want to provide tabulars for some given sets of parameters, as they are too special and probably will lead to no physical insight. We only mention the property shown in Fig. 10.2 (b): For all systems of this type we have studied until now, we obtained a negligible correlation energy. Thus, the Hartree-Fock approximation almost always describes the ground- and equilibrium states of the system sufficiently. This statement can also be extended to any systems of the form shown in Fig. 10.2 (a), that are described by a few bound states. The corresponding correlation energies are roughly two orders smaller as in the harmonic oscillator. We will return to the finite box model in the non-equilibrium calculations in the next chapter,

there starting from the Hartree-Fock groundstate. For now, we turn to a potential which yields higher correlation contributions and which is defined by only one parameter.

One-dimensional Coulomb model atom

The one-dimensional Coulomb potential [1] is defined by

$$v(x) \;=\; -\frac{N}{\sqrt{x^2+1}}\,, \tag{10.1}$$

where N is the nuclear charge. Consequently, also the screening parameter α in the Coulomb interaction is set to one. The value is chosen in order to allow the particles to pass each other. This model has e.g. been used in [6].
In particular, we investigate the one-dimensional Helium model with $N = 2$ particles. Due to the small particle number and the single dimension, the many-body Schrödinger equation becomes a two-dimensional scheme. This allows for a solution on a spatial grid by the methods collected in 5.2. For ionization processes this is likely the most convenient form. However, higher dimensions than two are hard to treat in this way.
The Hamiltonian of the Helium system is given by

$$\hat{H}(x_1,x_2,t) \;=\; \hat{h}^0(x_1) \;+\; \hat{h}^0(x_2) \;+\; E(t)\,(x_1+x_2) \;+\; \frac{1}{\sqrt{(x_1-x_2)^2+1}}\,, \tag{10.2}$$

and is interpreted as a one-particle operator for a two-dimensional state. To determine the groundstate of the 1D Helium model, this operator is discretized on a spatial grid and diagonalized. For the grid we used a discretization of $\Delta x = 0.05$, while the boundaries were given by $-40 \leq x_1, x_2 \leq 40$. The corresponding potential and groundstate density are shown in Fig. 10.3. The density $n(x_1, x_2)$ yields the probability, that particle one is localized at x_1 and particle two at x_2. We also applied the NEGF schemes as well as Configuration Interaction, that is just

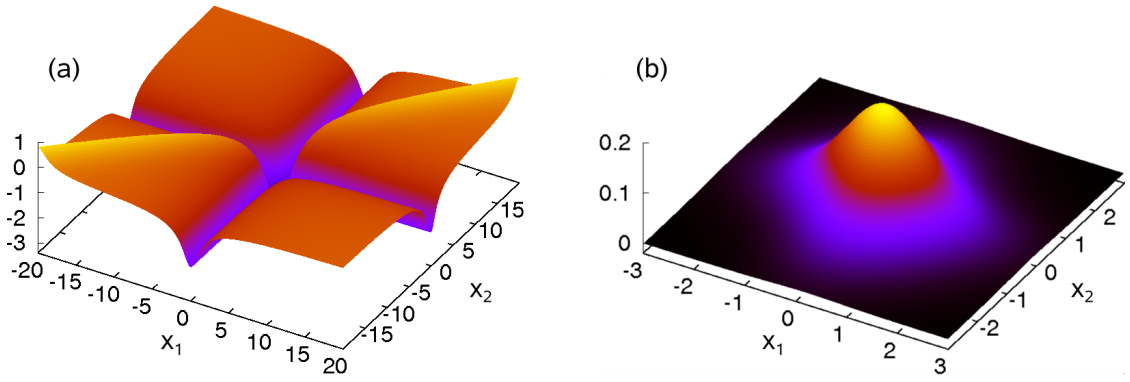

Figure 10.3.: *Interpretation of the one-dimensional Helium model as a two-dimensional one-particle problem. (a) Two-dimensional potential. The Coulomb potential is situated at the axes, while the wall on the diagonal accounts for the interaction. (b) The groundstate density due to the interaction is elliptically shaped.*

[1] For a discussion on "one-dimensional Coulomb" see section 8.4.

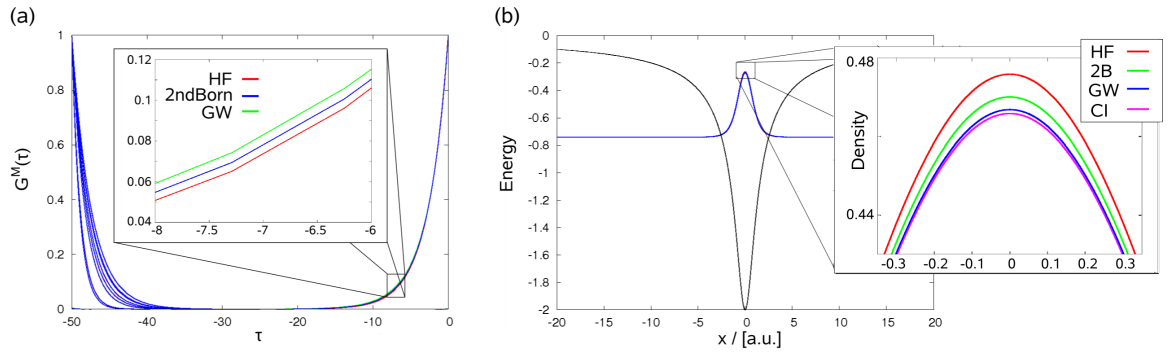

Figure 10.4.: *Equilibrium quantities of the one-dimensional Helium model. (a) Diagonal elements of the Matsubara Green functions in Hartree-Fock, second Born and GW approximation. (b) Groundstate densities. The GW density apparently yields the best approximation to the exact CI density.*

the above approach in a basis. In summary, we obtained the following results for the total energies:

HF	2ndBorn	GW	CI	2D SE
−2.224	−2.231	−2.236	−2.235	−2.238

The Green function and CI calculations were performed with $N_b = 10$ basisfunctions. The two-dimensional Hamiltonian was discretized by $N_x = 4000$ gridpoints and a grid spacing of $\Delta x = 0.01$ in each direction. The result from the diagonalization was checked to converge.
The second Born and GW results are very close to the exact result. In comparison to CI, the GW result overestimates the correlation energy. This behavior has already been observed in chapter 8.

Three-dimensional box model atom

Three-dimensional systems of course yield an incomparably richer description of the real world than one-dimensional models. One advantage of the basis approach is, that we have an easy access to higher dimensions. All we need to do, is to start from another set of electron integrals. In Appendix A, we examine the calculation of the three-dimensional electron integrals in central potentials. A restriction is only given by the degeneracy of three-dimensional basis states – a calculation of comparable accuracy is likely to need the cubic power of basis functions than in one dimension. However, regarding further information, for instance angular momentum conservation, one can still reduce the size.
In Tab. 10.1, we present some exemplary results obtained from the Matsubara Green function in second Born approximation.

10.3. Ionization potentials and the spectral function

As mentioned in the theory part, the correlated equilibrium Green function covers the information on the one-particle ionization energies and electron affinities. In fact, we have several alternatives for their calculation. One is given by the extended Koopmans theorem, that has already been introduced in section 8.3. The ionization energies there are obtained by a variational principle,

λ	E_{tot}	E_{single}	E_{HF}	E_{corr}	Part. Number	Symmetry
1	-17.311	-18.537	1.233	-0.007	1.9999	$6.68 \cdot 10^{-10}$
2	-14.870	-18.513	3.702	-0.060	1.9999	$4.40 \cdot 10^{-9}$
3	-12.452	-18.475	6.178	-0.154	1.9998	$1.92 \cdot 10^{-7}$
4	-10.050	-18.406	8.635	-0.279	1.9997	$4.47 \cdot 10^{-5}$

Table 10.1.: *The energy contributions to the groundstate of a three-dimensional box, in which two spin-restricted particles are trapped. The results were obtained from the Matsubara Green function in second Born approximation, whereby the UPM parameters were $p = 15$, $u = 4$ and $\beta = 50$. The calculation of the symmetry is defined in Eq. (8.17).*

that was casted in the form of a generalized eigenvalue problem.
Another possibility is offered by the (equilibrium) spectral function , which is defined in [13]:

$$A(x,\omega) \;=\; -\frac{1}{\pi}\, G^M(x,x;\omega)\,. \tag{10.3}$$

$G^M(x,x;\omega)$ is the Fourier transformation of the Matsubara Green function. As it can be recognized from the Lehmann representation of the Green function, the spectral function has poles at the excitation energies respectively the electron affinities. A third alternative is given by the analytic continuation of the previous expression to nonequilibrium

$$A(1,2) \;=\; G^{>}(1,2) \;-\; G^{<}(1,2)\,, \tag{10.4}$$

followed by a conversion to relative and center of mass coordinates and a Fourier transformation with respect to the relative time.

In the following we apply the equilibrium approaches to the Matsubara Green function. Therefore we consider again the one-dimensional Helium model for an inverse temperature of $\beta = 50$ and a coupling parameter of $\lambda = 1$. First, we find the self-consistent solution of the Dyson equation. Again we use the Hartree-Fock-, second Born- and GW approximation. By a solution of the generalized eigenvalue problem (8.37), we then obtain the approximated ionization energies:

	HF	2ndBorn	GW
EKT	0.749	0.749	0.735

While Hartree-Fock and second Born yield the same result, the excitation energy from GW is a little lower. The GW result could have been expected, because the ionization energies from Hartree-Fock do not account for a relaxation of the ionized system and thus the ionization potential should be smaller than the one obtained from Hartree-Fock. We can only guess, why second Born yields the same result as Hartree-Fock: Probably the relaxation energy and the correlation energy contributions cancel each other. In addition, we calculated the spectral function. The required Fourier transform was performed after a zero-padding of the Matsubara Green function to enhance the resolution. If we mention the structure of the diagonal entries, Fig. 10.4 (a), this can be done without any further effort. The result can be seen in Fig. 10.5. There, we have plotted the diagonal elements of the spectral function matrix. As can be seen, its peaks agree very well with the results from the extended Koopmans theorem.
A further information offered by the spectral function is the spectral density given by the width of the curves. In Hartree-Fock approximation, one would expect sharp peaks, while correlation effects should broaden the curves. This is caused by the particle collision, that smear out the

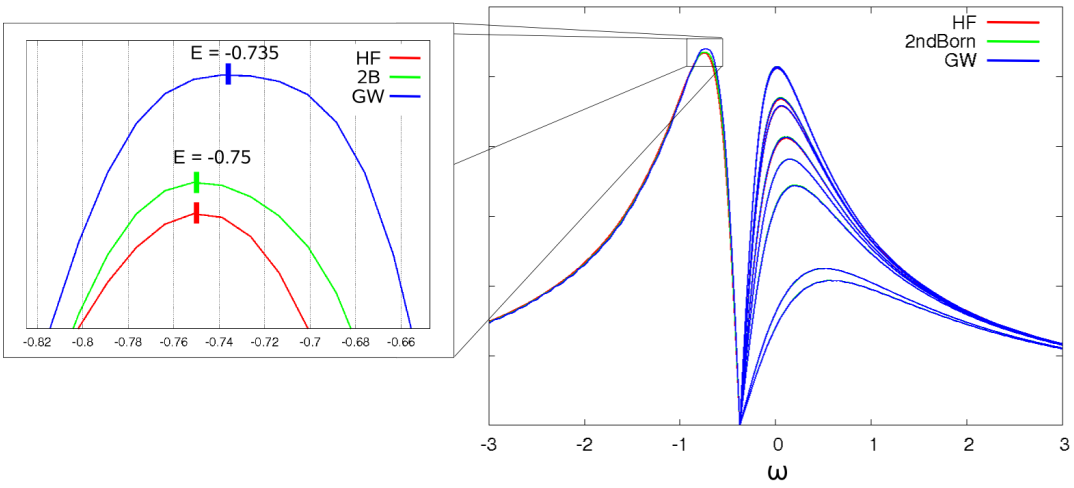

Figure 10.5.: *The spectral function for the one-dimensional Helium model. The position of the peak specifies the ionization energy (peaks below 0) respectively the electron affinity (above zero). The ionization energies agree perfectly with the ones obtained by the extended Koopmans theorem.*

delta-function like mean-field energies. With some goodwill, this can also be observed from Fig. 10.5. However, for a determination of the spectral properties beside the excitation energies, the nonequilibrium approach, Eq. 10.4 has been found more convenient – although its numerically effort is much larger.

Approximation scheme on the two-electron integrals

The calculation of the two-electron integrals, Eq. (6.6), constitutes the bottleneck of the Hartree-Fock formalism. Likewise, in the solution of the correlated Dyson equation and the Kadanoff-Baym equations, the main effort is spend in computing the self-energy expressions. For this reason we introduce an approximation scheme on the two-electron integrals, that was mainly suggested by the continuum model. There we can assume the continuum as non-interacting and non-reacting on the bound states, what yields a good approximation, at least for small occupation numbers of the continuum states. The problem of particle interaction is then reduced to the small subsystem given by the atom.[2] Practically this is achieved by setting all two-electron integrals to zero, that have at least larger index than the number of highest bound state. Thereby all self-energy calculations may be truncated at this value.
This scheme is easily extendible. We can choose a number n between 0 and 4 and calculate the two-electron integrals only, if n indices exceed the highest bound-state (or any other appropriately chosen state). $n = 4$ denotes the full scheme, where all integrals are calculated, and any smaller n reduces the calculation of the two-electron integrals to $\mathcal{O}(N_b^n)$. In Tab. 10.2,ionization e we show the results of different choices of n, that were obtained in a spin-polarized Helium potential. The number of basis functions was $N_b = 12$, and the cutoff index was set to 4.

[2]This is a practical implementation of the embedding scheme used in [49], however, not that elegant.

approx	order	HF	2ndBorn	CI
0	const	-1.806	-1.806	-1.8111
1	$\mathcal{O}(N_b)$	-1.810	-1.8070	-1.8162
2	$\mathcal{O}(N_b^2)$	-1.8108	-1.8128	-1.8139
3	$\mathcal{O}(N_b^3)$	-1.8108	-1.8128	-1.8139
4 (full)	$\mathcal{O}(N_b^4)$	-1.8108	-1.8128	-1.8139

Table 10.2.: *Results from the presented approximation scheme obtained from Hartree-Fock and Configuration Interaction calculations for a spin-restricted one-dimensional Helium model.*

Auger processes

From the equilibrium state we can also obtain information about the kinetic energy of an Auger-ionized electron. In the following we examine the standard procedures for a one-dimensional spin-polarized Beryllium model, $v(x) = -4/\sqrt{x^2+1}$. One approach for the determination of the Auger electron energy is given by formula (2.29), $E_{kin} = E_A - E_B - E_C$. We can directly apply it to the Hartree-Fock energies. However, the formula neglects relaxation processes, as it assumes the (double) ionized system to have the same orbitals.
Within CI a very natural description can be given. The initial groundstate can be described by the occupation vector (1,1,1,1,0,0,..), indicating that the four lowest Hartree-Fock orbitals are occupied.[3] The system with ionized core hole is then given by the vector (0,1,1,1,0,0,..), respectively (1,0,1,1,0,0,..), while the doubly ionized final states are (1,1,0,0,...),(1,0,1,0,...) or (1,0,0,1,0,...).
The difference between the energy of an $N = 3$ particle-state and a final $N = 2$ particle state will yield the Auger-electron energy. It is exact except for the approximation through Hartree-Fock orbitals and the assumption, that the Auger electron is emitted from the totally relaxed state. The results in Tab. 10.3 reveal a great impact of relaxation effects on the actual system. As expected, the exact results are lower than the approximate ones, since relaxation processes diminish the energy of the system.

Though this approach may yield accurate predictions for the energy, apparently it is unable to answer questions related to the dynamics. However, just the time-resolved Auger process is of great current interest. For instance, it is important to know on which time-scales Auger emission and relaxation occur and how both effects affect each other. The simulation of this processes by means of the collected time-evolution schemes constitutes a future goal. However, this probably

transition	HF	CI
(012)	0.722	0.5654
(013)	1.059	0.871
(023)	1.623	1.448
(123)	0.438	0.2728

Table 10.3.: *The kinetic energy of the Auger electron in a one-dimensional spin-polarized Beryllium model. The nomenclature is the same as in Chapter 2. For example (012) means that the hole in orbital* 0 *was filled up with the electron from orbital* 1*, while at the same time the Auger electron is emitted from orbital* 2*.*

[3] This holds exactly only for single-particle basis of natural orbitals, the eigenvectors of the density matrix, whose calculation is explained in chapter 7. For the present we restrict us to the basis Hartree-Fock orbitals, for which this assumption is already an approximation – whether a good one for $\lambda = 1$.

requires the inclusion of photons into the model – as it is e.g. done in the Jaynes-Cummings model – and thus new theoretical investigations.

11. Nonequilibrium calculations

The previous chapter has examined the thermodynamic equilibrium state of fermionic ensembles trapped in various potentials. The present chapter is now devoted to the analysis of time-dependent processes in nonequilibrium. Within the nonequilibrium Green function formalism, the reaction of the system to external fields of arbitrary strength in principle can be treated non-perturbatively. A possible restriction only emerges from the finite basis size. Here, we consider the interaction of the particle system with electromagnetic fields. As examined in chapter 2, in dipole approximation the field enters the many-body Hamiltonian as

$$v_{ext}(\mathbf{r}, t) \;=\; E(t)\,\mathbf{r}\,. \tag{11.1}$$

Further we restrict ourselves to wavepackets with Gaussian envelopes,

$$E(t) \;=\; E_0\,\cos(\omega(t-t_0)\,)\,\mathrm{e}^{-\frac{(t-t_0^2)}{2\Delta t^2}}\,. \tag{11.2}$$

If monochromatic pulses are needed, the variance Δt is set to a large value.
In the following work, we focus exclusively on one-dimensional potentials, more precisely, on the basic finite-box model as well as on the Helium model. Besides, we only consider the groundstate to avoid a thermal occupation of continuum states. Correspondingly, the inverse temperature β is placed at a sufficiently large value. As it was checked in the previous chapters, $\beta = 50$ is an adequate choice.
In contrast to the previous equilibrium calculations, which only required a moderate basis size, in nonequilibrium the introduced model meets its limits. In the presented calculations we do not exceed a basis size of $N_b = 100$ functions, while the full and unconditioned description of ionization processes is likely to need the hundredfold.[1]

11.1. Ideal calculations

We can learn a lot about the properties of our basic model, if we consider the ideal case, i.e. one particle. To avoid self-interaction of the particle, or more precisely the interaction between fractional occupied orbitals, also the coupling parameter λ must be set to zero.

Comparison between KB and the TDSE

A first affirmation of the Kadanoff-Baym simulations, explained in Chapter 9, is obtained by a comparison with solutions of the single-particle Schrödinger equation in coordinate space. For the ideal case, $\lambda = 0$, the solution of the KKBE corresponds to the solution of the Schrödinger equation in basis representation. By assuming the spatial results to be exact, these calculations

[1] This statement is based on talks at the conference "Interaction of free-electron-laser radiation with matter: recent experimental achievements, challenges for theory" at DESY in Hamburg.

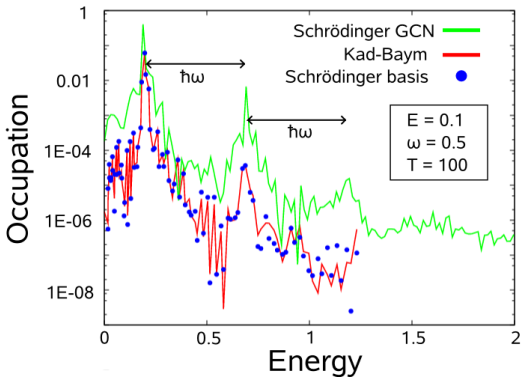

Figure 11.1: *Ionization spectrum of one particle in a finite box of depth $V_0 = -2$ and width $a = 1$, that is excited by a monochromatic wave. The green curve shows the result from a finite difference calculation with the generalized Crank-Nicolson method. The blue dots are obtained from a projection of the spatial solution on the basis functions, while the red curve is the result from an (ideal) Kadanoff-Baym calculation.*

yield the first – and probably best – test for the quality of a given continuum.
The comparison is done in terms of the energy spectra of the ionized particle, which present crucial quantities for ionization processes. The spectrum is calculated with two methods: In basis representation, the occupation number of a state is naturally obtained as the respective diagonal element of the Green function. A simple plot of the occupation numbers against the energy of the state yields the energy spectrum. In spatial representation, by projection of the final wavefunction on the Hartree-Fock basis, we can proceed in a similar way. In addition, we applied the procedure used in [50]: at a certain point outside the atom, the detector, the incoming wavefunction is stored and Fourier-transformed with respect to time. The result then is outlined against $k^2/2$. This procedure is only valid for the free particle, and thus no external field may affect the wavefunction at the position of the detector. Obviously, a monochromatic dipole field does not satisfy this condition. Yet we regard the result as an approximation.
In Fig. 11.1 the two methods are examined. The results from the basis representation methods are in good agreement, and deviate only at the upper boundary, where the incompleteness of the basis set becomes sensible. A comparison with the Fourier method in spatial representation reveals a poor agreement of the relative height. At least, the position of the peaks at multiples of the photon energy is well reproduced.

The resolution of one spectral line

An important question in the search for the "right" continuum is the question of the resolution of one basis state. Or reformulated, how much deviation from a resonant state is allowed to be furthermore resonant? For an answer, we performed calculations for $N = 2$ spin-polarized particles and $N_b = 2$ basis functions in a finite box of depth $V_0 = -10$ and width $a = 0.5$, that has only one basis state at $E_0 \approx -0.3$. The second state is chosen as the second basis function in order to obtain a non-zero dipole matrix – we could not use the third state as it has the same parity than the groundstate and therefore would lead to no transitions. The energy of the second state is now varied by the continuum box width, that is chosen in the range $b = 5$ to $b = 50$, and each time the system is propagated under the action of an electromagnetic wave with frequency $\omega = 0.5$ and different amplitudes. By plotting the basis state occupation numbers against their energies, we obtain the transition induced by the wave.
The results are shown in Fig. 11.2. For an amplitude of $E = 0.01$, they look very similar to the theoretical curve obtained from first order perturbation theory, Eq. (2.1). The zeros of the transition curves are located at a distance of roughly $2\pi/T$ and thus also behave as predicted. Looking at the transitions induced by a strong field of $E = 0.1$, we see that the relative heights of the peaks is strikingly modified, while the respective width has only barely changed. The

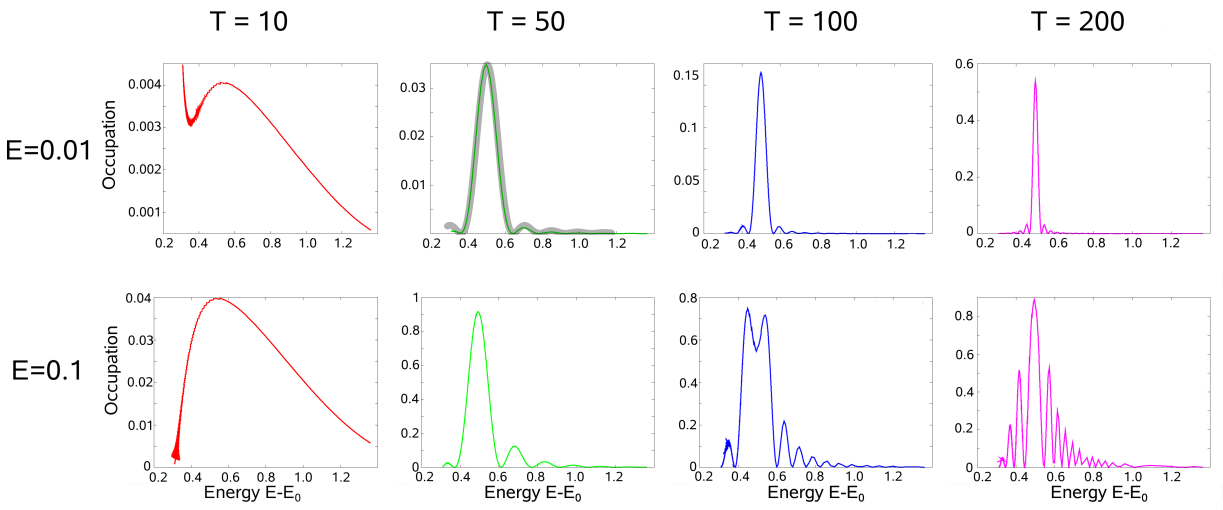

Figure 11.2.: *The resolution of one spectral line. The calculations were carried out for two non-interacting spin-restricted particles in a finite box. We used only two finite-box basis functions, one of which is a bound state and the other is a continuum state, whose energy is varied by the continuum box width. Plotted is the occupation of the continuum basis function after a monochromatic pulse with frequency $\omega = 0.5$ and different amplitudes E and evolution time T. In the $E = 0.01$, $T = 50$ picture the first order perturbation theory result is underlayed in grey.*

first-order perturbation result fails to describe the height of the peaks, what could have been also guessed from the Keldysh-Parameter, that is given by $\gamma = 3.5$.
The transition therefore depends strongly on the field strength, what makes it difficult for strong fields to apply the approximation scheme mentioned before.

The different concepts of ionization

In our basis approach, we can choose out of different concepts of ionization. The first and obvious one, that we will apply most of the time, is the probability for a particle not to be in a bound state. It is obtained by a trace over the density matrix, that involves only the continuum basis states. The other – for spatial calculations only – concept is given by the probability for a particle to be outside a reasonable chosen radius. The integration of the (one-particle) density over the outer region then yields the ionization probability, and if higher particle densities are available, we can also resolve different contributions to it – see the exact solution of the 1D-Coulomb model downwards.[2]
In Fig. 11.3 we checked the equivalence of the two ionization concepts.

Exclusion of basis functions

As it was mentioned above, in actual calculations we are very restricted in the number of basis functions. For the program as it is now implemented – without the use of parallel or vector architecture – the absolute limit for ideal and Hartree-Fock calculations is $N_b \approx 200$ basis functions, while for correlated Kadanoff-Baym calculations $N_b \approx 30$. If a good continuum resolution respectively a wide energy region is needed, this is not sufficient. A way around these restrictions

[2]The correlated one-body Green function offers only the one-particle density, while the two-body Green function must be approximated - e.g. as in (4.4) through Hartree-Fock.

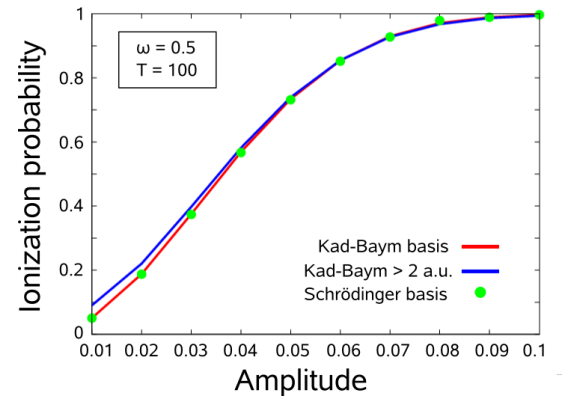

Figure 11.3: *The different concepts of ionization. The red curve and the green dots show the probability not to be in a bound state - both calculations, Schrödinger and Kadanoff-Baym, again yield the same result. The blue curve shows the probability to be outside of the radius $R = 2$ obtained from the one-particle Green function. The model atom consists of a box with $E_0 = -0.3$ and $a = 1$. The wave is monochromatic.*

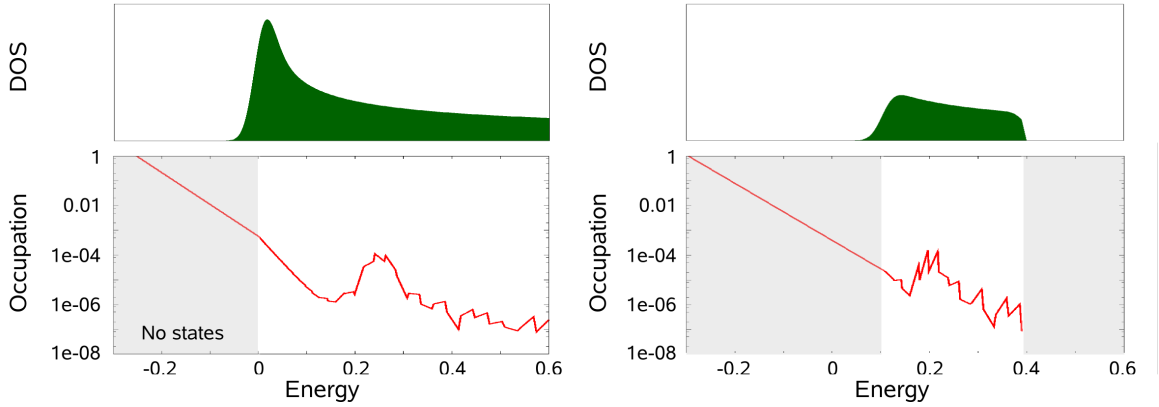

Figure 11.4.: *Approximation scheme for the density of states (DOS). $N = 2$ spin-restricted particles in a finite box were propagated to $T = 100$ under action of a monochromatic wave with $E = 0.01$ and $\omega = 0.5$. Left: Solution of the full problem with $N_b = 100$. Right: Only the energy region between 0.1 and 0.4 is taken into account. The number of basis functions is $N_b = 29$.*

can be made by means of some a priori information. For example, if we expect the ionized spectrum in accordance with Fermi's golden rule, we could drop the non-resonant states. Though this can yield a great numerical ease, it is also risky and should not be used without comparisons to benchmark calculations – if available. By a neglect of basisfunctions, also the particle density will be affected.

Figure 11.4 shows the densities of states (DOS) for a one-dimensional continuum box plus an approximated density, as well as an exemplary calculation with both DOS. We propagated $N = 2$ spin-restricted particles in Hartree-Fock approximation to time $T = 100$ under the action of a monochromatic field with $E = 0.01$ and $\omega = 0.5$. The results show an acceptable agreement in the considered energy region.

In the code there is the possibility to exclude both, some specified basis states or energy regions. This can be used, to drop the deep-lying, non-resonant continuum states with all too narrow energy distance.

Restrictions of the model

As it was mentioned in the introduction of this chapter, the main problem of the present Kadanoff-Baym approach is the small limit in the possible number of basisfunctions . Within this work, we did not consider more than $N_b = 100$ basisfunctions. For this choice, an ideal or Hartree-Fock calculation with $N_t = 1000$ timesteps takes a little less than one day – given a precomputed

set of electron integrals. In the following, we estimate a relation between the basis size and the accessible field strength. We performed calculations on an ideal system with $N = 1$ and $N_b \ll 80$, that are shown in Fig. 11.5. There, the system has been evolved with $N_b = 80$ basisfunctions to yield a reference result. For this calculation, the occupation numbers of the states after the pulse are plotted in the upper pictures. The red curve in the lower pictures shows the sum of these occupation numbers up to the basisfunction, that is given by the x-coordinate.
Next, we propagated the system for all numbers of basisfunctions smaller than $N_b = 80$ and plotted the calculated ionization probability. One could guess, that these two curves show a similar behavior, and this is true for a moderate field amplitude of $E = 0.01$. However, if the amplitude increases, strange things happen: Obviously, the increase of the basisfunction can lead to a significantly change of the result, although it is actually believed to yield an improved description of the system. For the amplitude of $E = 0.1$, we see that the region of instability is located around the first peak. For $N_b \geq 60$, the result converges towards the reference result. Further we reveal, that the case $E = 1.0$ is not accessible for the present number of basis functions, if at the same time an adequate continuum resolution is desired. Unfortunately, we can not present a proper explanation of this behavior. We only mention, that one has to be careful in the interpretation of the calculational results.

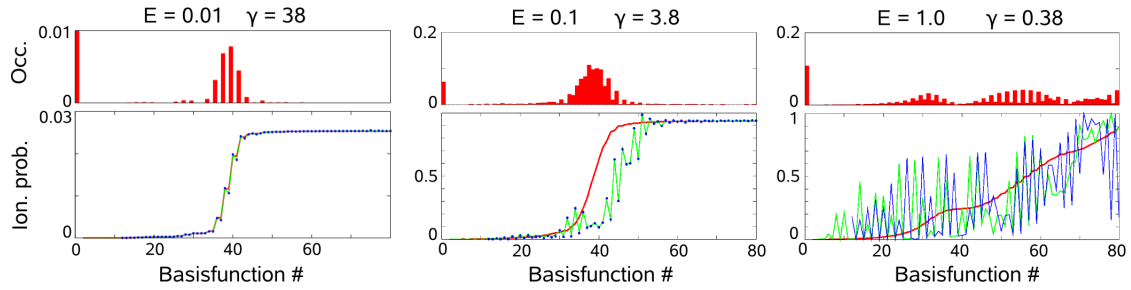

Figure 11.5.: *The influence of the electric field on the continuum. One particle in the groundstate with energy $E = -0.3$ is evolved in time under the action of a monochromatic field with $\omega = 0.5$ and varying amplitude. The continuum width is $2b = 200$. The upper pictures show the occupation of the system with $N_b = 80$ basisfunctions at $T = 100$, that serves as a reference. In the lower pictures different ionization probabilities are plotted against the number of basisfunctions. The red curves show the reference occupation summed up to the basisfunction given on the abscissa. The green curves illustrates the ionization probability obtained from a calculation with $N_b = x$, i.e. with the basisfunction given on the abscissa.*

11.2. Mean-field and correlated calculations

Having estimated the properties of the continuum model, we now include the particle interaction in the description. For the following calculations, we use a finite-box model with a depth of $V_0 = -10$ and a width $2a = 0.5$. The continuum box width is chosen as $2b = 200$, while $N_b = 100$ basis functions are incorporated. Further we use the continuum approximation as introduced in the previous chapter, so all continuum states are considered as non-interacting. The bound state at $E = -0.3$ is occupied by two spin-restricted interacting electrons.

Ionization probability

The ionization probability marks a central quantity in the description of ionization processes. A large part of the following work is devoted to its determination and interpretation. In Fig. 11.6, we outlined the ionization probability for different sets of parameters. The electromagnetic waves, that are applied to the basic system, are assumed to be monochromatic, i.e. the variance of the Gaussian Δt envelope is set to a large value.
In Fig. 11.6 (a), the ionization probability is plotted against the intensity for different frequencies. We can see, that for larger frequencies the curve shows a linear characteristic. As ω decreases, the curves continuously deviate from this linear trend and seem to converge against a fixed value. The explanation can be given in terms of the Keldysh parameter γ, as illustrated in the graphic. For a larger ω, the field oscillates too fast for an electron to tunnel out of the confinement. In this regime perturbation theory holds, that predicts a linear growth with the intensity. For a smaller frequency, the Keldysh parameter also decreases, and the strong-field effects collected in Chapter 2 obviously become important. For a γ smaller than three, perturbation theory definitely fails.
Right beside, in Fig. 11.6 (b), the ionization probability is outlined against the frequency of the wave. At the frequencies $\omega = 0.1$ and $\omega = 0.2$, all curves show a significant decay. In this region, the energy of one photon is not sufficient to ionize the electron, so that for an ionization more photon absorptions are required. Later, we will focus on this multi-photon ionization separately. For frequencies larger than $\omega = 0.3$, the curves increase up to a certain value, from which on they remain constant. Again the description can be given within the Keldysh-picture. By considering the first-order perturbation expression, Eq. (2.20), we recognize that it is independent of the

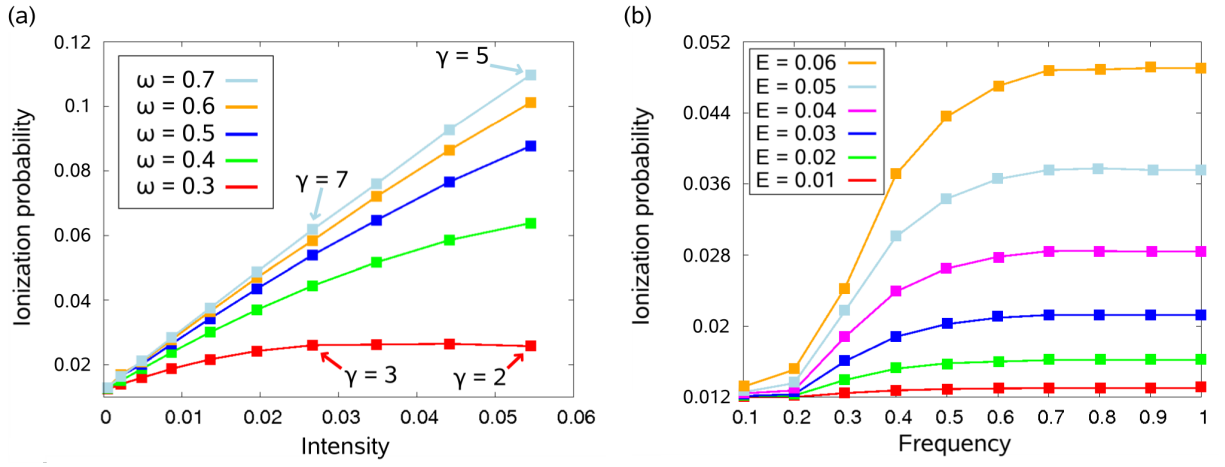

Figure 11.6.: *Ionization probabilities for different parameters. (a) Variation of the intensity. (b) Variation of the frequency.*

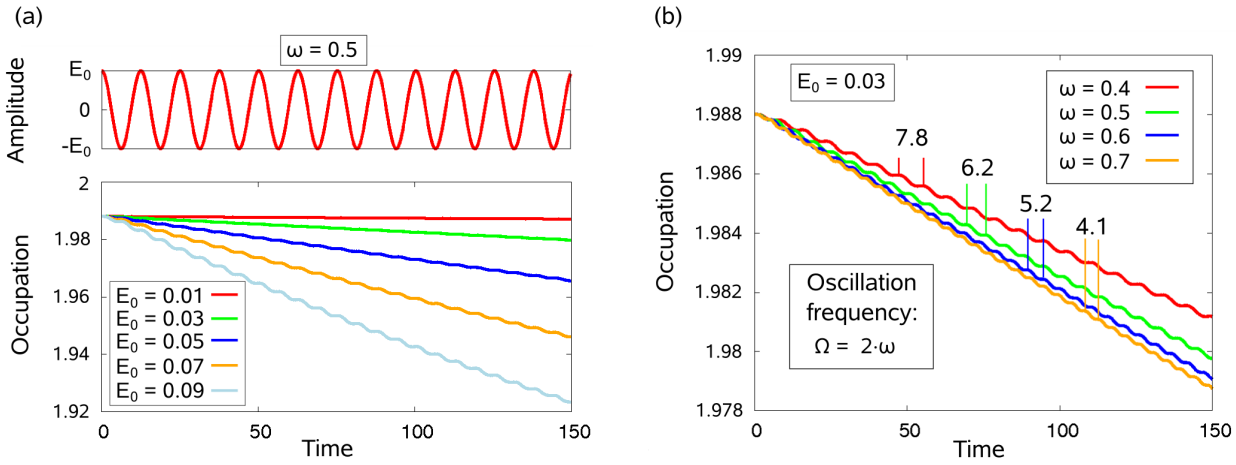

Figure 11.7.: *Time-dependent occupation of the first orbital. (a) Variation of the field amplitude for* $\omega = 0.5$*. As predicted by perturbation theory, the orbital occupation decreases nearly linear in time, while the slope of this line is proportional to the intensity. (b) The same for a fixed amplitude* $E = 0.03$ *and varying frequencies. According to perturbation theory, the frequency plays a minor role in the ionization probability.*

Figure 11.8: *A closer look at the time-dependent occupation shown in Fig. 11.7. The ionization rate is largest in the region between two extrema, when the velocity of the particles is large. At the time of the extrema, it has almost stopped.*

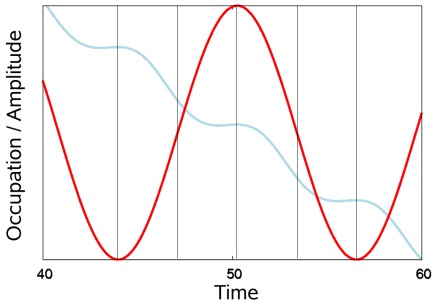

absolute frequency. Thus, the constancy of the ionization probability curves corresponds to the validity of perturbation theory. Consequently, for larger amplitudes the constant regions begin at larger frequencies.

We proceed by looking at the time-dependent occupation numbers shown in Fig. 11.7. In the left picture, they are plotted for different field amplitudes. We reveal a linear decrease, that is also predicted by the perturbative description. Accordingly, the slope of the curves decreases as E_0^2. In Fig. 11.7 (b), we compared the time-dependent occupation for different frequencies. The curves show a small dependence on the frequency. As it was previously explained, this corresponds to the validity of the perturbation theory. Furthermore, we have measured the duration of the oscillations in the occupation number by an average over twenty cycles. The corresponding frequency, $\omega = 2\pi/T$ turns out to be the double of the field frequency. This behavior is now explained.

A closer look at the oscillations of the occupation number and the field in Fig. 11.8 reveals, at which times the ionization rate is largest. This happens between two extrema of the external field, when the electrons have gathered an amount of energy from the field. At this time, the kinetic energy of the electrons is largest. This agrees with an intuitive picture: To get out of some confinement, a particle has to be fast enough.

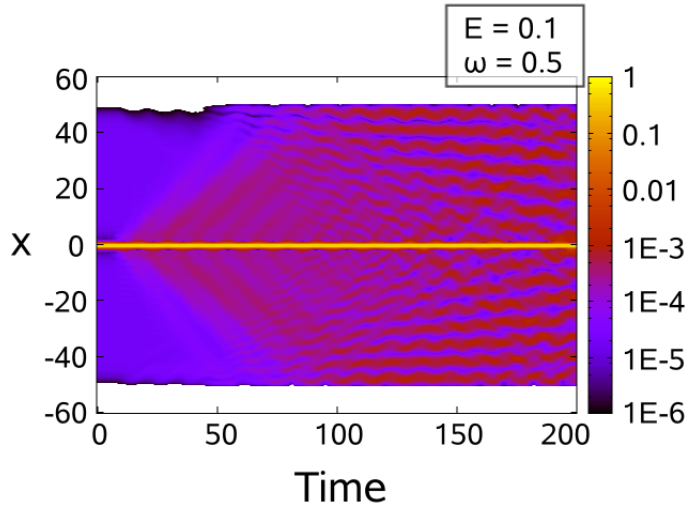

Figure 11.9: *Logarithmic plot of the time-dependent density of a spin-restricted $N = 2$ particle system in Hartree-Fock approximation. The structures in the density are caused by interference between the emitted and reflected fraction.*

Time-dependent density

The time-dependent density can be obtained from the Green function as explained in Chapter 9. Figure 11.9 shows the density from a calculation, in which the field amplitude was $E = 0.1$ and the frequency $\omega = 0.5$. We chose a finite-box model with a continuum width of $2b = 50$. After the system has evolved a certain time, we observe the formation of a structure in the density. It is caused by an interference between the emitted density fraction and the density fraction that has been reflected at the boundaries. Thus, the densities have no physical relevance. We could diminish the interference effects by use of appropriate optical potentials, i.e. complex potentials with a negative imaginary part. As one can reveal from a glance at the continuity equation, such a potential leads to a decay in the particle number. Its implementation is in basis representation not that straightforward as in coordinate space and will be part of the future work.

Multi-photon processes

The basic model also allows for a natural description of multi-photon processes. The continuum energy range then has to be chosen large enough to resolve the multiple photon peaks. With the possibility to exclude certain basis functions, we can also distinguish between real multi-photon processes, where the electron has crossed a virtual state, and sequential ionization, in which the particle occupies a real state between two photon absorptions. In the following this question bears no relevance, since we investigate the transition from the previously introduced model atom. It has only a single bound state at $E = -0.3$, which is occupied by two spin-restricted electrons. The frequency of the applied electromagnetic waves now is smaller than the energy gap, $\omega = 0.1$ and $\omega = 0.2$. It yields a continuation of Fig. 11.6 (a), in which only frequencies $\omega \geq 0.3$ were considered.
In Fig. 11.10, the energy spectrum of an ionized electron is shown, that has absorbed at least four photons. The first peak at $E = 4\hbar\omega$ is obtained with a fine resolution. However, the other peaks show an unexpected behavior. First, they are not located at multiples of the photon energy. Additionally, the respective height is larger than the one of the first peak. However, as known from perturbation theory, it should decrease with I^n, where n is the peak order.
In Fig. 11.11, we examined the validity of the perturbation theory. For a frequency of $\omega = 0.2$, the particle must receive two photons to become ionized. The ionization probability should therefore

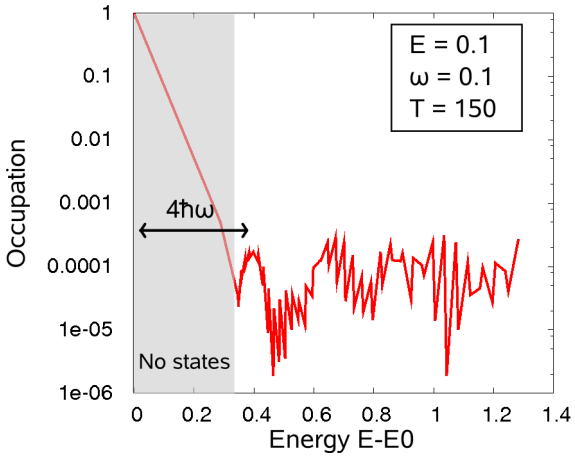

Figure 11.10: *Occupation of the continuum caused by multi-photon transitions. An electromagnetic wave of frequency $\omega = 0.1$ is applied to a finite box system with $N = 2$ spin-restricted particles in the groundstate $E_0 = -0.3$. Thus, for the ionization four photons are needed. The first peak at $E = 4\hbar\omega$ is clearly observable, while the resolution to the other expected peaks is poor.*

be proportional to I^2, and its outline against the intensity clearly affirms this prediction. Likewise for a frequency of $\omega = 0.1$, we expect a cubic behavior. However, the fitted cubic function does not match the curve. The reason for this can be explained by the Keldysh parameter. It becomes too large for an application of perturbation theory. The fit against a curve with a variable exponent yields $n = 1.83$. This behavior can also be observed in the experiment: If the Keldysh parameter approaches one, the ionization probability is better described by a smaller power than expected from perturbation theory. For the experimental results and further explanation see Ref. [2].

Double ionization of Helium

We also tried to investigate the sequential double ionization of Helium, or more precisely the corresponding effect in the 1D Helium model, $v(x) = -2/\sqrt{x^2+1}$. The respective equilibrium results of the model have already been presented in the previous chapter.

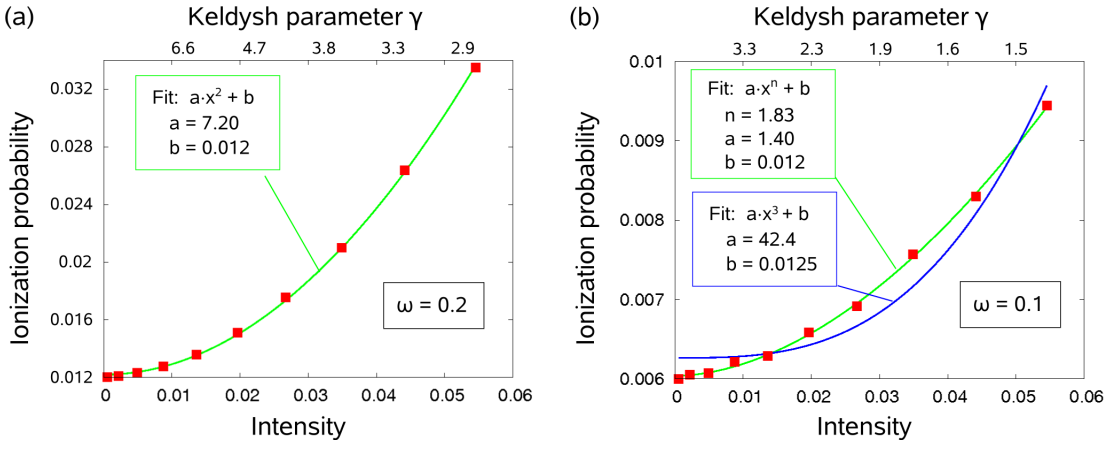

Figure 11.11.: *Ionization probability plotted against intensity and Keldysh parameter in the multi-photon regime. The system is evolved to $T = 150$ under action of a monochromatic wave. (a) For a frequency of $\omega = 0.2$, two photons are needed to ionize the particle. Perturbation theory predicts a ionization probability proportional to I^2, which is well confirmed by the fit curve. (b) For $\omega = 0.1$, three photons are required for an ionization. As the Keldysh parameters approaches one, perturbation theory breaks down. The ionization probability then is better characterized by a smaller exponent, here by $n \approx 1.83$.*

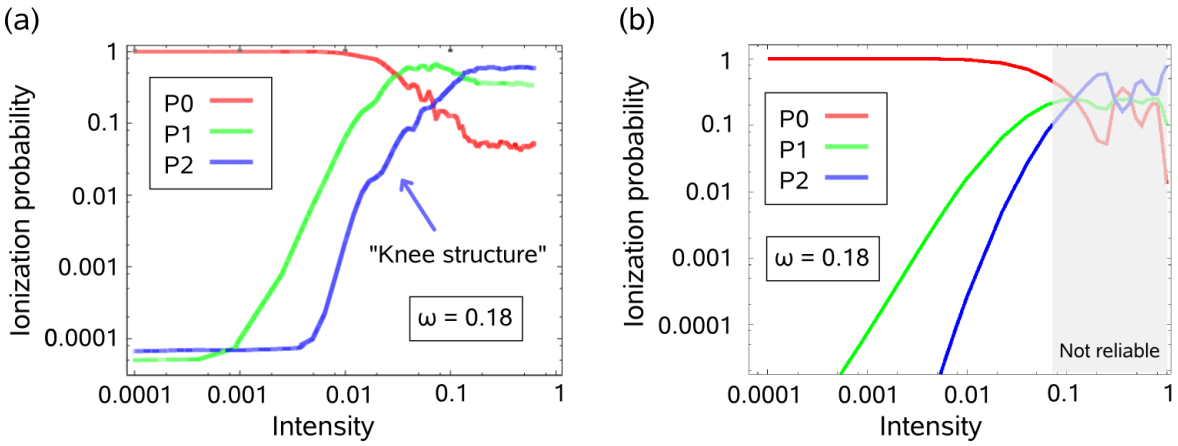

Figure 11.12.: *Ionization and double ionization probability of the one-dimensional Helium model plotted against the intensity. $P1$ and $P2$ denote the probability, that after the pulse one respectively two particles are outside of a radius $R = 10$. $P0$ gives the probability that no particle is ionized. (a) Result from the solution of the 2D Schrödinger equation. In the double ionization curve, one clearly observes the knee structure caused by the interaction of the re-scattered particle. (b) Corresponding Hartree-Fock result from a calculation with $N_b = 40$ basis functions. The knee structure disappears. Due to the small basis, the grey underlayed results are not reliable.*

As explained in Chapter 2, for special parameters of the electromagnetic wave[3], the ionized electron is driven back to the atom, where it may collide with the other electron. This interaction has a great impact on the ionization process of the confined electron, which results in a double-ionization curve, that shows the characteristic "Knee" structure.
To the groundstate we apply electromagnetic waves with the frequency $\omega = 0.18$ and varying intensities. The average and variance of the Gaussian envelope are $t_0 = 40$ and $\Delta t = 10$, and the system is evolved to time $T = 80$. After the pulse, we calculate the particular contributions to the ionization probability. An electron thereby is recognized as ionized, if it is located outside the radius $R = 10$. By an integration of the two-particle density over the inner or outer region, we obtain the contributions to the ionization probability, see Ref. [6]. This separation in the respective contributions is only possible, if we have access to the two-particle density.[4]
The results in Fig. 11.12 (a) were obtained by a propagation of the spatial solution of the stationary two-dimensional Schrödinger equation, as it is shown in Fig. 10.3. In the double ionization curve, the knee is clearly observable.
Our aim now was the description of this many body effect within the NEGF formalism. We expanded the Green function in $N_b = 40$ HF-orbitals, where the two particles had to be considered as spin-restricted. This Green function then was propagated in real time under action of the same wave. To arrange the result in the same way as in the exact calculation, the two-particle density is needed. In Hartree-Fock, it is simply given as the product of the one-particle densities. In Fig. 11.12 (b) the different contributions to the ionization from a Hartree-Fock calculation are presented. We reveal the well-known result, that the Hartree-Fock mean-field approach is not able to describe the knee structure.
Consequently, we tried to apply the second Born approximation. However, there are some major problems to be solved. First, as explained above, the two-particle density is essential. But the correlated one-particle Green function only covers the one-particle density, and the two-particle

[3]For a specification of the parameters see Ref. [2]. Roughly, double ionization occurs at small frequencies and larger amplitudes, i.e. at $\gamma < 1$.
[4]Likewise, to yield the N-particle ionization probability, we need the N-particle density.

quantity is hard to obtain, see Ref. [51]. Although higher particle densities can be reached in principle, they are much too complex for a numerical treatment.
In addition, even if we had solved these problems, the numerical solution of the Kadanoff-Baym equations is a very hard task. A second Born calculation with just the same parameters as in the Hartree-Fock case ($N_b = 40$,$N_t = 200$) has been started. For HF, the simulation lasts roughly 5 minutes. In contrast, the second Born calculation was stopped after a month, when it had reached 40 from 200 time-steps.
In summary, we have to state that the NEGF approach to double (not to say triple,...) ionization is very questionable. This statement also holds for other problems, in which information on higher-particle density matrices is required.

12. Conclusion and outlook

Conclusion

The goal of the present work was to investigate ionization processes in the framework of nonequilibrium Green functions. Therefore, we adopted a standard model for the description of an atom and the surrounding continuum, which in principle allows for an accurate treatment of the arising effects. The model continuum consists of an infinitely deep box, whose boundaries are chosen sufficiently separated to ensure an adequate energy-level spacing, whereas the model atom can be of arbitrary form. Here, we have considered three cases: the finite box, the harmonic oscillator and the Coulomb potential. In equilibrium they were studied in one, two and three dimensions, while for nonequilibrium calculations we have restricted ourselves to one dimension.

A main part of the thesis concentrates on the derivation of several numerical schemes. Likewise, we attached a great importance to their efficient implementation, for what a couple of state-of-the-art libraries are used. Certainly, the nonequilibrium Green functions lie at the heart of the investigations. For the numerical treatment, we followed the approach of Nils Erik Dahlen, Robert van Leeuwen and Adrian Stan, which is able to deal with inhomogeneous systems. It provides the expansion of the Green function in a suitable basis, with which the Dyson equation and the Kadanoff-Baym equations gain matrix structure. In contrast to earlier approaches, for the obtainment of the equilibrium state, the Dyson equation is solved self-consistently in imaginary-time space rather than in frequency space. This yields a natural starting point for the time evolution. The Kadanoff-Baym equations are solved on the whole two-time plane under full consideration of initial correlations.
Within this work, the self-energy is obtained within three common schemes, namely in Hartree-Fock, second Born and GW approximation, where the latter one is until now only available in equilibrium calculations. While the implementation of Hartree-Fock and second Born caused no further difficulties, the treatment of GW has been unknown. To this end an efficient algorithm has been developed and tested on a couple of examples.

From the main topic, several other schemes arose. The stationary one-particle Schrödinger equation is solved to achieve an initial basis, and likewise its time-dependent counterpart to determine single-particle reference results. For both, high-order schemes were introduced. Further, the solutions of the Roothaan-Hall equations are found to provide the Hartree-Fock basis expansion, and also the unrestricted Hartree-Fock algorithm is considered. As an original contribution we introduced the canonical treatment of the Hartree-Fock equations and demonstrated the ensemble differences in the presence of interactions. Finally, basing on the latter point, the stationary and time-dependent Configuration Interaction approach has been implemented to yield exact reference results.

In all the mentioned many-body methods the description of spin was included, what meets the final outlook in the preceeding work on nonequilibrium Green functions [18]. Further, we examined the influence of different basis sets and pointed out the advantages of analytical basis functions.

In each numerical section, the presented methods were applied to the harmonic oscillator, the standard example of a well-tempered system. Our intention thereby was not to repeat the results of Ref. [18], but to amend them. In this light, some interesting and new results were obtained. They include the canonical and grand-canonical comparisons on the Hartree-Fock level as well as the GW approximation results, whereas the latter were probably achieved for the first time. Further, we compared the results of all different calculations and pointed out the quality of the respective schemes.

For the investigation of the actual topic, ionization processes, the introduced model was studied by means of the methods above. In particular it was tried to work out its advantages and restrictions. The solutions of the Kadanoff-Baym equations for the noninteracting, one-particle system were compared to the results of the one-particle Schrödinger equation and yielded a good agreement. The necessary preliminaries and tests for an adequate continuum were collected, and an approximation scheme to modify the density of states has been invented.
Further, the equilibrium state has been determined for different model atoms and dimensions. The spectral function has been provided as well as results from the Extended Koopmans theorem, and both were shown to yield the same ionization energies. Moreover, the equilibrium approach to the kinetic energy of an Auger electron has been presented.
In nonequilibrium, the model system was propagated under action of an electromagnetic wave with Gaussian envelope. The ionization probabilities have been calculated for different sets of parameters and also the multi-photon transition was considered. The results were compared to the ones from perturbation theory, and the relation to the Keldysh parameter has been stated. Also, we investigated the double-ionization of a one-dimensional Helium model.

In summary, we have to state, that the NEGF approach to ionization processes is questionable. This is due to two general reasons: (i) The numerical effort of correlated calculations based on the presented method is too heavy for the required system size, and (ii) the Green function does not offer all necessary quantities in an easy way.

Outlook

Due to the detailed concern on the numerical basics, we gathered a wide overview on general quantum many-body theory and, in particular, on the nonequilibrium Green function formalism. Therefore, a large list of interesting problems arose. Most of them are not exclusively related to ionization processes, but rather mark principal questions in the application. In the following we shortly collect the most interesting directions.

- **Canonical ensemble**: Like for the Hartree-Fock scheme, the treatment of the Green function could be extended to the canonical formalism, see Ref. [52] for the theoretical footing. This could be advantageous when considering strongly coupled systems, in which the chemical potential naturally deviates from the one found in Hartree-Fock calculations.
- **Time-dependent GW**: The GW approximation, which has been established only on the imaginary time axis of the Keldysh-contour, should be extended to real-time evolution.
- **Embedding self-energy approach**: For larger systems, one can reduce the problem and restrict the view to the region of interest, while the interaction with the environment can be included in an embedding self-energy. For instance, the region of interest can be the atom in an atom-continuum model or a center molecule in between two leads [49].

- **Periodic potentials**: A first step towards the solid could be taken by considering periodic potentials, such as the Kronig-Penney model. With this we would obtain the band structure. The basis would be given by Bloch-states.
- **Quantized external fields**: The time-resolved treatment of Auger processes and spontaneous emission probably requires the quantization of the external field. The NEGF formalism thus has to be applied to the models known from quantum optics.
- **Real molecules, pseudo potentials**: Within our basis approach, it requires no further effort to treat molecules besides the calculation of the multi-center electron integrals. For large atoms and molecules pseudopotentials, as they are used in DFT, could be invented. This would also remove the need to describe deep-lying core states in the ionization.
- **Symmetrization of UHF**: We have shown how the Hartree-Fock method can produce a symmetry breaking. A way around this is to use unrestricted Hartree-Fock calculations, where the asymmetry is presumed, and afterwards apply certain symmetrizing procedures to the solution [32].

We conclude by announcing the most important goal. After comparing the efficiency of time-dependent Configuration Interaction and the propagation of the correlated Kadanoff-Baym equations, we observed that for the presented calculations CI is 10 - 100 times faster than KB (using $N \leq 4$ particles and $N_b \approx 15$ basisfunctions). Remember that the effort of (full) CI grows factorially with $\binom{N_b}{N}$, while KB grows only by a certain power (e.g. $O(N_b^8)$ for second Born). Thus the Kadanoff-Baym approach as it is given in this work only makes sense, if we can go beyond those regions, where the two effort-curves intersect.
The work of the future therefore will concentrate on a new implementation of the algorithms on parallel and/or vector-architectures.

A. Calculation of the two-electron integrals in 3D central potentials

The solutions of the Schrödinger equation in central potentials are given by (5.8):

$$\psi_{nlm}(\mathbf{r}) \;=\; \frac{u_{nl}(r)}{r}\; \mathrm{Y}_{lm}(\theta,\varphi) \tag{A.1}$$

For the calculation of the two-electron integrals,

$$w_{(n_1l_1m_1),(n_2l_2m_2),(n_3l_3m_3),(n_4l_4m_4)} = \int d^3\mathbf{r}\; d^3\mathbf{r'}\; \psi^*_{(n_1l_1m_1)}(\mathbf{r})\; \psi^*_{(n_3l_3m_3)}(\mathbf{r'})\; \frac{1}{|\mathbf{r}-\mathbf{r'}|}\; \psi_{(n_2l_2m_2)}(\mathbf{r})\; \psi_{(n_4l_4m_4)}(\mathbf{r'})\,, \tag{A.2}$$

we can use the multipole-expansion,

$$\frac{1}{|\mathbf{r}-\mathbf{r'}|} = \sum_{l=0}^{\infty} \frac{4\pi}{2l+1}\; \frac{r_<^l}{r_>^{l+1}}\; \sum_{m=-l}^{l} (-1)^m\; Y_{l,m}(\varphi,\theta)\; Y_{l,-m}(\varphi',\theta')\,. \tag{A.3}$$

(φ,θ), (φ',θ') are the angles of $\mathbf{r}$ respectively $\mathbf{r'}$, and $r_> = \max(r,r')$, $r_< = \min(r,r')$. After insertion of (A.3) in (A.2) we obtain

$$\begin{aligned} w_{(n_1l_1m_1),(n_2l_2m_2),(n_3l_3m_3),(n_4l_4m_4)} = {} & \sum_{l=0}^{\infty} \frac{4\pi}{2l+1} \int dr\; dr'\; u^*_{n_1,l_1}(r) u_{n_2,l_2}(r) u^*_{n_3,l_3}(r') u_{n_4,l_4}(r')\; \frac{r_<^l}{r_>^{l+1}} \\ & \cdot \sum_{m=-l}^{l} (-1)^m \int d\varphi\; d\theta\; \sin(\theta)\; Y^*_{l_1,m_1}(\varphi,\theta)\; Y_{l,m}(\varphi,\theta)\; Y_{l_2,m_2}(\varphi,\theta) \\ & \cdot \int d\varphi'\; d\theta'\; \sin(\theta')\; Y^*_{l_3,m_3}(\varphi',\theta')\; Y_{l,-m}(\varphi',\theta')\; Y_{l_4,m_4}(\varphi',\theta')\,. \end{aligned} \tag{A.4}$$

The integrals over three spherical harmonics are analytically solvable, see Ref. [53], p. 803 :

$$\begin{aligned} & \int_0^{2\pi} \int_0^{\pi} d\varphi\; d\theta\; \sin(\theta)\; Y^*_{l_1,m_1}(\varphi,\theta)\; Y_{l,m}(\varphi,\theta)\; Y_{l_2,m_2}(\varphi,\theta) \\ & \qquad = \sqrt{\frac{(2l+1)(2l_2+1)}{4\pi(2l_1+1)}}\; C(l\; l_2\; l_1|0\; 0\; 0)\; C(l\; l_2\; l_1|m\; m_2\; m_1)\,. \end{aligned} \tag{A.5}$$

$C(\;\ldots\;|\;\ldots\;)$ thereby denote the Clebsch-Gordan coefficients.

The integral vanishes, unless

(i) $\quad |l_1 - l_2| \le l \le l_1 + l_2$

(ii) $m_1 - m_2 = m$

(iii) $l_1 + l_2 + l$ even

We insert (A.5) in (A.4) and restrict the sum to those indices, for which the integral is non-zero:

$$w_{(n_1 l_1 m_1),(n_2 l_2 m_2),(n_3 l_3 m_3),(n_4 l_4 m_4)} = \sum_{l=\max(|l_1-l_2|,|l_3-l_4|)}^{\min(l_1+l_2,l_3+l_4)} A_l^{n_1 l_1, n_2 l_2, n_3 l_3, n_4 l_4} \int dr\ dr'\ u^*_{n_1,l_1}(r) u_{n_2,l_2}(r) u^*_{n_3,l_3}(r') u_{n_4,l_4}(r')\ \frac{r_<^l}{r_>^{l+1}} \quad \text{(A.6)}$$

Thereby we defined

$$A_l^{l_1 m_1, l_2 m_2, l_3 m_3, l_4 m_4} = \sqrt{\frac{(2l_2+1)(2l_4+1)}{(2l_1+1)(2l_3+1)}}\ C(l\ l_2\ l_1|0\ 0\ 0)\ C(l\ l_4\ l_3|0\ 0\ 0) \cdot \sum_{m=-l}^{l} (-1)^m\ C(l\ l_2\ l_1|m\ m_2\ m_1)\ C(l\ l_4\ l_3|-m\ m_4\ m_3)\,. \quad \text{(A.7)}$$

Together with restriction (ii), the sum over m evaluates to

$$A_l^{l_1 m_1, l_2 m_2, l_3 m_3, l_4 m_4} = \sqrt{\frac{(2l_2+1)(2l_4+1)}{(2l_1+1)(2l_3+1)}}\ C(l\ l_2\ l_1|0\ 0\ 0)\ C(l\ l_4\ l_3|0\ 0\ 0) \cdot \delta_{m_1-m_2,m_4-m_3}\ (-1)^{m_1-m_2}\ C(l\ l_2\ l_1|m_1-m_2\ m_2\ m_1)\ C(l\ l_4\ l_3|m_3-m_4\ m_4\ m_3)\,. \quad \text{(A.8)}$$

If we further define

$$R_l^{n_1 l_1, n_2 l_2, n_3 l_3, n_4 l_4} = \int dr\ dr'\ u^*_{n_1,l_1}(r) u_{n_2,l_2}(r) u^*_{n_3,l_3}(r') u_{n_4,l_4}(r')\ \frac{r_<^l}{r_>^{l+1}}\,,$$

we obtain the final expression for the two-electron integrals:

$$w_{(n_1 l_1 m_1),(n_2 l_2 m_2),(n_3 l_3 m_3),(n_4 l_4 m_4)} = \delta_{m_1-m_2,m_4-m_3} \sum_{l=\max(|l_1-l_2|,|l_3-l_4|)}^{\min(l_1+l_2,l_3+l_4)} A_l^{n_1 l_1, n_2 l_2, n_3 l_3, n_4 l_4} \cdot R_l^{n_1 l_1, n_2 l_2, n_3 l_3, n_4 l_4}\,. \quad \text{(A.9)}$$

The sum runs in steps of two and has to be performed only, if $(l1+l2) \mod 2 \neq (l3+l4) \mod 2$, i.e. if $(l1+l2)$ and $(l3+l4)$ have different parity. For each summand now, the radial integral has to be computed once.

Bibliography

[1] C. C. Gerry and P. L. Knight, *Introductory quantum optics* (Cambridge university press, 2005).

[2] I. V. Hertel, *Atome und Moleküle und optische Physik 1.* (Springer, 2008).

[3] I. V. Hertel, *Atome und Moleküle in starken Laserfeldern.* (2003), URL `http://staff.mbi-berlin.de/hertel/lehrseminar_kurzpuls/vortraege/9_hertel_starke-felder.pdf`.

[4] A. S. Kheifets, I. A. Ivanov, and I. Bray, Journal of Physics: Conference Series **88** (2007).

[5] D. Bauer and F. Ceccherini, Optics Express **8** (2001).

[6] N. E. Dahlen and R. van Leeuwen, Physical Review Letters A **64** (2001).

[7] A. Szabo and N. Ostlund, *Modern Quantum chemistry: Introduction to advanced electronic structure theory* (Dover publications Inc., Mineola, New York, 1996), ISBN 0521884071.

[8] L. P. Kadanoff and G. Baym, *Quantum statistical mechanics* (W.A. Benjamin, New York, 1962).

[9] R. van Leeuwen and N. E. Dahlen, *An Introduction to Nonequilibrium Green Functions. Lecture notes.* (2005).

[10] H. Haug and A. P. Jauho, *Quantum kinetics in transport and optics of semiconductors* (Springer, 1998).

[11] A. L. Fetter and J. D. Walecka, *Quantum theory of many particle systems* (Dover Publication Inc., 1971).

[12] W. Nolting, *Grundkurs Theoretische Physik 7: Viel-Teilchen-Theorie* (Springer, 2005).

[13] W. H. Dickhoff and D. van Neck, *Many body theory exposed ! Propagator description of quantum mechanics in many-body systems* (World Scientific Publishing, 2005).

[14] L. Keldysh, *"Real-time nonequilibrium Green's functions" in "Progress in nonequilibrium Green's functions II" edited by Michael Bonitz and Dirk Semkat* (World Scientific Publishing, 2002).

[15] L. Keldysh, Zh. Eksp. Teor. Fiz. **47** (1964).

[16] M. Bonitz and D. Semkat, *Introduction to computational methods in many-body theory* (Rinton press, 2006).

[17] R. van Leeuwen and N. E. Dahlen, *Introduction to the Keldysh formalism. Lecture notes.* (2006).

[18] K. Balzer, *Nonequilibrium Greensfunction approach to artificial atoms. Diploma thesis.* (2007).

[19] D. Semkat, D. Kremp, and M. Bonitz, Phys. Rev. E **59** (1999).

[20] G. Baym, Phys. Rev. **127** (1962).

[21] R. van Leeuwen and N. E. Dahlen, *Conserving approximations in nonequilibrium Green function and density functional theory* (2004).

[22] R. D. Mattuck, *A guide to Feynman diagrams in the many-body problem* (Dover Publications Inc., 1976).

[23] L. Hedin, Phys. Rev. **139** (1965).

[24] W. van Dijk and F. M. Toyama, Physical Review E (Statistical, Nonlinear, and Soft Matter Physics) **75**, 036707 (2007).

[25] M. A. Heroux and J. M. Willenbring, Tech. Rep. SAND2003-2952, Sandia National Laboratories (2003).

[26] T. Fließbach, *Quantenmechanik. Lehrbuch zur theoretischen Physik III, 3. Auflage* (Spektrum Akademischer Verlag, 2000).

[27] W. H. Press, S. A. Teukolsky, W. T. Vetterling, and B. P. Flannery, *Numerical Recipes 3rd Edition: The Art of Scientific Computing* (Cambridge University Press, New York, 2007), ISBN 0521884071.

[28] I. V. Puzynin, A. V. Selin, and S. I. Vinitsky, Computer Physics Communications **123** (1999).

[29] I. V. Puzynin, A. V. Selin, and S. I. Vinitsky, Computer Physics Communications **126** (2000).

[30] S. Chin and C. Chen, ArXiv Physics e-prints (2000), `physics/0012017`.

[31] C. C. J. Roothaan, Rev. Mod. Phys. **32** (1960).

[32] U. D. Giovannini, F. Cavaliere, R. Cenni, M. Sassetti, and B. Kramer, Physical Review B (Condensed Matter and Materials Physics) **77**, 035325 (2008).

[33] K. Schönhammer, American Journal of Physics **68** (2000).

[34] H. J. Schmidt and J. Schnack (1998), `cond-mat/9803151`.

[35] S. Gümüş and T. Özdoğan, Chinese Journal of chemistry **22** (2004).

[36] C. F. Bunge, J. A. Barrientos, A. V. Bunge, and J. A. Cogordan, Phys. Rev. A **46** (1992).

[37] M. Rontani, C. Cavazzoni, D. Bellucci, and G. Goldoni, The Journal of Chemical Physics **124**, 124102 (2006).

[38] N. E. Dahlen and R. van Leeuwen, The Journal of Chemical Physics **122**, 164102 (2005).

[39] A. Stan, N. E. Dahlen, and R. van Leeuwen, EPL **76** (2006).

[40] S. I. Yoshifumi Noguchi, Yohei Kudo and K. Ohno, The Journal of Chemical Physics **123**, 144112 (2005).

[41] A. Bergström, Nordisk Mat. Tidskr. 20, 138–142, 159, Math. Sci. Net., available at 'http://hem.passagen.se/scientor' (1972).

[42] K. S. Thygesen and A. Rubio, Physical Review B (Condensed Matter and Materials Physics) **77**, 115333 (2008).

[43] D. W. Smith and O. W. Day, J. Chem. Phys. **62** (1975).

[44] R. v. L. A. S. K. Balzer, M. Bonitz (2008), arXiv:0810.2425.

[45] H. S. Köhler, N. H. Kwong, and H. A. Yousif, Computer Physics Communications **123** (1999).

[46] N. E. Dahlen, R. van Leeuwen, and A. Stan, Journal of Physics: Conference Series **35** (2006).

[47] N. E. Dahlen and R. van Leeuwen (2007), arXiv:cond-mat/0703411.

[48] M. Bonitz, K. Balzer, and R. van Leeuwen, Physical Review B (Condensed Matter and Materials Physics) **76**, 045341 (2007).

[49] P. Myohanen, A. Stan, G. Stefanucci, and R. van Leeuwen, arXiv:0808.3483 (2008).

[50] S. Bauch, *Coulomb scattering and ionization processes in strong laser fields. Diploma thesis.* (2008).

[51] R. van Leeuwen, N. E. Dahlen, and A. Stan, Physical Review B **74** (2006), arXiv:cond-mat/0609694.

[52] P. C. Kwok and J. W. F. Woo, Phys. Rev. A **3** (1971).

[53] G. Arfken and H. Weber, *Mathematical methods for physicists. Fourth edition.* (Academic press, 2005).

Nachwort

Da liegt sie nun vor mir, meine Diplomarbeit, und hinter mir liegt das arbeitsreichste Jahr meines Lebens. Doch ich bin weit davon entfernt mich zu beschweren – es war sehr erfüllend an diesem faszinierenden Thema zu arbeiten. Nun, nach getaner Arbeit empfinde ich ein Gefühl des Dankes (oder ist es doch Schlafentzug, mhhh, nein Dank). Ich möchte Prof. Michael Bonitz danken, dass er mir die Möglichkeit gab, durch freies Arbeiten die eigenen Ideen zu verwirklichen, mich aber dann doch immer wieder im richtigen Moment zum eigentlichen Thema zurückholte. Hätte ich noch ein bißchen häufiger darauf gehört, wären wahrscheinlich mehr Ergebnisse zur Ionisation entstanden. Ganz besonders danken möchte ich ihm für die Möglichkeit einer Promotion, in der ich diesbezüglich Besserung gelobe. Ebenso möchte ich Prof. Pehlke danken, der immer ein offenes Ohr für Fragen hatte. Und weiter gehts mit der Arbeitsgruppe: Auch wenn ich häufig meinen Arbeitsplatz auf die heimische Couch verlagert habe, wars im Büro und beim Kaffee-Klatsch doch meistens sehr lustig. Hervorheben möchte ich zunächst Karsten Balzer, meinen Universal-Ansprechpartner in Sachen Greensfunktionen – gab es eigentlich einen Tag, an dem ich nicht seine hervoragende Diplomarbeit in einem PC-Fenster geöffnet hatte? Weiter sage ich Danke an meine Zimmergenossen Hanno Kählert und Torben Ott für viele interessante Gespräche und auch für das Korrekturlesen dieser Arbeit. Dafür und für eine schöne Konferenz in Hamburg danke ich auch Sebastian Bauch. Ein besonderer Dank geht an meine Freunde Lasse Rosenthal und Martin Heimsoth, mit denen ich viele schöne Abende während des gesamten Studiums verbracht habe.
Nun bleibt noch meine Familie. Ich möchte meinen Eltern sehr, sehr danken für die jahrelange Unterstützung und dafür, dass sie einfach cool sind. Schließlich geht mein ganzer Dank an meine Freundin Melanie Eberlein, für ihre Liebe, ihre große Geduld und dafür, dass sie mir während dieser Arbeit das Schönste aller Geschenke gemacht hat: unseren Sohn Benjamin.

Eidesstattliche Erklärung

Die vorliegende Arbeit ist von mir selbstständig und nur unter Zuhilfenahme der angegebenen Quellen und Hilfsmittel angefertigt worden.

Kiel, _____ _____